6 Power Flows

Tennessee Valley Authority (TVA) Regional Operations Center (Courtesy of TVA.)

Successful power system operation under normal balanced three-phase steady-state conditions requires the following:

1. Generation supplies the demand (load) plus losses.
2. Bus voltage magnitudes remain close to rated values.
3. Generators operate within specified real and reactive power limits.
4. Transmission lines and transformers are not overloaded.

The power flow (sometimes also called the *load flow*) is the basic tool for investigating these requirements. The power flow determines the voltage magnitude and angle at each bus in a power system under balanced three-phase steady-state conditions. It also computes real and reactive power flows for all equipment interconnecting the buses, as well as equipment losses.

Both existing power systems and proposed changes, including new generation and transmission, are of interest.

Conventional nodal or loop analysis is not suitable for power flow studies because the input data for loads are normally given in terms of power, not impedance. Also, generators are considered to be power sources, not voltage or current sources. The power flow problem is therefore formulated as a set of nonlinear algebraic equations suitable for computer solution.

Sections 6.1 through 6.3 review some basic methods, including direct and iterative techniques for solving algebraic equations. Then Sections 6.4 through 6.6 formulate the power flow problem, specify input data, and present two solution methods: Gauss-Seidel and Newton-Raphson. Means for controlling power flows are discussed in Section 6.7. Sections 6.8 and 6.9 introduce sparsity techniques and a fast decoupled power flow method, while Section 6.10 discusses the dc power flow, and Section 6.11 considers the power flow representation of wind turbine generators. Formulations for economic dispatch and optimal power flow are given in Sections 6.12 and 6.13

Since balanced three-phase steady-state conditions are assumed, this chapter uses only positive-sequence networks. Also, all power flow equations and input/output data are given in per unit (p.u.).

CASE STUDY

During this century, renewable energy sources, including solar and wind generation, are projected to substantially increase in the United States and worldwide. High penetrations of wind and solar generation can induce increased cycling of fossil-fueled power plants. The following case study examines the operational impacts of up to 35% wind and solar penetrations in the western United States. The primary impact of displacing fuel, as well as displacing fuel costs and emissions associated with fossil-fueled power plants, and the secondary impact of increased cycling, including costs and emissions associated with cycling of fossil-fueled power plants, are analyzed.

Finding Flexibility: Cycling the Conventional Fleet

By Debra Lew, Greg Brinkman, Nikhil Kumar, Steve Lefton, Gary Jordan, and Sundar Venkataraman

Adding new generation, load, or transmission to the grid changes the operation of the incumbent power system. Wind and solar generation plants are no different, but their impact on the rest

of the grid is exacerbated by the facts that wind and solar energy is nondispatchable and such generators produce variable output. And because wind and solar effectively bid into the market at very low or negative cost, they are preferred resources in the dispatch stack. They are used by system operators whenever possible, unless there are generator operating limits or transmission constraints.

At low wind and solar penetrations or with low-variability resources (e.g., from high geographic diversity), the impact on the rest of the system may be small. But at high penetrations or with high-variability resources, wind and solar can induce increased cycling of the fossil-fueled fleet. This means that coal and gas generators may be asked to start up and shut down, ramp up and down, or operate at minimum generation levels more frequently. Cycling has impacts on emissions and on the wear-and-tear costs of the fossil-fueled fleet.

Coal and gas generators tend to have additional emissions at start-up and possibly also during ramps. Emissions are also affected by the output level of the generator. For example, units tend to be less efficient at partial load, thus increasing the carbon dioxide (CO_2) rates at minimum generation levels.

Starts and ramps also lead to increased wear and tear on the unit components and systems. Temperature and pressure changes lead to stresses that can result in premature component failure, an increased need for maintenance and overhauls, and more frequent repairs.

The primary impact of a MWh of wind or solar energy is to displace a MWh of other generation, typically fossil-fueled generation. Displacing a MWh of fossil-fueled generation displaces the costs and emissions associated with that fuel. But a secondary impact of this wind and solar energy can be to increase cycling of the fossil-fueled generators. As we have said, there are wear-and-tear costs and emissions impacts associated with cycling. This raises two questions: how big are those secondary impacts, and do they significantly negate the primary impacts that wind and solar energy bring to the table? Some recent analyses have claimed that wind actually increases overall emissions or that the avoided emissions from wind have been significantly overestimated.

Many integration studies have examined the impacts of high penetrations of wind power on particular systems and on the operation of the conventional fleet. Very few have considered cycling impacts in detail, partly because of the lack of data on cycling costs and emissions. This article describes the first study that combines detailed data on wear-and-tear costs and the emissions impacts of cycling with operational simulations of the entire western U.S. grid with high penetrations of wind and solar to determine these impacts.

The Western Wind and Solar Integration Study: Phase 2

In 2011, GE Energy, Intertek AIM, the National Renewable Energy Laboratory (NREL), and RePPAE began the Western Wind and Solar Integration Study Phase 2 (WWSIS-2). This study built on the Phase 1 effort, which had examined up to 35% wind and solar penetrations in subregions in the Western Interconnection and mitigation options for integrating those resources. The conclusion of Phase 1 was that several changes in operating practices would be needed to integrate the wind and solar energy. The two most important of these were increased balancing area coordination and intrahour scheduling. There are many efforts being considered now in the western United States to implement these changes, including the creation of an energy imbalance market.

The goal of WWSIS-2 was to investigate the cycling impacts on the fossil-fueled fleet in detail and to determine if the wear-and-tear costs and the impacts on emissions significantly reduced the benefits of wind and solar power. The point of this study was not to determine whether wind and solar plants should be built, but rather to understand what the impacts on the fossil-fueled fleet would be if wind and solar were built to a high penetration—especially the impacts on costs and emissions.

To do this, we simulated future power system operations under varying levels of wind and solar penetration. Any simulation of the grid requires simplifying assumptions in order to develop a model that can be run with a reasonable amount of computing power and time. Power system operation in a future scenario with high penetrations of wind and solar is likely to be different from today. Additionally, we did not have access to confidential information such as bilateral contracts for power or transmission flows. The key differences between our model and today's operation are:

- We assumed a natural gas price that varied subregionally but averaged US$4.60/million Btu across the interconnection. We did not model a carbon tax or any renewable energy incentive, such as the production tax credit.
- We did not model bilateral contracts for power or transmission flows but assumed a least-cost unit commitment and economic dispatch.
- We modeled the nearly 40 standalone balancing authorities as 20 zones, each holding its own contingency and flexibility reserves, with no hurdle rates between them.

New Data Sets

NREL analyzed measured emissions from every power plant in the United States (using the Environmental Protection Agency's continuous emissions-monitoring data) to determine incremental emissions due to a start or ramp as well as emissions rates from part loading. This analysis

was used to create a unit-specific emissions data set for cycling and noncyclic operation. These unit-specific emissions were used in the detailed operational simulations. For display purposes, however, we have averaged the data by unit type to show high-level results.

Heat rates as a function of load were examined for combined cycle (CC), combustion turbine (CT), coal, and gas steam units. Table 1 shows the resulting penalties for operating at part load. This penalty is defined as the percentage increase in emissions rate (lb/MWh) when the average unit is operating at 50% of maximum capacity. CC units are the most efficient at full load and part load; CC and CT units have the most significant emissions penalties for operating at 50% compared with 100% of maximum generation, however.

NO_x emissions as a function of load were analyzed similarly and are shown in Table 1. Steam units (coal and gas) emit approximately an order of magnitude more NO_x per MWh than gas CC units and CT units. Although part-load operation leads to an NO_x penalty for the CC and CT units, such operation was found to benefit the coal-fired steam units. For example, coal units operating at 50% were found to emit 14% less NO_x per MWh compared with full-loading operation; gas CC units were found to emit 22% more NO_x per MWh at 50% load compared with full load. Most of the NO_x from all units is created from nitrogen in the combustion air ("thermal" NO_x), as opposed to in the fuel, so flame temperature is likely a primary driver of NO_x emissions.

Type of Unit	CO_2 (%)	NO_x (%)
Coal	5	−14
Gas CC	9	22
Gas CT	18	15
Gas steam	6	−14

TABLE 1
Emissions penalty for part-load operation

Because of the significant part-time usage of pollution control equipment for SO_2, it was impossible to create part-load emission curves.

Starting an off-line, fossil-fueled unit increases emissions for two reasons. First, it takes fuel to bring the unit online, and that fuel adds emissions without adding energy to the grid. Second, starts can increase emissions rates because most pollution-control equipment does not become fully effective until flame and flue gas temperatures are in the proper range. Table 2 shows the start penalties for different types of units and different emissions. For example, a coal unit emits 1.98 lb/MW of capacity of excess NO_x during start-up. This is equivalent to operating the unit at full load for approximately 30 minutes.

Ramping, or load-following, emissions were estimated in a similar way to the start-up emissions. A ramp was defined as an increase of output of 30% of maximum capacity (e.g., from 70% to 100% of maximum

Type of Unit	Heat Input per Start (Millions Btu/MW)	NO_x per Start (lb/MW)	SO_2 per Start (lb/MW)
Coal	16.5	1.98	3.9
Gas CC	2.0	0.53	n/a
Gas CT	3.5	0.79	n/a
Gas steam	13.7	0.84	n/a

TABLE 2
Start-up emissions per MW of capacity

capacity). Table 3 presents generation-weighted averages. Ramping emissions are much lower than start-up emissions. The most significant ramping emission impact is the NO_x emissions from coal units (equivalent to 10–15 minutes of full-load operation).

While emissions at various operating levels are reasonably well understood, many utilities in the western United States do not know the wear-and-tear costs of cycling their fossil-fueled units. First, they have not needed to know these costs because until very recently, many of these plants, which were designed as base load plants, were not cycled. Second, determining these costs is complex because cycling operation today may not have cost implications until several years in the future.

Intertek AIM studied wear-and-tear costs from cycling for hundreds of fossil-fueled units around the world. For each unit, Intertek AIM had determined a best fit and a lower-bound and upper-bound fit for cycling costs, where the bounds reflected the uncertainty range for that plant. While specific data from those studies were confidential, aggregated data from those studies could be used as generic wear-and-tear costs for similar units that have not been studied. In this way, we were able to define variable operations and maintenance (VOM) costs for a hot, warm, and cold start; a ramp (typical); and for noncyclic operation for different types of plants. Table 4 shows the lower-bound costs for the different plant types.

Upper-bound costs were also used in this study. The raw

Type of Unit	Heat Input per Ramp (Millions Btu/MW)	NO_x per Ramp (lb/MW)	SO_2 per Ramp (lb/MW)
Coal	0.57	0.73	0.82
Gas CC	0.08	0.00	n/a
Gas CT	0.28	0.02	n/a
Gas steam	−0.09	0.05	n/a

TABLE 3
Ramping emissions per MW of capacity

	Small Subcritical Coal	Large Subcritical Coal	Super-Critical Coal	Gas, Combined Cycle	Gas, Large-Frame Combustion Turbine	Gas, Aero-derivative Combustion Turbine	Gas, Steam
Hot start (US$/MW)	94	59	54	35	32	19	36
Warm start (US$/MW)	157	65	64	55	126	24	58
Cold start (US$/MW)	147	105	104	79	103	32	75
Ramp (US$/MW)	3.34	2.45	1.96	0.64	1.59	0.63	1.92
Noncyclic operation (US$/MWh)	2.82	2.68	2.96	1.02	0.57	0.66	0.92

TABLE 4

Lower-bound median costs for cycling for various generation types

upper-bound data is confidential, however; only aggregated results can be presented here. All the cycling cost estimates used for this study are for typical units of various types; they are not unit-specific. The worst units for cycling are older base load power plants that should be retrofitted prior to significant cycling, using countermeasures such as procedure and chemistry changes and hardware retrofits. Without these measures, cycling could potentially lead to costly high-impact, low-probability events. Ongoing studies are examining the costs and benefits of retrofitting coal- and gas-fired power plants for increased flexibility.

Five Scenarios: Wind versus Solar

We used these new data sets in a commercial production simulation tool, PLEXOS, to model grid operations of the Western Interconnection on a 5-minute time step, because wind and solar output varies within the hour. We used the Western Electricity Coordinating Council (WECC) Transmission Expansion Policy Planning Committee (TEPPC) 2020 data set as a basis for our model, because it has been widely vetted among western U.S. utilities. A key change in assumptions was the natural gas price: the 2020 case average gas price was high, so we used the 2022 average gas price of US$4.60/million Btu.

We created five scenarios to examine increasing penetration levels of variable generation and also to compare wind with solar. Solar included rooftop photovoltaics (PV), utilityscale PV, and concentrating solar power (CSP) with six hours of

thermal storage. The scenarios were as follows:

- **No renewables:** 0 MW wind, 0 MW solar (0% wind, 0% solar)
- **TEPPC:** 27,900 MW wind; 7074 MW PV; 4352 MW CSP (9.4% wind, 3.6% solar)
- **High wind:** 63,840 MW wind; 20,064 MW PV; 6536 MW CSP (25% wind, 8% solar)
- **High mix:** 43,118 MW wind; 40,374 MW PV; 13,997 MW CSP (16.5% wind, 16.5% solar)
- **High solar:** 23,357 MW wind; 61,941 MW PV; 21,526 MW CSP (8% wind, 25% solar).

Penetration levels refer to energy, not capacity, and are penetration levels for the U.S. portion of the Western Interconnection only, because data for Canada and Mexico were lacking. The scenario without any renewables is an unrealistic one because existing wind and solar plants have been removed, but it was created to examine the impacts of all the wind and solar on the system.

Table 5 shows the penetration levels for each scenario. Wind and solar were nominally built to 33% energy penetration considering the historical weather patterns of 2004, 2005, and 2006. The analysis was for the load and weather pattern of 2006, which had a typical solar profile but better wind than the average of the years 2004–2006. After curtailment (curtailment includes CSP storage curtailment, some of which is built into the design of the generator), the 2006 penetration levels are 30–33% of U.S. load in the Western Interconnection and 24–26% of total load in the Western Interconnection. Because Canada and Mexico have relatively small connections with the United States in the Western Interconnection (compared with the total size of the U.S. portion), the impacts of renewables in the United States should be compared with the nominal 33% penetration numbers. Certain outputs, such as total change in emissions throughout the Western Interconnection, should be compared with the total Western Interconnection penetration levels (nominally 26%).

	2006 Penetration Level Across U.S. WECC After All Curtailment	2006 Penetration Level Across All WECC After All Curtailment
TEPPC	13.2	10.5
High wind	32.6	26.0
High mix	32.2	25.6
High solar	30.2	24.1

TABLE 5

Renewable energy penetration levels

To bring resources to load, we expanded the capabilities of existing transmission paths by iterating production cost runs until shadow prices across paths were within fixed, consistent cutoff values.

Simulating Western Grid Operations

We committed base load units one day ahead using synthesized day-ahead wind and solar forecasts. We

then committed gas units four hours ahead using synthesized four-hour-ahead wind and solar forecasts. Finally, we ran a 5-minute real-time dispatch.

Balancing the system can be more challenging with higher penetrations of variable generation. We therefore increased operating reserves to accommodate the wind and solar, as shown in Table 6. We used dynamic reserve requirements, and Table 6 shows the average level of operating reserves held throughout the year. We did not increase contingency reserves, which were held zonally, because neither wind nor solar plants were the single largest contingency. We adjusted other operating reserves, however, based on the wind and solar output during each hour of the year. Regulating reserves were held equivalent to 1% of load plus 90% of the 10-minutes wind and solar variability. The high wind and solar penetrations required up to 10% more regulating reserves than the scenario without any renewables. We also held a new reserve category—"flexibility reserves"—to account for the 60-minutes variability of wind and solar. These amounted to 1–3% of the installed capacity of the wind and solar generating facilities.

All of this work was overseen by a technical review committee consisting of about 50 utility staff members, researchers, and power plant experts. They met approximately every other month to review inputs, assumptions, methodologies, and results.

System Operation with High Penetrations of Wind and Solar

We analyzed the 5-minute operational simulations, with a focus on cycling impacts of the coal and gas units. All results reflect the specific characteristics of the generators and transmission of the Western Interconnection.

During the summer, load is high, and the impacts of variable generation on cycling are modest. In the spring and fall, however, load is low, and both wind and solar output are high, resulting in challenging operational conditions. This makes for a low net load: net load is the load minus the variable generation. Five-minute dispatch from the most challenging week of the year, as defined by the minimum net load condition,

Scenario	Contingency (MW)	Regulation (MW)	Flexibility (MW)
No renewables	3361	1120	0
TEPPC	3361	1158	1193
High wind	3361	1236	2599
High mix	3361	1211	2035
High solar	3361	1207	1545

TABLE 6

Contingency, regulating, and flexibility reserves

is shown in Figure 1. At low penetrations, as shown in Figure 1(a), there is little impact on the rest of the system except on the minimum net load day of March 29. For the high-wind scenario, shown in Figure 1(b), however, most of the gas CC generation has been displaced; there is curtailment on March 29; and coal generation declines markedly over the week. In the high-solar scenario, shown in Figure 1(c), the high midday

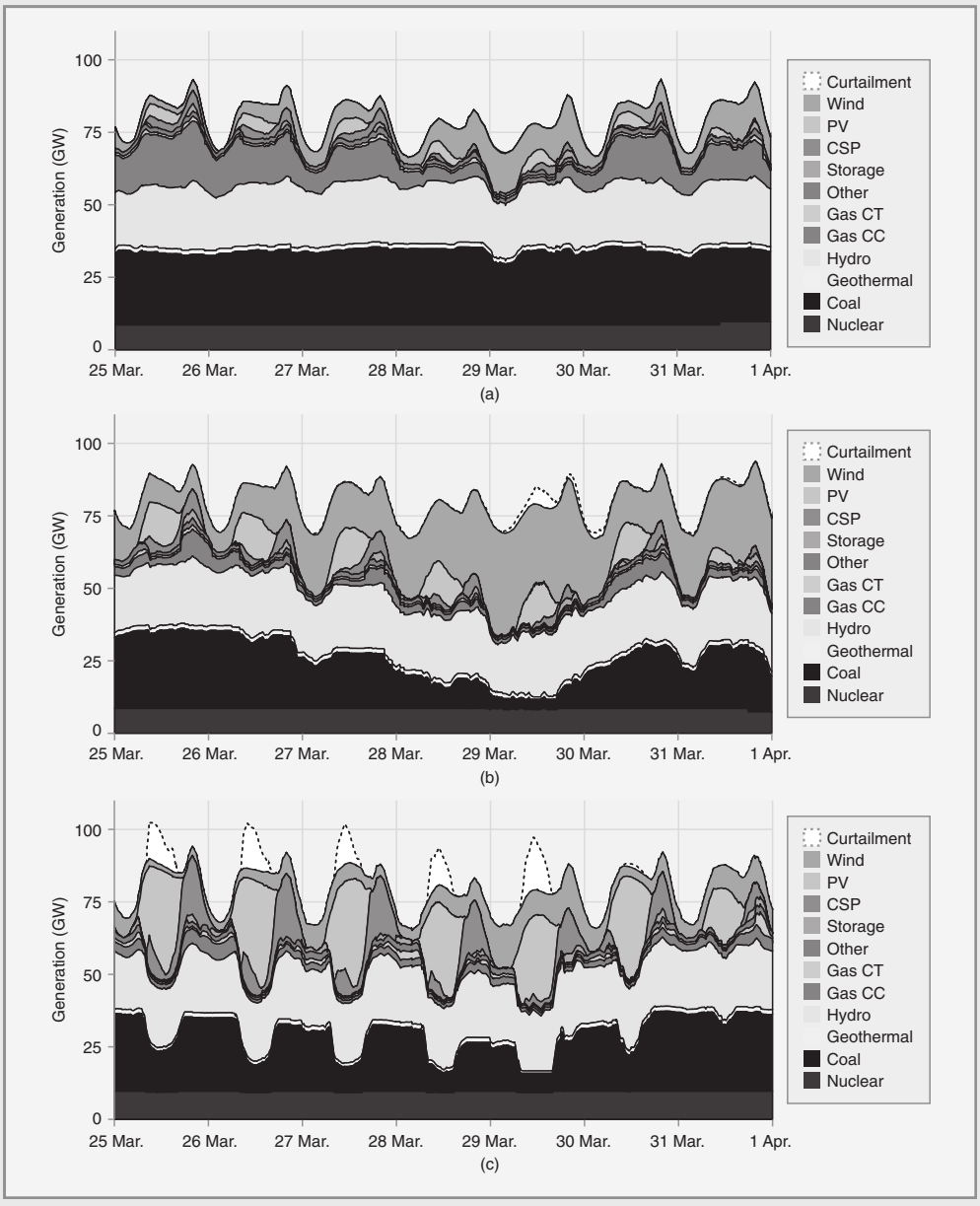

Figure 1 Five-minute dispatch stacks for the (a) TEPPC, (b) high-wind, and (c) high-solar scenarios for a week in March. This week represented the most challenging week, as defined by the minimum net load condition.

output leads to curtailment and the backing down of coal generation on a nearly daily basis in the middle of the day. Gas CT units turn on in the evening to help meet the evening load peak.

Despite these challenges, we find that the system can operate and balance load and generation. There were no regulating reserve violations and very few contingency reserve violations. Figure 2 shows that wind and solar mostly displace gas CC generation. Displacement of coal increased with increasing penetrations of wind because gas tends to be decommitted or backed down already at night, when there are high levels of wind. Curtailment of potential wind and solar generation on an annual basis was as much as 5% in the high-penetration scenarios. The high-mix scenario saw the least curtailment (1.6%).

The biggest impact from wind and solar on cycling of other generation is the increased ramping of the coal units, as shown in Figure 3(b). Starts for coal units, as shown in Figure 3(a), change little. Gas CCs start more with low wind and solar penetrations, but at high penetrations starts are similar to those in the scenario with no renewables. Gas CTs cycle more with high solar penetrations and less with high wind penetrations.

Figure 4 depicts coal starts and ramps for the challenging week in March. At low penetrations, there is little change in coal commitments, and the coal units are typically running at or near full output. In the high-penetration scenarios, coal capacity is shut down approximately each week, and the coal is ramped up and down each day, especially with high penetrations of solar.

Emissions Reductions Are Significant

We find that wind- and solar-induced cycling offsets a very small percentage of the wind- and solar-induced emissions reductions of CO_2, NO_x, and SO_2 across the Western Interconnection that are more than offset by the emissions reductions due

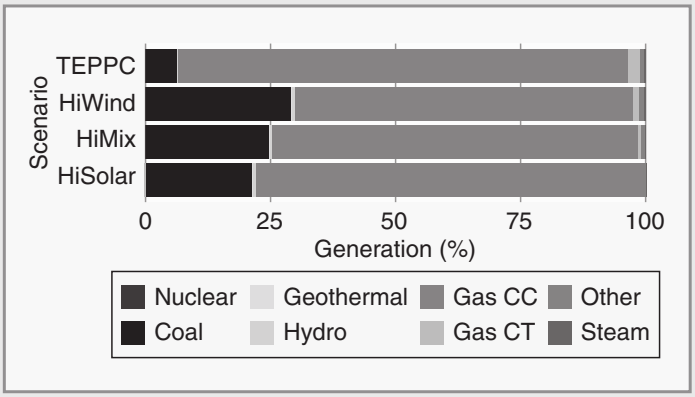

Figure 2 Generation displaced by wind and solar, as compared with the scenario without any renewables

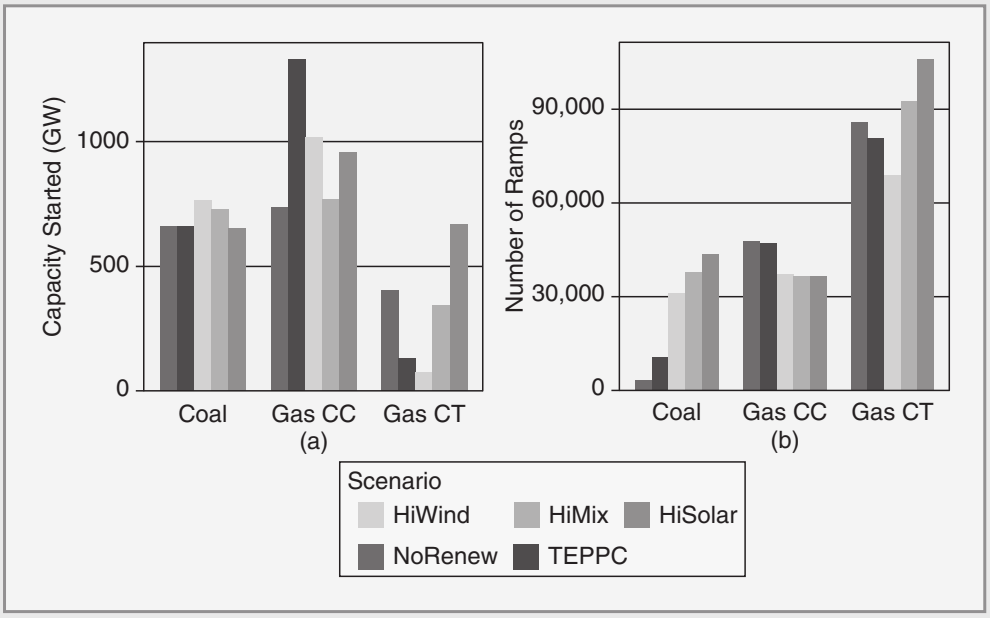

Figure 3 (a) Capacity started and (b) total number of ramps for each plant type by scenario for one year

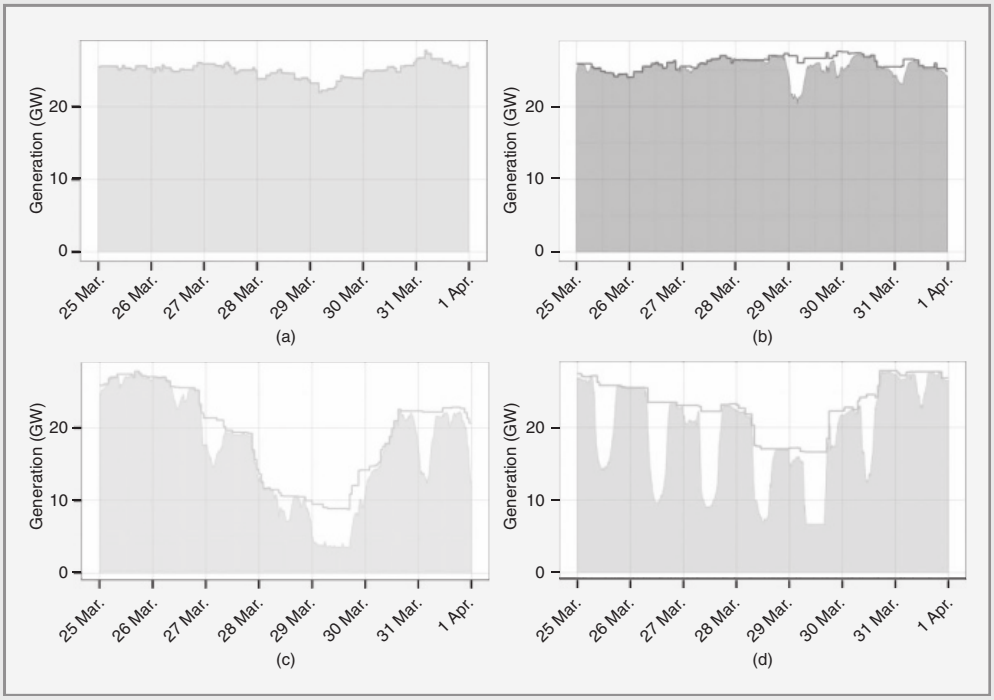

Figure 4 Capacity committed (solid line) and dispatched (shaded area) for coal units during a sample week in March. The white area between the solid line and the shaded area illustrates how far the capacity is backed down (a) no renewables, (b) TEPPC, (c) high wind, and (d) high solar.

to the displacement of fossil-fueled generation. Compared with the scenario without any renewables, the high-penetration scenarios (nominally 33% wind and solar in the U.S. portion of the Western Interconnection, resulting in 26% wind and solar across the interconnection) reduce CO_2 by 29–34%, NO_x by 16–22%, and SO_2 by 14–24%, including the cycling impacts. CO_2 emissions are reduced by a greater percentage than the wind and solar penetration level because wind and solar preferentially displace fossil-fueled generation, while typically the generation in the western United States is a combination of hydro, nuclear, fossil-fueled, and other renewable generation.

Figure 5(a) shows the total CO_2 emissions for each scenario. Ramping had no significant impact on CO_2 emissions, so those estimates are not shown. The start-up CO_2 emissions (shown by the thin, dark line at the top of each bar) were negligible in all cases. Figure 5(b) shows the CO_2 emissions saved by each MWh of wind/solar. Avoided CO_2—considering part-load, ramping, and start impacts—was 1100–1190 lb/MWh of wind and solar produced in the high-penetration scenarios (see Table 7). CO_2 emissions from starts were negligible here as well. We also calculated the part-load penalty— which was the incremental CO_2 emissions from part loading—as negligible. These values reflect aggregate emissions across the Western Interconnection; any specific plant might have lower or higher emissions than those shown here.

From the fossil-fueled plant perspective, average CO_2 emission rates of coal, CCs, and CTs change only slightly with wind and solar, as shown in Figure 6(a). Figure 6(b)

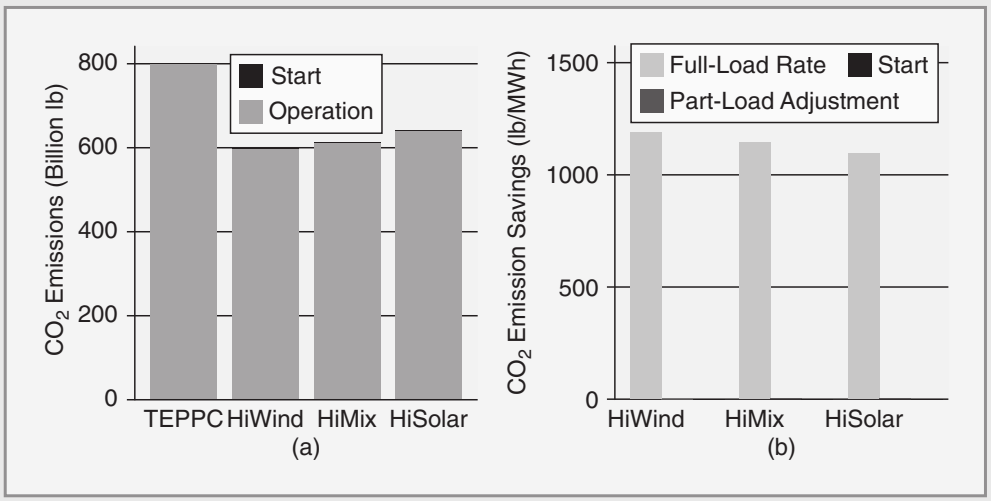

Figure 5 CO_2 emissions by scenario: (a) absolute CO_2 emissions for operation and starts and (b) CO_2 emissions reductions compared with the scenario without renewables, separated into the constant emissions rate assumption and adjustments for part load and starts. Ramping emissions are excluded because they have no significant impact on CO_2 emissions.

Scenario	Avoided CO_2 (lb/MWh)	Avoided NO_x (lb/MWh)	Avoided SO_2 (lb/MWh)
High wind	1190	0.92	0.56
High mix	1150	0.80	0.44
High solar	1100	0.72	0.35

TABLE 7

Emissions avoided per MWh of wind and solar, considering part-load, ramping, and start impacts. Part-load impacts were not included for SO_2 because of inadequate data

shows that adding wind and solar can positively or negatively affect emissions rates, depending on the plant type and scenario. For coal and CC units, wind and solar generally improves emissions rates by up to 1%. The largest negative impact of wind- and solar-induced cycling is found in the high-wind scenario and for the CT units, where the emissions rate increases by 2%. This is on average; individual units might be more or less affected.

Figure 7 shows the analysis for NO_x emissions. There was a negligible impact of starts on NO_x. Ramping

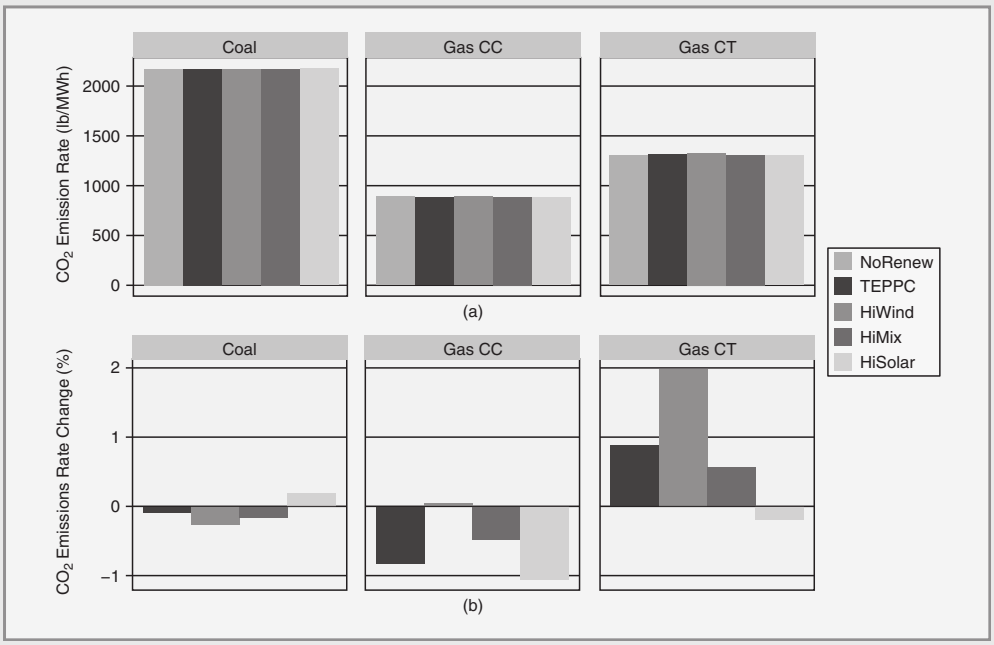

Figure 6 (a) Average CO_2 emission rates by plant type (defined as CO_2 emissions divided by MWh of coal, CC, or CT generation) for each scenario and (b) changes in emissions rates as compared with the scenario without renewables

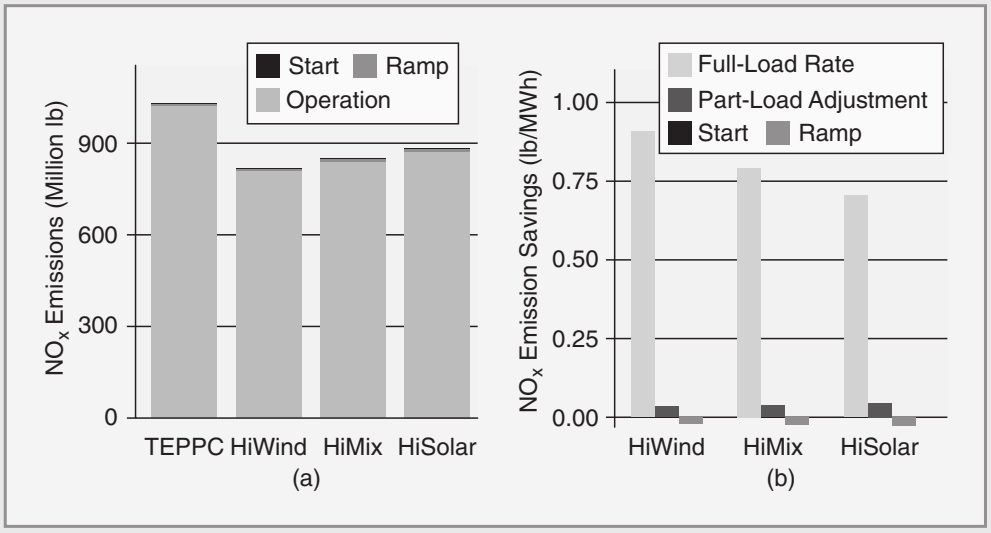

Figure 7 NO_X emissions by scenario: (a) absolute NO_X emissions for operation, ramps, and starts, and (b) NO_X emissions reductions compared with the scenario without renewables, separated into the constant emissions rate assumption and adjustments for part-load, ramps, and start impacts

reduced the avoided NO_x by 2–4%. This is shown in Figure 7(b) as a small negative contribution. Part-loading impacts, on the other hand, increased avoided NO_x by 4–6%. On average, coal units in the western United States emit less NO_x per MWh of generation at part load. The net impact of considering cycling improved avoided NO_x emissions from wind and solar by 1–2%.

Figure 8 shows the emissions analysis for SO_2. Because there were inadequate data to create SO_2 emission part-load curves, part-load impacts were not studied for SO_2. Ramping impacts on avoided SO_2 were modest for the high-penetration scenarios, reducing avoided SO_2 by 2–5%. Start-up emissions affected the avoided emissions rates by significantly less than 1%.

Wind- and Solar-Induced Cycling Operational Costs

The production simulation analysis undertaken in this study quantifies (1) the operational impacts of wind and solar displacing other generation and (2) the cycling costs induced by wind and solar. Operational costs (the industry term is production cost) include fuel, noncyclic VOM, and cycling costs. Cycling costs includes costs for starts, ramps and start-up fuel.

Under the scenarios studied, we find that the high wind and solar penetrations affect the grid by displacing US$7 billion/year in fuel costs and inducing an increase of US$35–157 million/year in cycling costs of fossil-fueled plants. The overall production cost for each scenario is shown in Figure 9, with the lower- and upper-bound uncertainty ranges shown.

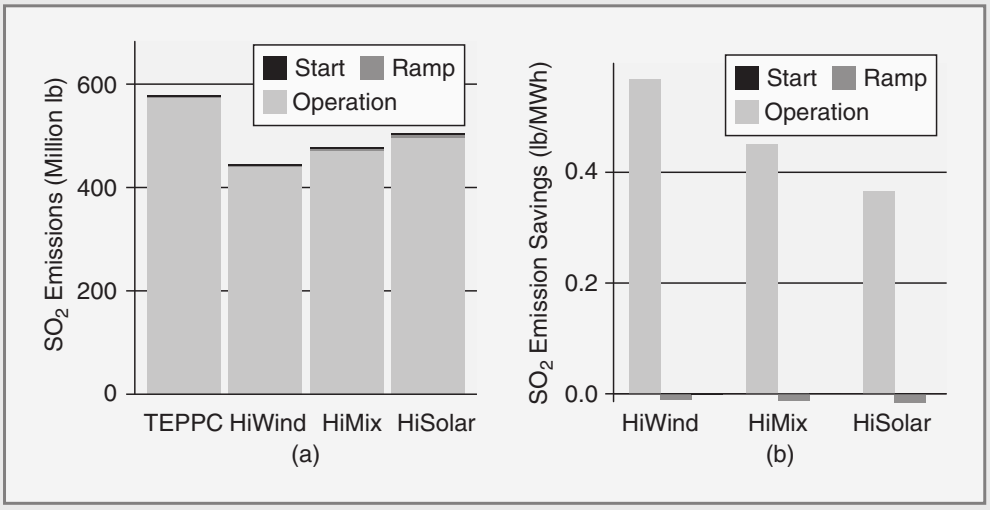

Figure 8 SO_2 emissions by scenario: (a) absolute SO_2 emissions for operation, ramping, and starts and (b) SO_2 emission reductions compared with the scenario without renewables, separated into the constant emissions rate assumption and adjustments for ramps, and start impacts. Part-load impacts were not studied because of inadequate data.

At an average gas price of US$4.60/million Btu, fuel dominates the production cost savings as wind and solar penetration increases. It is important to note that production cost does not include the capital costs of renewable or thermal generation or transmission.

Figure 10 details the cycling costs of each scenario. The cycling costs range from about US$270 million in the scenario without renewables, using lower-bound costs, to about US$800 million in the high-solar scenario, using upper-bound

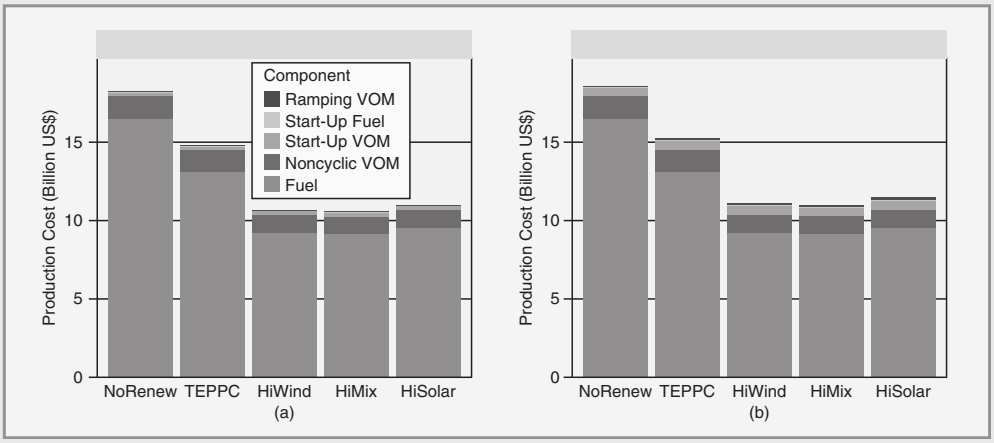

Figure 9 Production cost for each scenario showing the (a) lower-bound and (b) upper-bound cycling costs. These costs do not include capital costs of renewable or thermal generation or transmission.

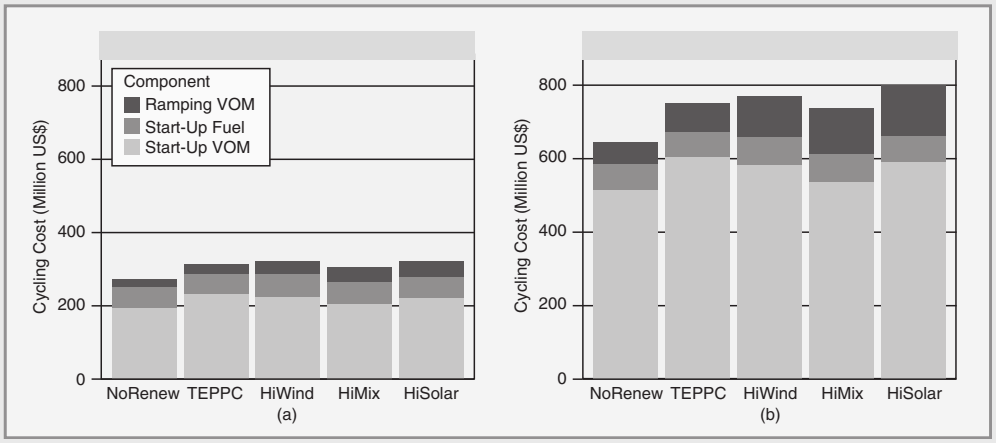

Figure 10 Production cost components resulting from cycling, showing the (a) lower-bound and (b) upper-bound wear-and-tear costs for each scenario. Cost components have been broken down into starts, start fuel, and ramping costs.

cycling costs. Interestingly, the high-mix scenario has a higher wind and solar penetration but lower cycling costs than the TEPPC scenario. In these scenarios, going from no wind and solar penetration to 13% nominal wind and solar penetration induces higher cycling costs than going from 13% to 33% penetration. On a per-MWh-of-fossil-fueled-generation basis, the increased cycling costs (compared with the scenario without any renewables) are US$0.18–0.44/MWh, US$0.52–1.24/MWh, US$0.47–1.14/MWh, and US$0.50–1.28/MWh for the TEPPC, high-wind, high-mix, and high-solar scenarios, respectively. The ranges represent the uncertainty range in the cycling cost inputs.

Figure 11 shows the lower-bound costs from the perspective of a coal, gas CC, or gas CT unit, in terms of cycling costs per MWh of that unit's generation. Must-run gas CT units were excluded from this plot, as they skew the results. Cycling costs for coal increase modestly with high penetrations of wind and solar. Cycling costs for gas CC units increase significantly with increased wind and solar penetration. But the largest cycling costs (per MWh) are borne by the gas CT units, which are operated as peakers and cycle the most. Interestingly, gas CT units see lower cycling costs in the TEPPC scenario than in the scenario without any renewables at all. And in the high-wind scenario, their cycling costs are similar to the scenario without renewables.

These cycling costs are comparable to the noncyclic VOM of approximately US$2/MWh. The impact of wind and solar on the economic viability of a fossil-fueled plant can be significant if that plant's energy production is displaced by wind and solar, its revenue is reduced, and it now bears an increased cycling cost. That fossil-fueled plant may still be needed to help balance the system or provide power on peak demand

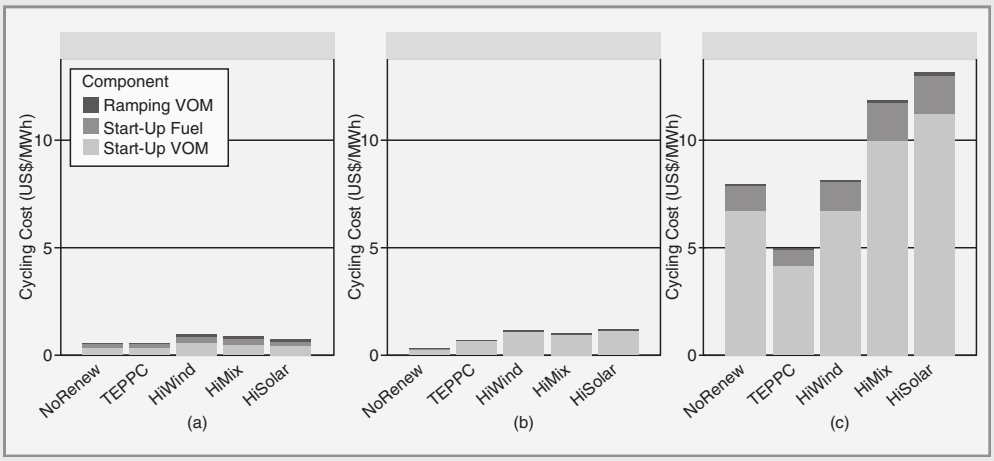

Figure 11 Lower-bound cycling cost for (a) coal, (b) gas CC units, and (c) gas CTs (excluding the must-run CTs). The total, system wide, lower-bound cycling costs were disaggregated by plant type and divided by MWh of generation for that plant type.

days. This raises a host of market and policy issues that require future analysis.

We performed a sensitivity analysis on the gas price to see if halving the price (to US$2.30/million Btu) or doubling it (to US$9.60/million Btu) significantly changed results. The US$9.60 gas price had little effect on operations. The US$2.30 gas price led to more gas usage and less coal usage, regardless of renewables on the system. The type of generation displaced by renewables was very similar for the three gas price estimates. Interestingly, the impact of wind and solar in the very low and very high gas price scenarios is to reduce overall cycling cost, because they displace starts for various unit types. The increase in cycling costs per MWh generated at fossil-fueled plants was similar in all the gas price scenarios. Units with increased cycling, however, will have a higher US$/MWh cost of generation and will probably see an increase in forced outage rates if adjustments to maintenance spending are not made.

An examination of the cycling impacts from a system perspective in Figure 12 shows the change in production cost (operational cost, not including capital or power purchase agreement costs) for each scenario as compared with the scenario without renewables. The primary operational impact of wind and solar is to displace a large amount of fuel cost (shown by the negative orange bars) and a small amount of noncyclic VOM (small negative blue bars). At this gas price (US$4.60/million Btu), the secondary impact of wind and solar is to incur the startup VOM, start-up fuel, and ramping VOM shown by the small positive bars. While it is important to remember that these operational costs do not include the capital costs of any generator or transmission, one can see

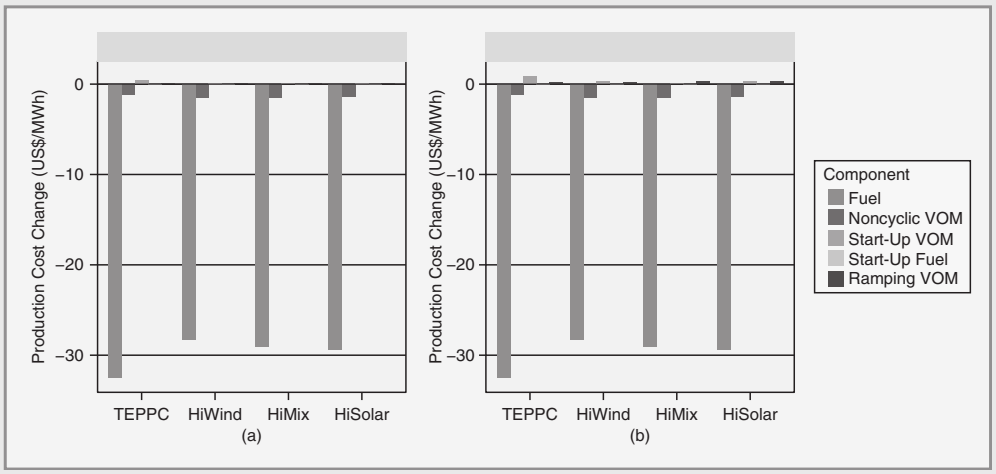

Figure 12 The change in production cost for each scenario relative to the scenario without renewables, per MWh of wind and solar generation, for the (a) lower-bound and (b) upper-bound wear-and-tear costs. Production costs do not include any fixed capital or power purchase agreement costs.

that the cycling costs are a small fraction of the costs of the fuel displaced. This cycling impact offsets the production cost reduction of wind and solar by US$0.14–0.67 per MWh of wind and solar generated. The net reduction in production cost compared with the scenario without renewables, including these cycling impacts, is approximately US$30 per MWh of wind and solar generated.

Wind Dominates Uncertainty, and Solar Dominates Variability

This study took advantage of recent advances in simulating large PV plants that allowed a comparison of the impacts of wind and solar on the grid. We conducted statistical analysis of variability and uncertainty (forecast error) to look at these impacts. We looked at extreme ramping events on an hourly and 5-minute basis and found that extreme ramping events were dominated by sunrise and sunset events. However, because we know when sunrise and sunset occur and, in fact, the path of the sun through the sky each day, we can plan for these events. When the solar diurnal variability is removed, PV variability due to weather is found to be similar to wind variability.

Statistical analysis of forecast errors showed that our day-ahead forecast errors were driven by wind uncertainty. Day-ahead solar forecasts were more accurate than day-ahead wind forecasts. Because forecast accuracy improves as one approaches the time in question, the four-hour-ahead forecasts were much more accurate, as shown in Figure 13. We used a four-hour-ahead unit commitment to commit gas units, similar to operations of the California Independent System Operator. This helped mitigate the uncertainty of the wind day-ahead forecasts.

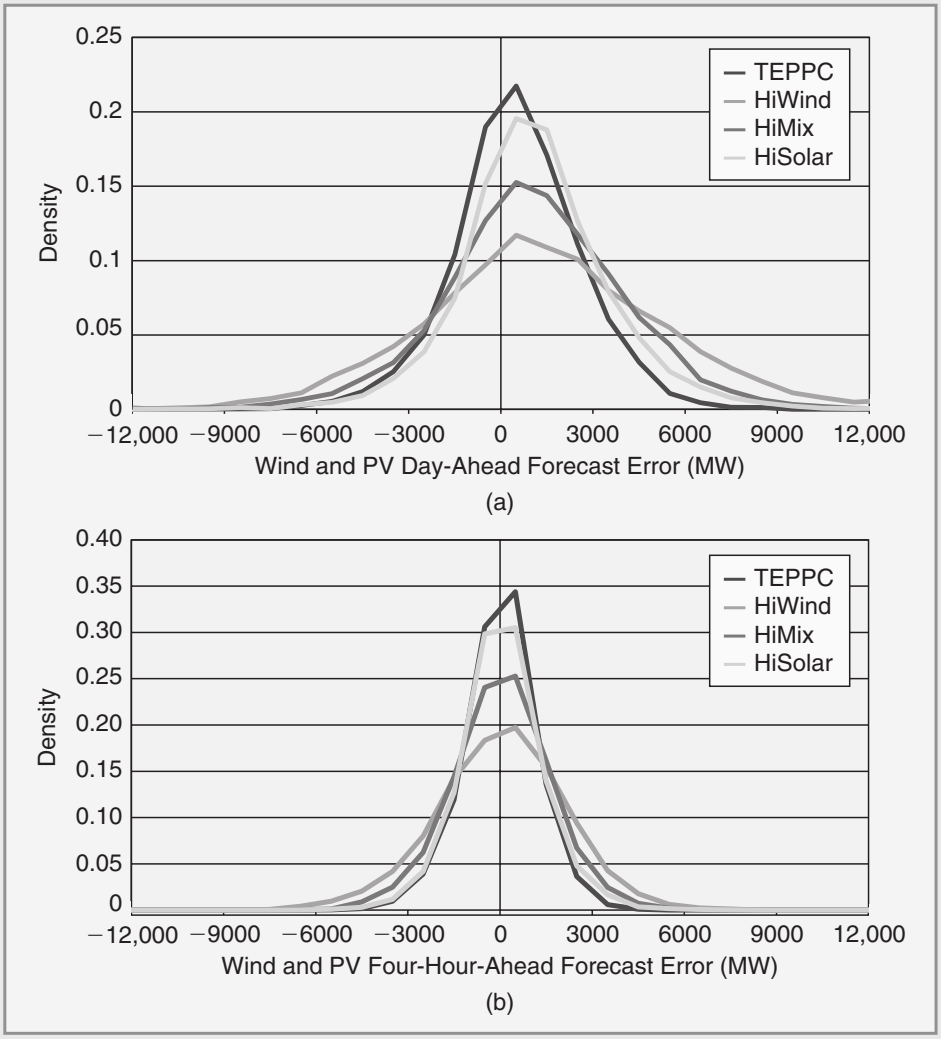

Figure 13 (a) Day-ahead and (b) four-hour-ahead wind and PV forecast errors for each scenario

Conclusions

For the first time, we have conducted an operational simulation of wind and solar impacts across the entire Western Interconnection using detailed data on cycling costs and cycling emissions. Our three high-penetration scenarios model a nominal 33% wind and solar penetration across the U.S. portion of the Western Interconnection, resulting in 26% nominal penetration across the entire Western Interconnection. We examine the primary operational impact of wind and solar in displacing fuel (and the costs and emissions associated with the fuel), along with the secondary impact of increased cycling (and the costs and emissions associated with cycling).

We found that wind- and solar-induced cycling has a small impact on avoided emissions of CO_2, NO_x, and SO_2. In our high-penetration scenarios, cycling reduces avoided CO_2 emissions by 0.2%, improves avoided NO_x by 1–2%, and lessens avoided SO_2 by up to 5%. The net result is that wind and solar in our high-penetration scenarios reduce CO_2 by 29–34%, NO_x by 16–22%, and SO_2 by 14–24%, inclusive of cycling impacts.

We also found that the secondary impact of increased cycling incurs costs that are a small fraction of the displaced fuel costs. In our high-penetration scenarios, wind and solar induce additional annual cycling costs of US$35–157 million. This same wind and solar also displaces about US$7 billion annually in fuel costs. In the high-penetration scenarios, the increase in cycling cost for the average fossil-fueled plant ranges from US$0.47–1.14 per MWh of fossil-fueled generation in the high-mix scenario to US$0.50–1.28 per MWh in the high-solar scenario. These additional costs, combined with reduced generation and revenue, beg the question of market and policy changes that may be required in a potential future with high levels of wind and solar energy.

For Further Reading

GE Energy. (2010). "Western wind and solar integration study." NREL. Golden, CO. NREL/SR-550-47434 [Online]. Available: http://www.nrel.gov/docs/fy10osti/47434.pdf.

N. Kumar, P. Besuner, S. Lefton, D. Agan, and D. Hilleman. (2012). "Power plant cycling costs." Intertek AIM. NREL. Sunnyvale, CA, Golden, CO. NREL/SR-5500-55433 [Online]. Available: http://www.nrel.gov/docs/fy12osti/55433.pdf.

D. Lew, G. Brinkman, E. Ibanez, A. Florita, M. Heaney, B.-M. Hodge, M. Hummon, G. Stark, J. King, S. Lefton, N. Kumar, D. Agan, G. Jordan, and S. Venkataraman. (2013). "The western wind and solar integration study phase 2." NREL. Golden, CO. NREL/TP-5500-55588. [Online]. Available: http://www.nrel.gov/docs/fy13osti/55588.pdf.

M. Milligan, K. Clark, J. King, B. Kirby, T. Guo, and G. Liu. (2013). "Examination of potential benefits of an energy imbalance market in the western interconnection." NREL. Golden, CO. NREL/TP-5500-57115. [Online]. Available: http://www.nrel.gov/docs/fy13osti/57115.pdf.

Biographies

Debra Lew is with the National Renewable Energy Laboratory, Golden, Colorado.

Greg Brinkman is with the National Renewable Energy Laboratory, Golden, Colorado.

Nikhil Kumar is with Intertek, Sunnyvale, California.

Steve Lefton is with Intertek and Global Utility Consultants LLC, Sunnyvale, California.

Gary Jordan is with GE Energy Consulting, Schenectady, New York.

Sundar Venkataraman is with GE Energy Consulting, Phoenix, Arizona. ■

6.1 DIRECT SOLUTIONS TO LINEAR ALGEBRAIC EQUATIONS: GAUSS ELIMINATION

Consider the following set of linear algebraic equations in matrix format:

$$\begin{bmatrix} \mathrm{A}_{11} & \mathrm{A}_{12} & \cdots & \mathrm{A}_{1N} \\ \mathrm{A}_{21} & \mathrm{A}_{22} & \cdots & \mathrm{A}_{2N} \\ \vdots & & \vdots & \\ \mathrm{A}_{N1} & \mathrm{A}_{N2} & \cdots & \mathrm{A}_{NN} \end{bmatrix} \begin{bmatrix} x_1 \\ x_2 \\ \vdots \\ x_N \end{bmatrix} = \begin{bmatrix} y_1 \\ y_2 \\ \vdots \\ y_N \end{bmatrix} \tag{6.1.1}$$

or

$$\mathbf{Ax} = \mathbf{y} \tag{6.1.2}$$

where **x** and **y** are N vectors and **A** is an $N \times N$ square matrix. The components of **x**, **y**, and **A** may be real or complex. Given **A** and **y**, the objective is to solve for **x**. Assume the det(**A**) is nonzero, so a unique solution to (6.1.1) exists.

The solution **x** can be obtained easily when **A** is an upper triangular matrix with nonzero diagonal elements. Then (6.1.1) has the form

$$\begin{bmatrix} \mathrm{A}_{11} & \mathrm{A}_{12} \ldots & & \mathrm{A}_{1N} \\ 0 & \mathrm{A}_{22} \ldots & & \mathrm{A}_{2N} \\ \vdots & & & \\ 0 & 0 \ldots & \mathrm{A}_{N-1,\,N-1} & \mathrm{A}_{N-1,N} \\ 0 & 0 \ldots 0 & & \mathrm{A}_{NN} \end{bmatrix} \begin{bmatrix} x_1 \\ x_2 \\ \vdots \\ x_{N-1} \\ x_N \end{bmatrix} = \begin{bmatrix} y_1 \\ y_2 \\ \vdots \\ y_{N-1} \\ y_N \end{bmatrix} \tag{6.1.3}$$

Since the last equation in (6.1.3) involves only x_N,

$$x_N = \frac{y_N}{\mathrm{A}_{NN}} \tag{6.1.4}$$

After x_N is computed, the next-to-last equation can be solved:

$$x_{N-1} = \frac{y_{N-1} - \mathrm{A}_{N-1,\,N} x_N}{\mathrm{A}_{N-1,\,N-1}} \tag{6.1.5}$$

In general, with $x_N, x_{N-1}, \ldots, x_{k+1}$ already computed, the kth equation can be solved as

$$x_k = \frac{y_k - \sum_{n=k+1}^{N} \mathrm{A}_{kn} x_n}{\mathrm{A}_{kk}} \qquad k = N, N-1, \ldots, 1 \tag{6.1.6}$$

This procedure for solving (6.1.3) is called *back substitution.*

If **A** is not an upper triangular, (6.1.1), it can be transformed to an equivalent equation with an upper triangular matrix. The transformation, called *Gauss*

elimination, is described by the following $(N-1)$ steps. During Step 1, use the first equation in (6.1.1) to eliminate x_1 from the remaining equations. That is, Equation 1 is multiplied by A_{n1}/A_{11} and then subtracted from equation n, for $n = 2, 3, \ldots, N$. After completing Step 1, we have

$$\begin{bmatrix} A_{11} & A_{12} & \cdots & A_{1N} \\ 0 & \left(A_{22} - \frac{A_{21}}{A_{11}}A_{12}\right) & \cdots & \left(A_{2N} - \frac{A_{21}}{A_{11}}A_{1N}\right) \\ 0 & \left(A_{32} - \frac{A_{31}}{A_{11}}A_{12}\right) & \cdots & \left(A_{3N} - \frac{A_{31}}{A_{11}}A_{1N}\right) \\ \vdots & \vdots & & \vdots \\ 0 & \left(A_{N2} - \frac{A_{N1}}{A_{11}}A_{12}\right) & \cdots & \left(A_{NN} - \frac{A_{N1}}{A_{11}}A_{1N}\right) \end{bmatrix} \begin{bmatrix} x_1 \\ x_2 \\ x_3 \\ \vdots \\ x_N \end{bmatrix}$$

$$= \begin{bmatrix} y_1 \\ y_2 - \frac{A_{21}}{A_{11}}y_1 \\ y_3 - \frac{A_{31}}{A_{11}}y_1 \\ \vdots \\ y_N - \frac{A_{N1}}{A_{11}}y_1 \end{bmatrix} \tag{6.1.7}$$

Equation (6.1.7) has the following form:

$$\begin{bmatrix} A_{11}^{(1)} & A_{12}^{(1)} & \cdots & A_{1N}^{(1)} \\ 0 & A_{22}^{(1)} & \cdots & A_{2N}^{(1)} \\ 0 & A_{32}^{(1)} & \cdots & A_{3N}^{(1)} \\ \vdots & \vdots & & \vdots \\ 0 & A_{N2}^{(1)} & \cdots & A_{NN}^{(1)} \end{bmatrix} \begin{bmatrix} x_1 \\ x_2 \\ x_3 \\ \vdots \\ x_N \end{bmatrix} = \begin{bmatrix} y_1^{(1)} \\ y_2^{(1)} \\ y_3^{(1)} \\ \vdots \\ y_N^{(1)} \end{bmatrix} \tag{6.1.8}$$

where the superscript (1) denotes Step 1 of the Gauss elimination.

During Step 2, use the second equation in (6.1.8) to eliminate x_2 from the remaining (third, fourth, fifth, and so on) equations. That is, Equation 2 is multiplied by $A_{n2}^{(1)}/A_{22}^{(1)}$ and subtracted from equation n, for $n = 3, 4, \ldots, N$.
After Step 2, there is

$$\begin{bmatrix} A_{11}^{(2)} & A_{12}^{(2)} & A_{13}^{(2)} & \cdots & A_{1N}^{(2)} \\ 0 & A_{22}^{(2)} & A_{23}^{(2)} & \cdots & A_{2N}^{(2)} \\ 0 & 0 & A_{33}^{(2)} & \cdots & A_{3N}^{(2)} \\ 0 & 0 & A_{43}^{(2)} & \cdots & A_{4N}^{(2)} \\ \vdots & \vdots & \vdots & & \vdots \\ 0 & 0 & A_{N3}^{(2)} & \cdots & A_{NN}^{(2)} \end{bmatrix} \begin{bmatrix} x_1 \\ x_2 \\ x_3 \\ x_4 \\ \vdots \\ x_N \end{bmatrix} = \begin{bmatrix} y_1^{(2)} \\ y_2^{(2)} \\ y_3^{(2)} \\ y_4^{(2)} \\ \vdots \\ y_N^{(2)} \end{bmatrix} \tag{6.1.9}$$

During step k, start with $\mathbf{A}^{(k-1)}\mathbf{x} = \mathbf{y}^{(k-1)}$. The first k of these equations, already triangularized, are left unchanged. Also, equation k is multiplied by $A_{nk}^{(k-1)}/A_{kk}^{(k-1)}$ and then subtracted from equation n, for $n = k+1, k+2, \ldots, N$.

After $(N-1)$ steps, the equivalent equation is $\mathbf{A}^{(N-1)}\mathbf{x} = \mathbf{y}^{(N-1)}$, where $\mathbf{A}^{(N-1)}$ is upper triangular.

EXAMPLE 6.1

Gauss elimination and back substitution: direct solution to linear algebraic equations

Solve

$$\left[\begin{array}{c|c} 10 & 5 \\ \hline 2 & 9 \end{array}\right]\begin{bmatrix} x_1 \\ x_2 \end{bmatrix} = \begin{bmatrix} 6 \\ 3 \end{bmatrix}$$

using Gauss elimination and back substitution.

SOLUTION

Since $N = 2$ for this example, there is $(N-1) = 1$ Gauss elimination step. Multiplying the first equation by $A_{21}/A_{11} = 2/10$ and then subtracting from the second,

$$\left[\begin{array}{c|c} 10 & 5 \\ \hline 0 & 9 - \frac{2}{10}(5) \end{array}\right]\begin{bmatrix} x_1 \\ x_2 \end{bmatrix} = \begin{bmatrix} 6 \\ 3 - \frac{2}{10}(6) \end{bmatrix}$$

or

$$\left[\begin{array}{c|c} 10 & 5 \\ \hline 0 & 8 \end{array}\right]\begin{bmatrix} x_1 \\ x_2 \end{bmatrix} = \begin{bmatrix} 6 \\ 1.8 \end{bmatrix}$$

which has the form $\mathbf{A}^{(1)}\mathbf{x} = \mathbf{y}^{(1)}$ where $\mathbf{A}^{(1)}$ is upper triangular. Now, using back substitution, (6.1.6) gives, for $k = 2$:

$$x_2 = \frac{y_2^{(1)}}{A_{22}^{(1)}} = \frac{1.8}{8} = 0.225$$

and, for $k = 1$,

$$x_1 = \frac{y_1^{(1)} - A_{12}^{(1)}x_2}{A_{11}^{(1)}} = \frac{6 - (5)(0.225)}{10} = 0.4875$$

EXAMPLE 6.2

Gauss elimination: triangularizing a matrix

Use Gauss elimination to triangularize

$$\begin{bmatrix} 2 & 3 & -1 \\ -4 & 6 & 8 \\ 10 & 12 & 14 \end{bmatrix} \begin{bmatrix} x_1 \\ x_2 \\ x_3 \end{bmatrix} = \begin{bmatrix} 5 \\ 7 \\ 9 \end{bmatrix}$$

SOLUTION

There are $(N-1) = 2$ Gauss elimination steps. During Step 1, subtract $A_{21}/A_{11} = -4/2 = -2$ times Equation 1 from Equation 2, and subtract $A_{31}/A_{11} = 10/2 = 5$ times Equation 1 from Equation 3, to give

$$\left[\begin{array}{c|c|c} 2 & 3 & -1 \\ \hline 0 & 6-(-2)(3) & 8-(-2)(-1) \\ \hline 0 & 12-(5)(3) & 14-(5)(-1) \end{array}\right] \begin{bmatrix} x_1 \\ x_2 \\ x_3 \end{bmatrix} = \begin{bmatrix} 5 \\ 7-(-2)(5) \\ 9-(5)(5) \end{bmatrix}$$

or

$$\begin{bmatrix} 2 & 3 & -1 \\ 0 & 12 & 6 \\ 0 & -3 & 19 \end{bmatrix} \begin{bmatrix} x_1 \\ x_2 \\ x_3 \end{bmatrix} = \begin{bmatrix} 5 \\ 17 \\ -16 \end{bmatrix}$$

which is $\mathbf{A}^{(1)}\mathbf{x} = \mathbf{y}^{(1)}$. During Step 2, subtract $A_{32}^{(1)}/A_{22}^{(1)} = -3/12 = -0.25$ times Equation 2 from Equation 3, to give

$$\left[\begin{array}{c|c|c} 2 & 3 & -1 \\ \hline 0 & 12 & 6 \\ \hline 0 & 0 & 19-(-.25)(6) \end{array}\right] \begin{bmatrix} x_1 \\ x_2 \\ x_3 \end{bmatrix} = \begin{bmatrix} 5 \\ 17 \\ -16-(-.25)(17) \end{bmatrix}$$

or

$$\begin{bmatrix} 2 & 3 & -1 \\ 0 & 12 & 6 \\ 0 & 0 & 20.5 \end{bmatrix} \begin{bmatrix} x_1 \\ x_2 \\ x_3 \end{bmatrix} = \begin{bmatrix} 5 \\ 17 \\ -11.75 \end{bmatrix}$$

which is triangularized. The solution $\mathbf{x}$ now can be easily obtained via back substitution.

Computer storage requirements for Gauss elimination and back substitution include N^2 memory locations for **A** and N locations for **y**. If there is no further need to retain **A** and **y**, then $\mathbf{A}^{(k)}$ can be stored in the location of **A**, and $\mathbf{y}^{(k)}$, as well as the solution **x**, can be stored in the location of **y**. Additional memory is also required for iterative loops, arithmetic statements, and working space.

Computer time requirements can be evaluated by determining the number of arithmetic operations required for Gauss elimination and back substitution. One can show that Gauss elimination requires $(N^3 - N)/3$ multiplications, $(N)(N - 1)/2$ divisions, and $(N^3 - N)/3$ subtractions. Also, back substitution requires $(N)(N - 1)/2$ multiplications, N divisions, and $(N)(N - 1)/2$ subtractions. Therefore, for very large N, the approximate computer time for solving (6.1.1) by Gauss elimination and back substitution is the time required to perform $N^3/3$ multiplications and $N^3/3$ subtractions.

For example, consider a digital computer with a 2×10^{-9} s multiplication time and 1×10^{-9} s addition or subtraction time. Solving $N = 10{,}000$ equations would require

$$\frac{1}{3}N^3(2 \times 10^{-9}) + \frac{1}{3}N^3(1 \times 10^{-9}) = \frac{1}{3}(10{,}000)^3(3 \times 10^{-9}) = 1000 \quad \text{s}$$

approximately plus some additional bookkeeping time for indexing and managing loops.

Since the power flow problem often involves solving power systems with tens of thousands of equations, by itself Gauss elimination would not be a good solution. However, for matrixes that have relatively few nonzero elements, known as sparse matrices, special techniques can be employed to significantly reduce computer storage and time requirements. Since all large power systems can be modeled using sparse matrices, these techniques are briefly introduced in Section 6.8.

6.2 ITERATIVE SOLUTIONS TO LINEAR ALGEBRAIC EQUATIONS: JACOBI AND GAUSS-SEIDEL

A general iterative solution to (6.1.1) proceeds as follows. First select an initial guess $\mathbf{x}(0)$. Then use

$$\mathbf{x}(i+1) = \mathbf{g}[\mathbf{x}(i)] \qquad i = 0, 1, 2, \ldots \tag{6.2.1}$$

where $\mathbf{x}(i)$ is the ith guess and **g** is an N vector of functions that specify the iteration method. Continue this procedure until the following stopping condition is satisfied, as

$$\left| \frac{x_k(i+1) - x_k(i)}{x_k(i)} \right| < \varepsilon \qquad \text{for all } k = 1, 2, \ldots, N \tag{6.2.2}$$

where $x_k(i)$ is the kth component of $\mathbf{x}(i)$ and ε is a specified *tolerance level.*

The following questions are pertinent:

1. Will the iteration procedure converge to the unique solution?
2. What is the convergence rate (how many iterations are required)?
3. When using a digital computer, what are the computer storage and time requirements?

These questions are addressed for two specific iteration methods: *Jacobi* and *Gauss-Seidel.** The Jacobi method is obtained by considering the kth equation of (6.1.1), as follows:

$$y_k = \mathrm{A}_{k1}x_1 + \mathrm{A}_{k2}x_2 + \cdots + \mathrm{A}_{kk}x_k + \cdots + \mathrm{A}_{kN}x_N \tag{6.2.3}$$

Solving for x_k,

$$\begin{aligned} x_k &= \frac{1}{\mathrm{A}_{kk}}[y_k - (\mathrm{A}_{k1}x_1 + \cdots + \mathrm{A}_{k,k-1}x_{k-1} + \mathrm{A}_{k,k+1}x_{k+1} + \cdots + \mathrm{A}_{kN}x_N)] \\ &= \frac{1}{\mathrm{A}_{kk}}\left[y_k - \sum_{n=1}^{k-1}\mathrm{A}_{kn}x_n - \sum_{n=k+1}^{N}\mathrm{A}_{kn}x_n\right] \end{aligned} \tag{6.2.4}$$

The Jacobi method uses the "old" values of $\mathbf{x}(i)$ at iteration i on the right side of (6.2.4) to generate the "new" value $x_k(i+1)$ on the left side of (6.2.4). That is,

$$x_k(i+1) = \frac{1}{\mathrm{A}_{kk}}\left[y_k - \sum_{n=1}^{k-1}\mathrm{A}_{kn}x_n(i) - \sum_{n=k+1}^{N}\mathrm{A}_{kn}x_n(i)\right] k = 1, 2, \ldots, N \tag{6.2.5}$$

The Jacobi method given by (6.2.5) also can be written in the following matrix format:

$$\mathbf{x}(i+1) = \mathbf{M}\mathbf{x}(i) + \mathbf{D}^{-1}\mathbf{y} \tag{6.2.6}$$

where

$$\mathbf{M} = \mathbf{D}^{-1}(\mathbf{D} - \mathbf{A}) \tag{6.2.7}$$

and

$$\mathbf{D} = \begin{bmatrix} \mathrm{A}_{11} & 0 & 0 & \cdots & 0 \\ 0 & \mathrm{A}_{22} & 0 & \cdots & 0 \\ 0 & \vdots & \vdots & & \vdots \\ \vdots & & & & 0 \\ 0 & 0 & 0 & \cdots & \mathrm{A}_{NN} \end{bmatrix} \tag{6.2.8}$$

For Jacobi, **D** consists of the diagonal elements of the **A** matrix.

The Gauss-Seidel method is given by

$$x_k(i+1) = \frac{1}{A_{kk}}\left[y_k - \sum_{n=1}^{k-1}\mathrm{A}_{kn}x_n(i+1) - \sum_{n=k+1}^{N}\mathrm{A}_{kn}x_n(i)\right] \tag{6.2.9}$$

*The Jacobi method is also called the Gauss method.

EXAMPLE 6.3

Jacobi method: iterative solution to linear algebraic equations

Solve Example 6.1 using the Jacobi method. Start with $x_1(0) = x_2(0) = 0$ and continue until (6.2.2) is satisfied for $\varepsilon = 10^{-4}$.

SOLUTION

From (6.2.5) with $N = 2$,

$$k = 1 \quad x_1(i+1) = \frac{1}{A_{11}}[y_1 - A_{12}x_2(i)] = \frac{1}{10}[6 - 5x_2(i)]$$

$$k = 2 \quad x_2(i+1) = \frac{1}{A_{22}}[y_2 - A_{21}x_1(i)] = \frac{1}{9}[3 - 2x_1(i)]$$

Alternatively, in matrix format using (6.2.6) through (6.2.8),

$$\mathbf{D}^{-1} = \left[\begin{array}{c|c} 10 & 0 \\ \hline 0 & 9 \end{array}\right]^{-1} = \left[\begin{array}{c|c} \frac{1}{10} & 0 \\ \hline 0 & \frac{1}{9} \end{array}\right]$$

$$\mathbf{M} = \left[\begin{array}{c|c} \frac{1}{10} & 0 \\ \hline 0 & \frac{1}{9} \end{array}\right]\left[\begin{array}{c|c} 0 & -5 \\ \hline -2 & 0 \end{array}\right] = \left[\begin{array}{c|c} 0 & -\frac{5}{10} \\ \hline -\frac{2}{9} & 0 \end{array}\right]$$

$$\left[\begin{array}{c} x_1(i+1) \\ \\ x_2(i+1) \end{array}\right] = \left[\begin{array}{c|c} 0 & -\frac{5}{10} \\ \hline -\frac{2}{9} & 0 \end{array}\right]\left[\begin{array}{c} x_1(i) \\ \\ x_2(i) \end{array}\right] + \left[\begin{array}{c|c} \frac{1}{10} & 0 \\ \hline 0 & \frac{1}{9} \end{array}\right]\left[\begin{array}{c} 6 \\ \\ 3 \end{array}\right]$$

The above two formulations are identical. Starting with $x_1(0) = x_2(0) = 0$, the iterative solution is given in the following table:

Jacobi

i	0	1	2	3	4	5	6	7	8	9	10
$x_1(i)$	0	0.60000	0.43334	0.50000	0.48148	0.48889	0.48683	0.48766	0.48743	0.48752	0.48749
$x_2(i)$	0	0.33333	0.20000	0.23704	0.22222	0.22634	0.22469	0.22515	0.22496	0.22502	0.22500

As shown, the Jacobi method converges to the unique solution obtained in Example 6.1.

The convergence criterion is satisfied at the 10th iteration, since

$$\left|\frac{x_1(10) - x_1(9)}{x_1(9)}\right| = \left|\frac{0.48749 - 0.48752}{0.48749}\right| = 6.2 \times 10^{-5} < \varepsilon$$

and

$$\left|\frac{x_2(10) - x_2(9)}{x_2(9)}\right| = \left|\frac{0.22500 - 0.22502}{0.22502}\right| = 8.9 \times 10^{-5} < \varepsilon$$

Comparing (6.2.9) with (6.2.5), note that Gauss-Seidel is similar to Jacobi except that during each iteration, the "new" values, $x_n(i + 1)$, for $n < k$ are used on the right side of (6.2.9) to generate the "new" value $x_k(i + 1)$ on the left side.

The Gauss-Seidel method of (6.2.9) also can be written in the matrix format of (6.2.6) and (6.2.7), where

$$\mathbf{D} = \begin{bmatrix} A_{11} & 0 & 0 & \cdots & 0 \\ A_{21} & A_{22} & 0 & \cdots & 0 \\ \vdots & \vdots & & & \vdots \\ A_{N1} & A_{N2} & \cdots & & A_{NN} \end{bmatrix} \tag{6.2.10}$$

For Gauss-Seidel, **D** in (6.2.10) is the lower triangular portion of **A**, whereas for Jacobi, **D** in (6.2.8) is the diagonal portion of **A**.

EXAMPLE 6.4

Gauss-Seidel method: iterative solution to linear algebraic equations

Rework Example 6.3 using the Gauss-Seidel method.

SOLUTION

From (6.2.9),

$$k = 1 \quad x_1(i + 1) = \frac{1}{A_{11}}[y_1 - A_{12}x_2(i)] = \frac{1}{10}[6 - 5x_2(i)]$$

$$k = 2 \quad x_2(i + 1) = \frac{1}{A_{22}}[y_2 - A_{21}x_1(i + 1)] = \frac{1}{9}[3 - 2x_1(i + 1)]$$

(*Continued*)

Using this equation for $x_1(i+1)$, $x_2(i+1)$ also can be written as

$$x_2(i+1) = \frac{1}{9}\left\{3 - \frac{2}{10}[6 - 5x_2(i)]\right\}$$

Alternatively, in matrix format, using (6.2.10), (6.2.6), and (6.2.7),

$$\mathbf{D}^{-1} = \left[\begin{array}{c|c} 10 & 0 \\ \hline 2 & 9 \end{array}\right]^{-1} = \left[\begin{array}{c|c} \frac{1}{10} & 0 \\ \hline -\frac{2}{90} & \frac{1}{9} \end{array}\right]$$

$$\mathbf{M} = \left[\begin{array}{c|c} \frac{1}{10} & 0 \\ \hline -\frac{2}{90} & \frac{1}{9} \end{array}\right]\left[\begin{array}{c|c} 0 & -5 \\ \hline 0 & 0 \end{array}\right] = \left[\begin{array}{c|c} 0 & -\frac{1}{2} \\ \hline 0 & \frac{1}{9} \end{array}\right]$$

$$\begin{bmatrix} x_1(i+1) \\ x_2(i+1) \end{bmatrix} = \left[\begin{array}{c|c} 0 & -\frac{1}{2} \\ \hline 0 & \frac{1}{9} \end{array}\right]\begin{bmatrix} x_1(i) \\ x_2(i) \end{bmatrix} + \left[\begin{array}{c|c} \frac{1}{10} & 0 \\ \hline -\frac{2}{90} & \frac{1}{9} \end{array}\right]\begin{bmatrix} 6 \\ 3 \end{bmatrix}$$

These two formulations are identical. Starting with $x_1(0) = x_2(0) = 0$, the solution is given in the following table:

Gauss-Seidel

I	0	1	2	3	4	5	6
$x_1(i)$	0	0.60000	0.50000	0.48889	0.48765	0.48752	0.48750
$x_2(i)$	0	0.20000	0.22222	0.22469	0.22497	0.22500	0.22500

For this example, Gauss-Seidel converges in 6 iterations, compared to 10 iterations with Jacobi.

The convergence rate is faster with Gauss-Seidel for some **A** matrices, but faster with Jacobi for other **A** matrices. In some cases, one method diverges while the other converges. In other cases both methods diverge, as illustrated by the next example.

EXAMPLE 6.5

Divergence of Gauss-Seidel method

Using the Gauss-Seidel method with $x_1(0) = x_2(0) = 0$, solve

$$\left[\begin{array}{c|c} 5 & 10 \\ \hline 9 & 2 \end{array}\right]\begin{bmatrix} x_1 \\ x_2 \end{bmatrix} = \begin{bmatrix} 6 \\ 3 \end{bmatrix}$$

SOLUTION

Note that these equations are the same as those in Example 6.1, except that x_1 and x_2 are interchanged. Using (6.2.9),

$$k = 1 \qquad x_1(i+1) = \frac{1}{A_{11}}[y_1 - A_{12}x_2(i)] = \frac{1}{5}[6 - 10x_2(i)]$$

$$k = 2 \qquad x_2(i+1) = \frac{1}{A_{22}}[y_2 - A_{21}x_1(i+1)] = \frac{1}{2}[3 - 9x_1(i+1)]$$

Successive calculations of x_1 and x_2 are shown in the following table:

Gauss-Seidel

i	0	1	2	3	4	5
$x_1(i)$	0	1.2	9	79.2	711	6397
$x_2(i)$	0	−3.9	−39	−354.9	−3198	−28,786

The unique solution by matrix inversion is

$$\begin{bmatrix} x_1 \\ x_2 \end{bmatrix} = \left[\begin{array}{c|c} 5 & 10 \\ \hline 9 & 2 \end{array}\right]^{-1}\begin{bmatrix} 6 \\ 3 \end{bmatrix} = \frac{-1}{80}\left[\begin{array}{c|c} 2 & -10 \\ \hline -9 & 5 \end{array}\right]\begin{bmatrix} 6 \\ 3 \end{bmatrix} = \begin{bmatrix} 0.225 \\ 0.4875 \end{bmatrix}$$

As shown, Gauss-Seidel does not converge to the unique solution; instead it diverges. Jacobi also diverges for this example.

If any diagonal element A_{kk} equals zero, then Jacobi and Gauss-Seidel are undefined, because the right-hand sides of (6.2.5) and (6.2.9) are divided by A_{kk}. Also, if any one diagonal element has too small a magnitude, these methods will diverge. In Examples 6.3 and 6.4, Jacobi and Gauss-Seidel converge, since the diagonals (10 and 9) are both large; in Example 6.5, however, the diagonals (5 and 2) are small compared to the off-diagonals, and the methods diverge.

In general, convergence of Jacobi or Gauss-Seidel can be evaluated by recognizing that (6.2.6) represents a digital filter with input y and output $x(i)$. The z-transform of (6.2.6) may be employed to determine the filter transfer function and its poles. The output $x(i)$ converges if and only if all the filter poles have magnitudes less than 1 (see Problems 6.16 and 6.17).

Rate of convergence is also established by the filter poles. Fast convergence is obtained when the magnitudes of all the poles are small. In addition, experience with specific **A** matrices has shown that more iterations are required for Jacobi and Gauss-Seidel as the dimension N increases.

Computer storage requirements for Jacobi include N^2 memory locations for the **A** matrix and $3N$ locations for the vectors **y**, **x**(i), and **x**$(i + 1)$. Storage space is also required for loops, arithmetic statements, and working space to compute (6.2.5). Gauss-Seidel requires N fewer memory locations, since for (6.2.9) the new value $x_k(i + 1)$ can be stored in the location of the old value $x_k(i)$.

Computer time per iteration is relatively small for Jacobi and Gauss-Seidel. Inspection of (6.2.5) or (6.2.9) shows that N^2 multiplications/divisions and $N(N - 1)$ subtractions per iteration are required [one division, $(N - 1)$ multiplications, and $(N - 1)$ subtractions for each $k = 1, 2, \ldots, N$]. But as was the case with Gauss elimination, if the matrix is sparse (i.e., most of the elements are zero), special sparse matrix algorithms can be used to substantially decrease both the storage requirements and the computation time.

6.3 ITERATIVE SOLUTIONS TO NONLINEAR ALGEBRAIC EQUATIONS: NEWTON-RAPHSON

A set of nonlinear algebraic equations in matrix format is given by

$$\mathbf{f}(\mathbf{x}) = \begin{bmatrix} f_1(\mathbf{x}) \\ f_2(\mathbf{x}) \\ \vdots \\ f_N(\mathbf{x}) \end{bmatrix} = \mathbf{y} \tag{6.3.1}$$

where **y** and **x** are N vectors and **f**(**x**) is an N vector of functions. Given **y** and **f**(**x**), the objective is to solve for **x**. The iterative methods described in Section 6.2 can be extended to nonlinear equations as follows. Rewriting (6.3.1).

$$0 = \mathbf{y} - \mathbf{f}(\mathbf{x}) \tag{6.3.2}$$

Adding **Dx** to both sides of (6.3.2), where **D** is a square $N \times N$ invertible matrix.

$$\mathbf{Dx} = \mathbf{Dx} + \mathbf{y} - \mathbf{f}(\mathbf{x}) \tag{6.3.3}$$

Premultiplying by $\mathbf{D}^{-1}$.

$$\mathbf{x} = \mathbf{x} + \mathbf{D}^{-1}[\mathbf{y} - \mathbf{f}(\mathbf{x})] \tag{6.3.4}$$

The old values **x**(i) are used on the right side of (6.3.4) to generate the new values **x**$(i + 1)$ on the left side. That is,

$$\mathbf{x}(i+1) = \mathbf{x}(i) + \mathbf{D}^{-1}\{\mathbf{y} - \mathbf{f}[\mathbf{x}(i)]\} \tag{6.3.5}$$

For linear equations, $\mathbf{f}(\mathbf{x}) = \mathbf{A}\mathbf{x}$ and (6.3.5) reduces to

$$\mathbf{x}(i+1) = \mathbf{x}(i) + \mathbf{D}^{-1}[\mathbf{y} - \mathbf{A}\mathbf{x}(z)] = \mathbf{D}^{-1}(\mathbf{D} - \mathbf{A})\mathbf{x}(i) + \mathbf{D}^{-1}\mathbf{y} \tag{6.3.6}$$

which is identical to the Jacobi and Gauss-Seidel methods of (6.2.6). For nonlinear equations, the matrix $\mathbf{D}$ in (6.3.5) must be specified.

One method for specifying $\mathbf{D}$, called *Newton-Raphson*, is based on the following Taylor series expansion of $\mathbf{f}(\mathbf{x})$ about an operating point $\mathbf{x}_0$.

$$\mathbf{y} = \mathbf{f}(\mathbf{x}_0) + \left.\frac{d\mathbf{f}}{d\mathbf{x}}\right|_{\mathrm{x}=\mathrm{x}_0} (\mathbf{x} - \mathbf{x}_0) \cdots \tag{6.3.7}$$

Neglecting the higher order terms in (6.3.7) and solving for $\mathbf{x}$,

$$\mathbf{x} = \mathbf{x}_0 + \left[\left.\frac{d\mathbf{f}}{d\mathbf{x}}\right|_{\mathbf{x}\,=\,\mathbf{x}_0}\right]^{-1} [\mathbf{y} - \mathbf{f}(\mathbf{x}_0)] \tag{6.3.8}$$

The Newton-Raphson method replaces $\mathbf{x}_0$ by the old value $\mathbf{x}(i)$ and $\mathbf{x}$ by the new value $\mathbf{x}(i+1)$ in (6.3.8). Thus,

$$\mathbf{x}(i+1) = \mathbf{x}(i) + \mathbf{J}^{-1}(i)\{\mathbf{y} - \mathbf{f}[\mathbf{x}(i)]\} \tag{6.3.9}$$

where

$$\mathbf{J}(i) = \left.\frac{d\mathbf{f}}{d\mathbf{x}}\right|_{\mathbf{x}=\mathbf{x}(i)} = \begin{bmatrix} \dfrac{\partial f_1}{\partial x_1} & \dfrac{\partial f_1}{\partial x_2} & \cdots & \dfrac{\partial f_1}{\partial x_N} \\ \dfrac{\partial f_2}{\partial x_1} & \dfrac{\partial f_2}{\partial x_2} & \cdots & \dfrac{\partial f_2}{\partial x_N} \\ \vdots & \vdots & & \vdots \\ \dfrac{\partial f_N}{\partial x_1} & \dfrac{\partial f_N}{\partial x_2} & \cdots & \dfrac{\partial f_N}{\partial x_N} \end{bmatrix}_{\mathbf{x}=\mathbf{x}(i)} \tag{6.3.10}$$

The $N \times N$ matrix $\mathbf{J}(i)$, whose elements are the partial derivatives shown in (6.3.10), is called the Jacobian matrix. The Newton-Raphson method is similar to extended Gauss-Seidel, except that $\mathbf{D}$ in (6.3.5) is replaced by $\mathbf{J}(i)$ in (6.3.9).

EXAMPLE 6.6

Newton-Raphson method: solution to polynomial equations

Solve the scalar equation $f(x) = y$, where $y = 9$ and $f(x) = x^2$. Starting with $x(0) = 1$, use (a) Newton-Raphson and (b) extended Gauss-Seidel with $\mathbf{D} = 3$ until (6.2.2) is satisfied for $\varepsilon = 10^{-4}$. Compare the two methods.

(*Continued*)

SOLUTION

a. Using (6.3.10) with $f(x) = x^2$,

$$\mathbf{J}(i) = \frac{d}{dx}(x^2)\bigg|_{x=x(i)} = 2x\bigg|_{x=x(i)} = 2x(i)$$

Using $\mathbf{J}(i)$ in (6.3.9),

$$x(i+1) = x(i) + \frac{1}{2x(i)}[9 - x^2(i)]$$

Starting with $x(0) = 1$, successive calculations of the Newton-Raphson equation are shown in the following table.

Newton–Raphson

i	0	1	2	3	4	5
$x(i)$	1	5.00000	3.40000	3.02353	3.00009	3.00000

b. Using (6.3.5) with $\mathbf{D} = 3$, the Gauss-Seidel method is

$$x(i+1) = x(i) + \frac{1}{3}[9 - x^2(i)]$$

The corresponding Gauss-Seidel calculations are as follows:

Gauss-Seidel (D = 3)

i	0	1	2	3	4	5	6
$x(i)$	1	3.66667	2.18519	3.59351	2.28908	3.54245	2.35945

As shown, Gauss-Seidel oscillates about the solution, slowly converging, whereas Newton-Raphson converges in five iterations to the solution $x = 3$. Note that if $x(0)$ is negative, Newton-Raphson converges to the negative solution $x = -3$. Also, it is assumed that the matrix inverse $\mathbf{J}^{-1}$ exists. Thus, the initial value $x(0) = 0$ should be avoided for this example.

EXAMPLE 6.7

Newton-Raphson method: solution to nonlinear algebraic equations

Solve

$$\begin{bmatrix} x_1 + x_2 \\ x_1 x_2 \end{bmatrix} = \begin{bmatrix} 15 \\ 50 \end{bmatrix} \qquad \mathbf{x}(0) = \begin{bmatrix} 4 \\ 9 \end{bmatrix}$$

Use the Newton-Raphson method starting with the above $\mathbf{x}(0)$ and continue until (6.2.2) is satisfied with $\varepsilon = 10^{-4}$.

SOLUTION

Using (6.3.10) with $f_1 = (x_1 + x_2)$ and $f_2 = x_1x_2$,

$$\mathbf{J}(i)^{-1} = \begin{bmatrix} \dfrac{\partial f_1}{\partial x_1} & \dfrac{\partial f_1}{\partial x_2} \\ \dfrac{\partial f_2}{\partial x_1} & \dfrac{\partial f_2}{\partial x_2} \end{bmatrix}^{-1}_{\mathbf{x}=\mathbf{x}(i)} = \begin{bmatrix} 1 & 1 \\ x_2(i) & x_1(i) \end{bmatrix}^{-1} = \frac{\begin{bmatrix} x_1(i) & -1 \\ -x_2(i) & 1 \end{bmatrix}}{x_1(i) - x_2(i)}$$

Using $\mathbf{J}(i)^{-1}$ in (6.3.9),

$$\begin{bmatrix} x_1(i+1) \\ x_2(i+1) \end{bmatrix} = \begin{bmatrix} x_1(i) \\ x_2(i) \end{bmatrix} + \frac{\begin{bmatrix} x_1(i) & -1 \\ -x_2(i) & 1 \end{bmatrix}}{x_1(i) - x_2(i)} \begin{bmatrix} 15 - x_1(i) - x_2(i) \\ 50 - x_1(i)x_2(i) \end{bmatrix}$$

Writing the preceding as two separate equations,

$$x_1(i+1) = x_1(i) + \frac{x_1(i)[15 - x_1(i) - x_2(i)] - [50 - x_1(i)x_2(i)]}{x_1(i) - x_2(i)}$$

$$x_2(i+1) = x_2(i) + \frac{-x_2(i)[15 - x_1(i) - x_2(i)] + [50 - x_1(i)x_2(i)]}{x_1(i) - x_2(i)}$$

Successive calculations of these equations are shown in the following table.

Newton-Raphson

i	0	1	2	3	4
$x_1(i)$	4	5.20000	4.99130	4.99998	5.00000
$x_2(i)$	9	9.80000	10.00870	10.00002	10.00000

Newton-Raphson converges in four iterations for this example.

Equation (6.3.9) contains the matrix inverse $\mathbf{J}^{-1}$. Instead of computing $\mathbf{J}^{-1}$, (6.3.9) can be rewritten as follows:

$$\mathbf{J}(i)\Delta\mathbf{x}(i) = \Delta\mathbf{y}(i) \tag{6.3.11}$$

where

$$\Delta\mathbf{x}(i) = \mathbf{x}(i+1) - \mathbf{x}(i) \tag{6.3.12}$$

and

$$\Delta\mathbf{y}(i) = \mathbf{y} - \mathbf{f}[\mathbf{x}(i)] \tag{6.3.13}$$

Then, during each iteration, the following four steps are completed:

STEP 1 Compute $\Delta\mathbf{y}(i)$ from (6.3.13).

STEP 2 Compute $\mathbf{J}(i)$ from (6.3.10).

STEP 3 Using Gauss elimination and back substitution, solve (6.3.11) for $\Delta\mathbf{x}(i)$.

STEP 4 Compute $\mathbf{x}(i+1)$ from (6.3.12).

Experience from power flow studies has shown that Newton-Raphson converges in many cases where Jacobi and Gauss-Seidel diverge. Furthermore, the number of iterations required for convergence is independent of the dimension

EXAMPLE 6.8

Newton-Raphson method in four steps

Complete the above four steps for the first iteration of Example 6.7.

SOLUTION

STEP 1 $$\Delta\mathbf{y}(0) = \mathbf{y} - \mathbf{f}[\mathbf{x}(0)] = \begin{bmatrix}15\\20\end{bmatrix} - \begin{bmatrix}4+9\\(4)(9)\end{bmatrix} = \begin{bmatrix}2\\14\end{bmatrix}$$

STEP 2 $$\mathbf{J}(0) = \left[\begin{array}{c|c} 1 & 1 \\ \hline x_2(0) & x_1(0)\end{array}\right] = \left[\begin{array}{c|c} 1 & 1 \\ \hline 9 & 4\end{array}\right]$$

STEP 3 Using $\Delta\mathbf{y}(0)$ and $\mathbf{J}(0)$, (6.3.11) becomes

$$\left[\begin{array}{c|c} 1 & 1 \\ \hline 9 & 4\end{array}\right]\begin{bmatrix}\Delta x_1(0)\\ \Delta x_2(0)\end{bmatrix} = \begin{bmatrix}2\\14\end{bmatrix}$$

Using Gauss elimination, subtract $J_{21}/J_{11} = 9/1 = 9$ times the first equation from the second equation, giving

$$\left[\begin{array}{c|c} 1 & 1 \\ \hline 0 & -5\end{array}\right]\begin{bmatrix}\Delta x_1(0)\\ \Delta x_2(0)\end{bmatrix} = \begin{bmatrix}2\\-4\end{bmatrix}$$

Solving by back substitution,

$$\Delta x_2(0) = \frac{-4}{-5} = 0.8$$

$$\Delta x_1(0) = 2 - 0.8 = 1.2$$

STEP 4 $$\mathbf{x}(1) = \mathbf{x}(0) + \Delta\mathbf{x}(0) = \begin{bmatrix}4\\9\end{bmatrix} + \begin{bmatrix}1.2\\0.8\end{bmatrix} = \begin{bmatrix}5.2\\9.8\end{bmatrix}$$

This is the same as computed in Example 6.7.

N for Newton-Raphson, but increases with N for Jacobi and Gauss-Seidel. Most Newton-Raphson power flow problems converge in fewer than 10 iterations [1].

6.4 THE POWER FLOW PROBLEM

The power flow problem is the computation of voltage magnitude and phase angle at each bus in a power system under balanced three-phase steady-state conditions. As a by-product of this calculation, real and reactive power flows in equipment such as transmission lines and transformers, as well as equipment losses, can be computed.

The starting point for a power flow problem is a single-line (oneline) diagram of the power system, from which the input data can be obtained. Input data consist of bus data, transmission line data, and transformer data.

As shown in Figure 6.1, the following four variables are associated with each bus k: voltage magnitude V_k, phase angle δ_k, net real power P_k, and reactive power Q_k supplied to the bus. At each bus, two of these variables are specified as input data, and the other two are unknowns to be computed by the power flow program. For convenience, the power delivered to bus k in Figure 6.1 is separated into generator and load terms. That is,

$$\begin{aligned} P_k &= P_{Gk} - P_{Lk} \\ Q_k &= Q_{Gk} - Q_{Lk} \end{aligned} \tag{6.4.1}$$

Each bus k is categorized into one of the following three bus types:

1. Swing bus (or slack bus)—There is only one swing bus, which for convenience is numbered bus 1 in this text. The swing bus is a reference bus for which $V_1 \underline{/\delta_1}$, is input data with the angle typically zero degrees and the voltage magnitude close to 1.0 per unit. The power flow computes P_1 and Q_1.

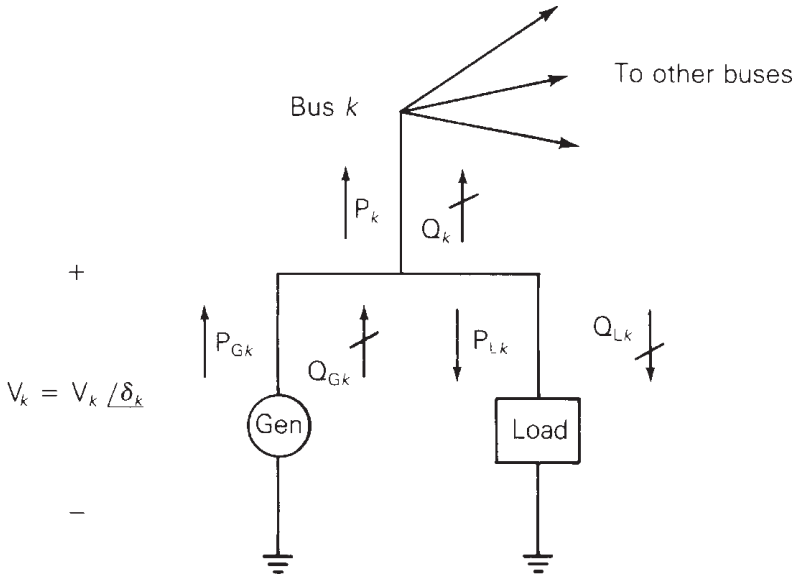

FIGURE 6.1
Bus variables V_k, δ_k, P_k, and Q_k

2. Load (PQ) bus—P_k and Q_k are input data. The power flow computes V_k and δ_k. Most buses in typical power flows are load buses.
3. Voltage controlled (PV) bus—P_k and V_k are input data. The power flow program computes Q_k and δ_k. Examples are buses to which generators, switched shunt capacitors, or static var systems are connected. Maximum and minimum reactive power (var) limits $Q_{Gk\max}$ and $Q_{Gk\min}$ that this equipment can supply are also input data. If an upper or lower reactive power limit is reached, then the reactive power output of the generator is held at the limit, and the bus is modeled as a PQ bus. Another example is a bus to which a tap-changing transformer is connected; the power flow then computes the tap setting.

Note that when bus k is a load bus with no generation, $P_k = -P_{Lk}$ is negative; that is, the real power supplied to bus k in Figure 6.1 is negative. If the load is inductive, $Q_k = -Q_{Lk}$ is negative.

Transmission lines are represented by the equivalent π circuit, shown in Figure 5.7. Transformers are also represented by equivalent circuits, as shown in Figure 3.9 for a two-winding transformer, Figure 3.20 for a three-winding transformer, or Figure 3.25 for a tap-changing transformer.

Input data for each transmission line include the per-unit equivalent π circuit series impedance Z' and shunt admittance Y', the two buses to which the line is connected, and maximum MVA rating. Similarly, input data for each transformer include per-unit winding impedances Z, the per-unit exciting branch admittance Y, the buses to which the windings are connected, and maximum MVA ratings. Input data for tap-changing transformers also include maximum tap settings.

The bus admittance matrix $\boldsymbol{Y}_{\text{bus}}$ can be constructed from the line and transformer input data. From (2.4.3) and (2.4.4), the elements of $\boldsymbol{Y}_{\text{bus}}$ are

$$\text{Diagonal elements: } Y_{kk} = \text{sum of admittances connected to bus } k$$

$$\text{Off-diagonal elements: } Y_{kn} = -(\text{sum of admittances connected between buses } k \text{ and } n) \quad k \neq n \tag{6.4.2}$$

EXAMPLE 6.9

Power flow input data and $\boldsymbol{Y}_{\text{bus}}$

Figure 6.2 shows a single-line diagram of a five-bus power system. Input data are given in Tables 6.1, 6.2, and 6.3. As shown in Table 6.1, bus 1, to which a generator is connected, is the swing bus. Bus 3, to which a generator and a load are connected, is a voltage-controlled bus. Buses 2, 4, and 5 are load buses. Note that the loads at buses 2 and 3 are inductive since $Q_2 = -Q_{L2} = -2.8$ and $-Q_{L3} = -0.4$ are negative.

For each bus k, determine which of the variables V_k, δ_k, P_k, and Q_k are input data and which are unknowns. Also, compute the elements of the second row of $\boldsymbol{Y}_{\text{bus}}$.

FIGURE 6.2

Single-line diagram for Example 6.9

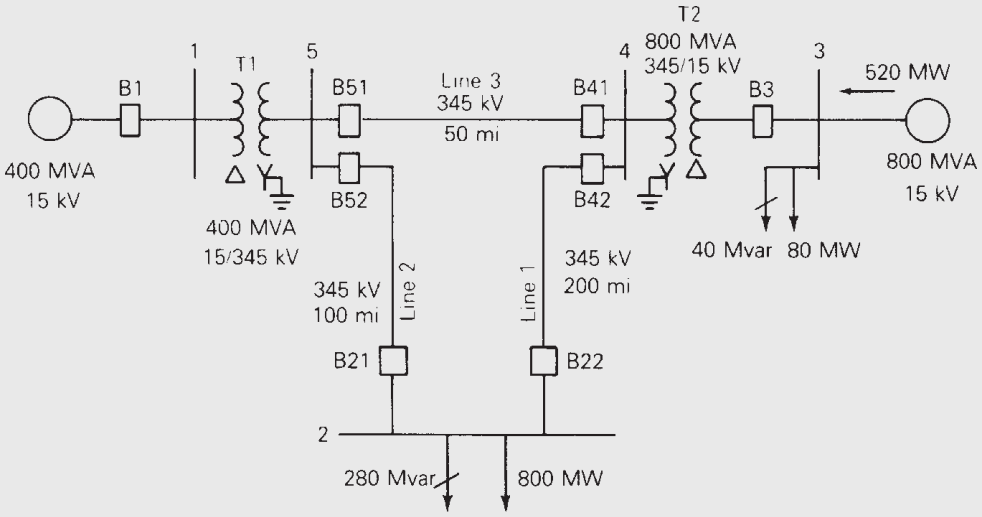

Bus	Type	V per unit	δ degrees	P_G per unit	Q_G per unit	P_L per unit	Q_L per unit	Q_{Gmax} per unit	Q_{Gmin} per unit
1	Swing	1.0	0	—	—	0	0	—	—
2	Load	—	—	0	0	8.0	2.8	—	—
3	Constant voltage	1.05	—	5.2	—	0.8	0.4	4.0	−2.8
4	Load	—	—	0	0	0	0	—	—
5	Load	—	—	0	0	0	0	—	—

TABLE 6.1

Bus input data for Example 6.9*

*S_{base} = 100 MVA, V_{base} = 15 kV at buses 1, 3, and 345 kV at buses 2, 4, 5

Bus-to-Bus	R′ per unit	X′ per unit	G′ per unit	B′ per unit	Maximum MVA per unit
2–4	0.0090	0.100	0	1.72	12.0
2–5	0.0045	0.050	0	0.88	12.0
4–5	0.00225	0.025	0	0.44	12.0

TABLE 6.2

Line input data for Example 6.9

(*Continued*)

Bus-to-Bus	R per unit	X per unit	G_c per unit	B_m per unit	Maximum MVA per unit	Maximum TAP Setting per unit
1–5	0.00150	0.02	0	0	6.0	—
3–4	0.00075	0.01	0	0	10.0	—

TABLE 6.3

Transformer input data for Example 6.9

Bus	Input Data	Unknowns
1	$V_1 = 1.0, \delta_1 = 0$	P_1, Q_1
2	$P_2 = P_{G2} - P_{L2} = -8$ $Q_2 = Q_{G2} - Q_{L2} = -2.8$	V_2, δ_2
3	$V_3 = 1.05$ $P_3 = P_{G3} - P_{L3} = 4.4$	Q_3, δ_4
4	$P_4 = 0, Q_4 = 0$	V_4, δ_4
5	$P_5 = 0, Q_5 = 0$	V_5, δ_5

TABLE 6.4

Input data and unknowns for Example 6.9

SOLUTION

The input data and unknowns are listed in Table 6.4. For bus 1, the swing bus, P_1 and Q_1 are unknowns. For bus 3, a voltage-controlled bus, Q_3 and δ_3 are unknowns. For buses 2, 4, and 5, load buses, V_2, V_4, V_5 and δ_2, δ_4, δ_5 are unknowns.

The elements of $\boldsymbol{Y}_{\text{bus}}$ are computed from (6.4.2). Since buses 1 and 3 are not directly connected to bus 2,

$$Y_{21} = Y_{23} = 0$$

Using (6.4.2),

$$Y_{24} = \frac{-1}{R'_{24} + jX'_{24}} = \frac{-1}{0.009 + j0.1} = -0.89276 + j9.91964 \quad \text{per unit}$$
$$= 9.95972 \underline{/95.143^\circ} \quad \text{per unit}$$

$$Y_{25} = \frac{-1}{R'_{25} + jX'_{25}} = \frac{-1}{0.0045 + j0.05} = -1.78552 + j19.83932 \quad \text{per unit}$$
$$= 19.9195 \underline{/95.143^\circ} \quad \text{per unit}$$

$$Y_{22} = \frac{1}{R'_{24} + jX'_{24}} + \frac{1}{R'_{25} + jX'_{25}} + j\frac{B'_{24}}{2} + j\frac{B'_{25}}{2}$$

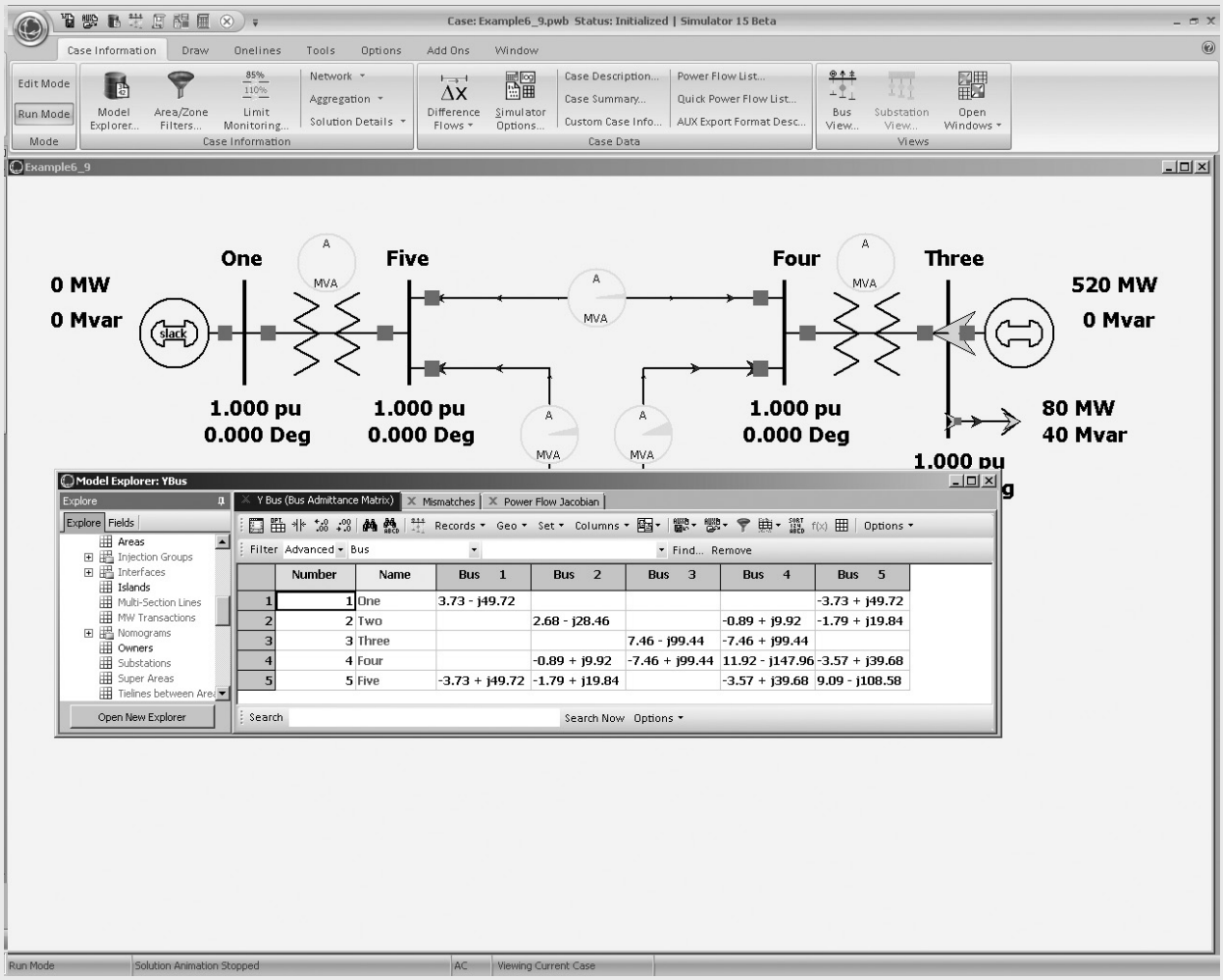

	Number	Name	Bus 1	Bus 2	Bus 3	Bus 4	Bus 5
1	1	One	3.73 - j49.72				-3.73 + j49.72
2	2	Two		2.68 - j28.46		-0.89 + j9.92	-1.79 + j19.84
3	3	Three			7.46 - j99.44	-7.46 + j99.44	
4	4	Four	-0.89 + j9.92	-7.46 + j99.44	11.92 - j147.96	-3.57 + j39.68	
5	5	Five	-3.73 + j49.72	-1.79 + j19.84		-3.57 + j39.68	9.09 - j108.58

FIGURE 6.3

Screen for Example 6.9

$$= (0.89276 - j9.91964) + (1.78552 - j19.83932) + j\frac{1.72}{2} + j\frac{0.88}{2}$$

$$= 2.67828 - j28.4590 = 28.5847\underline{/-84.624^\circ} \text{ per unit}$$

where half of the shunt admittance of each line connected to bus 2 is included in Y_{22} (the other half is located at the other ends of these lines).

This five-bus power system is modeled in PowerWorld Simulator case Example 6_9 (see Figure 6.3). To view the input data, first click on the **Edit Mode** button (on the far left-hand side of the ribbon) to switch into the Edit mode (the Edit mode is used for modifying system parameters). Then by selecting the **Case Information** tab, you can view tabular displays showing the various parameters for

(*Continued*)

the system. For example, use **Network**, **Buses** to view the parameters for each bus, and **Network**, **Lines and Transformers** to view the parameters for the transmission lines and transformers. Fields shown in blue on the screen can be directly changed simply by typing over them, and those shown in green can be toggled by clicking on them. Note that the values shown on these displays match the per unit values from Tables 6.1 to 6.3, except the power values are shown in actual MW/Mvar units.

The elements of $\boldsymbol{Y}_{\text{bus}}$ also can be displayed by selecting **Solution Details**, $\boldsymbol{Y}_{\text{bus}}$. Since the $\boldsymbol{Y}_{\text{bus}}$ entries are derived from other system parameters, they cannot be changed directly. Notice that several of the entries are blank, indicating that there is no transmission line or transformer directly connecting these two buses (a blank entry is equivalent to zero). For larger networks, most of the elements of the $\boldsymbol{Y}_{\text{bus}}$ are zero since any single bus usually only has a few incident lines (such sparse matrices are considered in Section 6.8). The elements of the $\boldsymbol{Y}_{\text{bus}}$ can be saved in a Matlab compatible format by first right-clicking within the $\boldsymbol{Y}_{\text{bus}}$ matrix to display the local menu, and then selecting **Save $\boldsymbol{Y}_{\text{bus}}$ in Matlab Format** from the local menu.

Finally, notice that no flows are shown on the oneline because the nonlinear power flow equations have not yet been solved, and the solution of these equations are covered next.

Using $\boldsymbol{Y}_{\text{bus}}$, the nodal equations for a power system network are written as

$$\mathbf{I} = \boldsymbol{Y}_{\text{bus}}\mathbf{V} \tag{6.4.3}$$

where $\mathbf{I}$ is the N vector of source currents injected into each bus and $\mathbf{V}$ is the N vector of bus voltages. For bus k, the kth equation in (6.4.3) is

$$I_k = \sum_{n=1}^{N} Y_{kn} V_n \tag{6.4.4}$$

The complex power delivered to bus k is

$$S_k = \mathrm{P}_k + j\mathrm{Q}_k = V_k I_k^* \tag{6.4.5}$$

Power flow solutions by Gauss-Seidel are based on nodal equations, (6.4.4), where each current source I_k is calculated from (6.4.5). Using (6.4.4) in (6.4.5),

$$\mathrm{P}_k + j\mathrm{Q}_k = V_k\left[\sum_{n=1}^{N} Y_{kn} V_n\right]^* \qquad k = 1, 2, \ldots, N \tag{6.4.6}$$

With the following notation,

$$V_n = \mathrm{V}_n e^{j\delta_n} \tag{6.4.7}$$

$$Y_{kn} = \mathrm{Y}_{kn} e^{j\theta_{kn}} = G_{kn} + jB_{kn} \qquad k,n = 1, 2, \ldots, N \tag{6.4.8}$$

(6.4.6) becomes

$$\mathrm{P}_k + j\mathrm{Q}_k = \mathrm{V}_k \sum_{n=1}^{N} \mathrm{Y}_{kn}\mathrm{V}_n e^{j(\delta_k - \delta_n - \theta_{kn})} \tag{6.4.9}$$

Taking the real and imaginary parts of (6.4.9), the power balance equations are written as either

$$\mathrm{P}_k = \mathrm{V}_k \sum_{n=1}^{N} \mathrm{Y}_{kn} \mathrm{V}_n \cos(\delta_k - \delta_n - \theta_{kn}) \tag{6.4.10}$$

$$\mathrm{Q}_k = \mathrm{V}_k \sum_{n=1}^{N} \mathrm{Y}_{kn} \mathrm{V}_n \sin(\delta_k - \delta_n - \theta_{kn}) \qquad k = 1, 2, \ldots, N \tag{6.4.11}$$

or when the Y_{kn} is expressed in rectangular coordinates as

$$\mathrm{P}_k = \mathrm{V}_k \sum_{n=1}^{N} V_n [G_{kn} \cos(\delta_k - \delta_n) + B_{kn} \sin(\delta_k - \delta_n)] \tag{6.4.12}$$

$$\mathrm{Q}_k = \mathrm{V}_k \sum_{n=1}^{N} V_n [G_{kn} \sin(\delta_k - \delta_n) - B_{kn} \cos(\delta_k - \delta_n)] \qquad k = 1, 2, \ldots, N \tag{6.4.13}$$

Power flow solutions by Newton-Raphson are based on the nonlinear power flow equations given by (6.4.10) and (6.4.11) [or alternatively by (6.4.12) and (6.4.13)].

6.5 POWER FLOW SOLUTION BY GAUSS-SEIDEL

Nodal equations $\mathbf{I} = \boldsymbol{Y}_{\text{bus}}\mathbf{V}$ are a set of linear equations analogous to $\mathbf{y} = \mathbf{Ax}$, solved in Section 6.2 using Gauss-Seidel. Since power flow bus data consists of P_k and Q_k for load buses or P_k and V_k for voltage-controlled buses, nodal equations do not directly fit the linear equation format; the current source vector $\mathbf{I}$ is unknown and the equations are actually nonlinear. For each load bus, I_k can be calculated from (6.4.5), giving

$$I_k = \frac{\mathrm{P}_k - j\mathrm{Q}_k}{V_k^*} \tag{6.5.1}$$

Applying the Gauss-Seidel method (6.2.9) to the nodal equations with I_k given above, obtain

$$V_k(i+1) = \frac{1}{Y_{kk}} \left[\frac{\mathrm{P}_k - j\mathrm{Q}_k}{V_k^*(i)} - \sum_{n=1}^{k-1} Y_{kn} V_n(i+1) - \sum_{n=k+1}^{N} Y_{kn} V_n(i) \right] \tag{6.5.2}$$

Equation (6.5.2) can be applied twice during each iteration for load buses, first using $V_k^*(i)$, then replacing $V_k^*(i)$, by $V_k^*(i+1)$ on the right side of (6.5.2).

For a voltage-controlled bus, Q_k is unknown but can be calculated from (6.4.11), giving

$$\mathrm{Q}_k = \mathrm{V}_k(i) \sum_{n=1}^{N} \mathrm{Y}_{kn} \mathrm{V}_n(i) \sin[\delta_k(i) - \delta_n(i) - \theta_{kn}] \tag{6.5.3}$$

Also,

$$\mathrm{Q}_{Gk} = \mathrm{Q}_k + \mathrm{Q}_{Lk}$$

If the calculated value of Q_{Gk} does not exceed its limits, then Q_k is used in (6.5.2) to calculate $V_k(i+1) = V_k(i+1)\underline{/\delta_k(i+1)}$. Then the magnitude $V_k(i+1)$ is changed to V_k, which is input data for the voltage-controlled bus. Thus, use (6.5.2) to compute only the angle $\delta_k(i+1)$ for voltage-controlled buses.

If the calculated value exceeds its limit $Q_{Gk\max}$ or $Q_{Gk\min}$ during any iteration, then the bus type is changed from a voltage-controlled bus to a load bus, with Q_{Gk} set to its limit value. Under this condition, the voltage-controlling device (e.g., generator, capacitor bank, static var compensator) is not capable of maintaining V_k as specified by the input data. The power flow then calculates a new value of V_k.

For the swing bus, denoted bus 1, V_1 and δ_1 *are* input data. As such, no iterations are required for the swing bus. After the iteration process has converged, one pass through (6.4.10) and (6.4.11) can be made to compute P_1 and Q_1.

EXAMPLE 6.10

Power flow solution by Gauss-Seidel

For the power system of Example 6.9, use Gauss-Seidel to calculate $V_2(1)$, the phasor voltage at bus 2 after the first iteration. Use zero initial phase angles and 1.0 per-unit initial voltage magnitudes (except at bus 3, where $V_3 = 1.05$) to start the iteration procedure.

SOLUTION

Bus 2 is a load bus. Using the input data and bus admittance values from Example 6.9 in (6.5.2),

$$V_2(1) = \frac{1}{Y_{22}}\left\{\frac{P_2 - jQ_2}{V_2^*(0)} - [Y_{21}V_1(1) + Y_{23}V_3(0) + Y_{24}V_4(0) + Y_{25}V_5(0)]\right\}$$

$$= \frac{1}{28.5847\underline{/-84.624^\circ}}\left\{\frac{-8 - j(-2.8)}{1.0\underline{/0^\circ}}\right.$$

$$\left. - [(-1.78552 + j19.83932)(1.0) + (-0.89276 + j9.91964)(1.0)]\right\}$$

$$= \frac{(-8 + j2.8) - (-2.67828 + j29.7589)}{28.5847\underline{/-84.624^\circ}}$$

$$= 0.96132\underline{/-16.543^\circ} \quad \text{per unit}$$

Next, the above value is used in (6.5.2) to recalculate $V_2(1)$;

$$V_2(1) = \frac{1}{28.5847\underline{/-84.624^\circ}}\left\{\frac{-8 + j2.8}{0.96132\underline{/16.543^\circ}} - [-2.67828 + j29.75829]\right\}$$

$$= \frac{-4.4698 - j24.5973}{28.5847\angle -84.624^\circ} = 0.87460\angle -15.675^\circ \quad \text{per unit}$$

Computations are next performed at buses 3, 4, and 5 to complete the first Gauss-Seidel iteration.

To see the complete convergence of this case, open PowerWorld Simulator case Example 6_10. By default, PowerWorld Simulator uses the Newton-Raphson method described in the next section since Gauss-Seidel, while being a useful technique for introducing the power flow to students, is now seldom used commercially. However, the free educational version of PowerWorld still allows cases to be solved with the Gauss-Seidel approach by selecting **Tools, Solve, Gauss-Seidel Power Flow**. To avoid getting stuck in an infinite loop if a case does not converge, PowerWorld Simulator places a limit on the maximum number of iterations. Usually for a Gauss-Seidel procedure this number is rather high, perhaps equal to 100 iterations. However, in this example to demonstrate the convergence characteristics of the Gauss-Seidel method, it has been set to a single iteration, allowing the voltages to be viewed after each iteration. To step through the solution one iteration at a time, just repeatedly select **Tools, Solve, Gauss-Seidel Power Flow**.

A common stopping criterion for the Gauss-Seidel is to use the scaled differences in the voltages from one iteration to the next (6.2.2). When the voltage differences for each bus are below a specified convergence tolerance ε, the problem is considered solved. An alternative approach, implemented in PowerWorld Simulator, is to examine the real and reactive mismatch equations, defined as the difference between the right- and left-hand sides of (6.4.10) and (6.4.11). PowerWorld Simulator continues iterating until all the bus mismatches are below an MVA (or kVA) tolerance. When single-stepping through the solution, the bus mismatches can be viewed after each iteration on the **Case Information, Mismatches** display. The solution mismatch tolerance can be changed on the Power Flow Solution page of the PowerWorld Simulator Options dialog (select **Tools, Simulator Options**, then select the **Power Flow Solution** category to view this dialog); the maximum number of iterations can also be changed from this page. A typical convergence tolerance is about 0.1 MVA.

6.6 POWER FLOW SOLUTION BY NEWTON-RAPHSON

Equations (6.4.10) and (6.4.11) are analogous to the nonlinear equation $\mathbf{y} = \mathbf{f}(\mathbf{x})$, solved in Section 6.3 by Newton-Raphson. The $\mathbf{x}$, $\mathbf{y}$, and $\mathbf{f}$ vectors for the power flow problem are defined as

$$\mathbf{x} = \begin{bmatrix} \delta \\ \mathbf{V} \end{bmatrix} = \begin{bmatrix} \delta_2 \\ \vdots \\ \delta_N \\ \mathrm{V}_2 \\ \vdots \\ \mathrm{V}_N \end{bmatrix}; \quad \mathbf{y} = \begin{bmatrix} \mathbf{P} \\ \mathbf{Q} \end{bmatrix} = \begin{bmatrix} \mathrm{P}_2 \\ \vdots \\ \mathrm{P}_N \\ \mathrm{Q}_2 \\ \vdots \\ \mathrm{Q}_N \end{bmatrix}$$

$$\mathbf{f}(\mathbf{x}) = \begin{bmatrix} \mathbf{P}(\mathbf{x}) \\ \mathbf{Q}(\mathbf{x}) \end{bmatrix} = \begin{bmatrix} \mathrm{P}_2(\mathbf{x}) \\ \vdots \\ \mathrm{P}_N(\mathbf{x}) \\ \mathrm{Q}_2(\mathbf{x}) \\ \vdots \\ \mathrm{Q}_N(\mathbf{x}) \end{bmatrix} \tag{6.6.1}$$

where all V, P, and Q terms are in per-unit and δ terms are in radians. The swing bus variables δ_1 and V_1 are omitted from (6.6.1), since they are already known. Equations (6.4.10) and (6.4.11) then have the following form:

$$y_k = \mathrm{P}_k = \mathrm{P}_k(\mathrm{x}) = \mathrm{V}_k \sum_{n=1}^{N} \mathrm{Y}_{kn} \mathrm{V}_n \cos(\delta_k - \delta_n - \theta_{kn}) \tag{6.6.2}$$

$$\begin{aligned} y_{k+N} &= \mathrm{Q}_\mathrm{k} = \mathrm{Q}_k(\mathrm{x}) = \mathrm{V}_\mathrm{k} \sum_{n=1}^{N} \mathrm{Y}_\mathrm{kn} \mathrm{V}_n \sin(\delta_k - \delta_n - \theta_{kn}) \\ k &= 2, 3, \ldots, N \end{aligned} \tag{6.6.3}$$

The Jacobian matrix of (6.3.10) has the form

$$\mathbf{J} = \begin{array}{c} \begin{matrix} \qquad\quad \mathbf{J}1 \qquad\qquad\qquad\quad & \mathbf{J}2 \end{matrix} \\ \left[\begin{array}{ccc|ccc} \dfrac{\partial \mathrm{P}_2}{\partial \delta_2} & \cdots & \dfrac{\partial \mathrm{P}_2}{\partial \delta_N} & \dfrac{\partial \mathrm{P}_2}{\partial \mathrm{V}_2} & \cdots & \dfrac{\partial \mathrm{P}_2}{\partial \mathrm{V}_N} \\ \vdots & & & \vdots & & \\ \dfrac{\partial \mathrm{P}_N}{\partial \delta_2} & \cdots & \dfrac{\partial \mathrm{P}_N}{\partial \delta_N} & \dfrac{\partial \mathrm{P}_N}{\partial \mathrm{V}_2} & \cdots & \dfrac{\partial \mathrm{P}_N}{\partial \mathrm{V}_N} \\ \hline \dfrac{\partial \mathrm{Q}_2}{\partial \delta_2} & \cdots & \dfrac{\partial \mathrm{Q}_2}{\partial \delta_N} & \dfrac{\partial \mathrm{Q}_2}{\partial \mathrm{V}_2} & \cdots & \dfrac{\partial \mathrm{Q}_2}{\partial \mathrm{V}_N} \\ \vdots & & & \vdots & & \\ \dfrac{\partial \mathrm{Q}_N}{\partial \delta_2} & \cdots & \dfrac{\partial \mathrm{Q}_N}{\partial \delta_N} & \dfrac{\partial \mathrm{Q}_N}{\partial \mathrm{V}_2} & \cdots & \dfrac{\partial \mathrm{Q}_N}{\partial \mathrm{V}_N} \end{array}\right] \\ \begin{matrix} \qquad\quad \mathbf{J}3 \qquad\qquad\qquad\quad & \mathbf{J}4 \end{matrix} \end{array} \tag{6.6.4}$$

Equation (6.6.4) is partitioned into four blocks. The partial derivatives in each block, derived from (6.6.2) and (6.6.3), are given in Table 6.5.

$n \neq k$

$$J1_{kn} = \frac{\partial P_k}{\partial \delta_n} = V_k Y_{kn} V_n \sin(\delta_k - \delta_n - \theta_{kn})$$

$$J2_{kn} = \frac{\partial P_k}{\partial V_n} = V_k Y_{kn} \cos(\delta_k - \delta_n - \theta_{kn})$$

$$J3_{kn} = \frac{\partial Q_k}{\partial \delta_n} = -V_k Y_{kn} V_n \cos(\delta_k - \delta_n - \theta_{kn})$$

$$J4_{kn} = \frac{\partial Q_k}{\partial V_n} = V_k Y_{kn} \sin(\delta_k - \delta_n - \theta_{kn})$$

$n = k$

$$J1_{kk} = \frac{\partial P_k}{\partial \delta_k} = -V_k \sum_{\substack{n=1 \\ n \neq k}}^{N} Y_{kn} V_n \sin(\delta_k - \delta_n - \theta_{kn})$$

$$J2_{kk} = \frac{\partial P_k}{\partial V_k} = V_k Y_{kk} \cos \theta_{kk} + \sum_{n=1}^{N} Y_{kn} V_n \cos(\delta_k - \delta_n - \theta_{kn})$$

$$J3_{kk} = \frac{\partial Q_k}{\partial \delta_k} = V_k \sum_{\substack{n=1 \\ n \neq k}}^{N} Y_{kn} V_n \cos(\delta_k - \delta_n - \theta_{kn})$$

$$J4_{kk} = \frac{\partial Q_k}{\partial V_k} = -V_k Y_{kk} \sin \theta_{kk} + \sum_{n=1}^{N} Y_{kn} V_n \sin(\delta_k - \delta_n - \theta_{kn})$$

$k, n = 2, 3, \ldots, N$

TABLE 6.5
Elements of the Jacobian matrix

Now apply to the power flow problem the four Newton-Raphson steps outlined in Section 6.3, starting with $\mathbf{x}(i) = \begin{bmatrix} \boldsymbol{\delta}(i) \\ \mathbf{V}(i) \end{bmatrix}$ at the ith iteration.

STEP 1 Use (6.6.2) and (6.6.3) to compute

$$\Delta \mathbf{y}(i) = \begin{bmatrix} \Delta \mathbf{P}(i) \\ \Delta \mathbf{Q}(i) \end{bmatrix} = \begin{bmatrix} \mathbf{P} - \mathbf{P}[\mathbf{x}(i)] \\ \mathbf{Q} - \mathbf{Q}[\mathbf{x}(i)] \end{bmatrix} \tag{6.6.5}$$

STEP 2 Use the equations in Table 6.5 to calculate the Jacobian matrix.

STEP 3 Use Gauss elimination and back substitution to solve

$$\left[\begin{array}{c|c} \mathbf{J}1(i) & \mathbf{J}2(i) \\ \hline \mathbf{J}3(i) & \mathbf{J}4(i) \end{array}\right] \begin{bmatrix} \Delta \boldsymbol{\delta}(i) \\ \Delta \mathbf{V}(i) \end{bmatrix} = \begin{bmatrix} \Delta \mathbf{P}(i) \\ \Delta \mathbf{Q}(i) \end{bmatrix} \tag{6.6.6}$$

STEP 4 Compute

$$\mathbf{x}(i+1) = \begin{bmatrix} \boldsymbol{\delta}(i+1) \\ \mathbf{V}(i+1) \end{bmatrix} = \begin{bmatrix} \boldsymbol{\delta}(i) \\ \mathbf{V}(i) \end{bmatrix} + \begin{bmatrix} \Delta\boldsymbol{\delta}(i) \\ \Delta\mathbf{V}(i) \end{bmatrix} \tag{6.6.7}$$

Starting with initial value $\mathbf{x}(0)$, the procedure continues until convergence is obtained or until the number of iterations exceeds a specified maximum. Convergence criteria are often based on $\Delta\mathbf{y}(i)$ (called *power mismatches*) rather than on $\Delta\mathbf{x}(i)$ (phase angle and voltage magnitude mismatches).

For each voltage-controlled bus, the magnitude V_k is already known, and the function $Q_k(\mathbf{x})$ is not needed. Therefore, V_k from the $\mathbf{x}$ vector can be omitted, as well as Q_k from the $\mathbf{y}$ vector. The column corresponding to partial derivatives with respect to V_k and the row corresponding to partial derivatives of $Q_k(\mathbf{x})$ can also be omitted from the Jacobian matrix. Alternatively, rows and corresponding columns for voltage-controlled buses can be retained in the Jacobian matrix. Then during each iteration, the voltage magnitude $V_k(i+1)$ of each voltage-controlled bus is reset to V_k which is input data for that bus.

At the end of each iteration, $Q_k(\mathbf{x})$ is computed using (6.6.3) and $Q_{Gk} = Q_k(\mathbf{x}) + Q_{Lk}$ for each voltage-controlled bus. If the computed value of Q_{Gk} exceeds its limits, then the bus type is changed to a load bus with Q_{Gk} set to its limit value. The power flow program also computes a new value for V_k.

EXAMPLE 6.11

Jacobian matrix and power flow solution by Newton-Raphson

Determine the dimension of the Jacobian matrix for the power system in Example 6.9. Also calculate $\Delta P_2(0)$ in Step 1 and $Jl_{24}(0)$ in Step 2 of the first Newton-Raphson iteration. Assume zero initial phase angles and 1.0 per-unit initial voltage magnitudes (except $V_3 = 1.05$).

SOLUTION

Since there are $N = 5$ buses for Example 6.9, (6.6.2) and (6.6.3) constitute $2(N-1) = 8$ equations, for which $\mathbf{J}(i)$ has dimension 8×8. However, there is one voltage-controlled bus, bus 3. Therefore, V_3 and the equation for $Q_3(\mathbf{x})$ could be eliminated, with $\mathbf{J}(i)$ reduced to a 7×7 matrix.

From Step 1 and (6.6.2),

$$\begin{aligned} \Delta P_2(0) = P_2 - P_2(x) = P_2 - V_2(0)\{ & Y_{21}V_1 \cos[\delta_2(0) - \delta_1(0) - \theta_{21}] \\ & + Y_{22}V_2 \cos[-\theta_{22}] + Y_{23}V_3 \cos[\delta_2(0) - \delta_3(0) - \theta_{23}] \\ & + Y_{24}V_4 \cos[\delta_2(0) - \delta_4(0) - \theta_{24}] \\ & + Y_{25}V_5 \cos[\delta_2(0) - \delta_5(0) - \theta_{25}]\} \end{aligned}$$

$$\Delta P_2(0) = -8.0 - 1.0\{28.5847(1.0)\cos(84.624°) + 9.95972(1.0)\cos(-95.143°) + 19.9159(1.0)\cos(-95.143°)\}$$
$$= -8.0 - (-2.89 \times 10^{-4}) = -7.99972 \text{ per unit}$$

From Step 2 and Jl given in Table 6.5

$$J1_{24}(0) = V_2(0)Y_{24}V_4(0)\sin[\delta_2(0) - \delta_4(0) - \theta_{24}]$$
$$= (1.0)(9.95972)(1.0)\sin[-95.143°]$$
$$= -9.91964 \text{ per unit}$$

To see the complete convergence of this case, open PowerWorld Simulator case Example 6_11 (see Figure 6.4). Select **Case Information, Network, Mismatches** to see the initial mismatches, and **Case Information, Solution Details, Power Flow Jacobian** to view the initial Jacobian matrix. As is common in commercial power flows, PowerWorld Simulator actually includes rows in the Jacobian for voltage-controlled buses. When a generator is regulating its terminal voltage, this row corresponds to the equation setting the bus voltage magnitude equal to the generator voltage setpoint. However, if the generator hits a reactive power limit, the bus type is switched to a load bus.

To step through the Newton-Raphson solution, from the ribbon select **Solve, Single Solution–Full Newton**. Ordinarily this selection would perform a complete Newton-Raphson iteration, stopping only when all the mismatches are less than the desired tolerance. However, for this case, in order to allow you to see the solution process, the maximum number of iterations has been set to 1, allowing the voltages, mismatches and the Jacobian to be viewed after each iteration. To complete the solution, continue to select **Single Solution—Full Newton** until the solution convergence to the values shown in Tables 6.6, 6.7, and 6.8 (in about three iterations).

Bus #	Voltage Magnitude (per unit)	Phase Angle (degrees)	Generation		Load	
			PG (per unit)	QG (per unit)	PL (per unit)	QL (per unit)
1	1.000	0.000	3.948	1.144	0.000	0.000
2	0.834	–22.407	0.000	0.000	8.000	2.800
3	1.050	–0.597	5.200	3.376	0.800	0.400
4	1.019	–2.834	0.000	0.000	0.000	0.000
5	0.974	–4.548	0.000	0.000	0.000	0.000
		TOTAL	9.148	4.516	8.800	3.200

TABLE 6.6
Bus output data for the power system given in Example 6.9

(*Continued*)

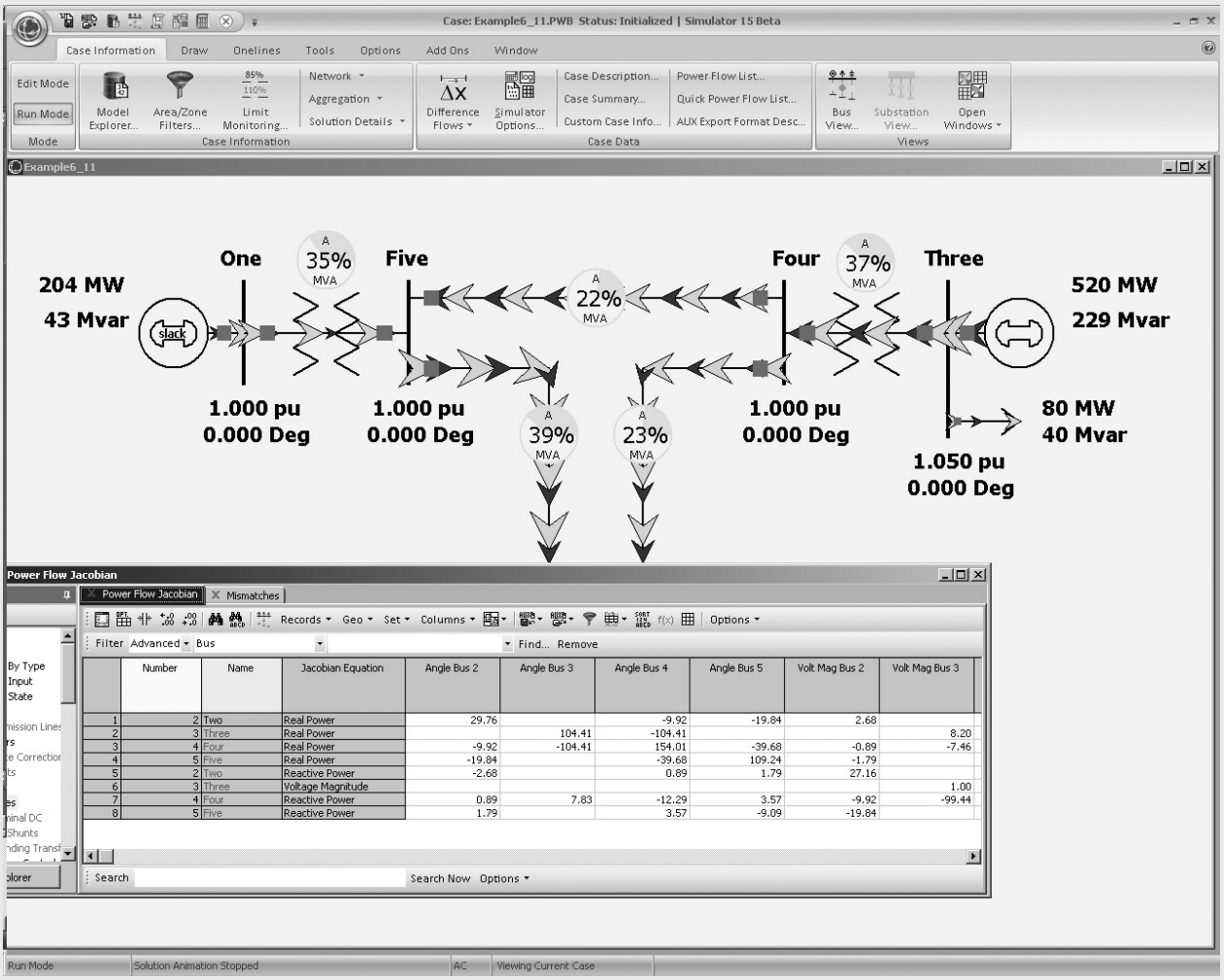

FIGURE 6.4

Screen for Example 6.11 showing Jacobian matrix at first iteration

Line #	Bus to Bus		P	Q	S
1	2	4	−2.920	−1.392	3.232
	4	2	3.036	1.216	3.272
2	2	5	−5.080	−1.408	5.272
	5	2	5.256	2.632	5.876
3	4	5	1.344	1.504	2.016
	5	4	−1.332	−1.824	2.260

TABLE 6.7

Line output data for the power system given in Example 6.9

Tran. #	Bus to Bus		P	Q	S
1	1	5	3.948	1.144	4.112
	5	1	−3.924	−0.804	4.004
2	3	4	4.400	2.976	5.312
	4	3	−4.380	−2.720	5.156

TABLE 6.8

Transformer output data for the power system given in Example 6.9

EXAMPLE 6.12

Power flow program: change in generation

Using the power-flow system given in Example 6.9, determine the acceptable generation range at bus 3, keeping each line and transformer loaded at or below 100% of its MVA limit.

SOLUTION

Load PowerWorld Simulator case Example 6_9. Select **Single Solution-Full Newton** to perform a single power flow solution using the Newton-Raphson approach. Then view the **Case Information** displays to verify that the PowerWorld Simulator solution matches the solution shown in Tables 6.6, 6.7, and 6.8. Additionally, the pie charts on the onelines show the percentage line and transformer loadings. Initially transformer Tl, between buses 1 and 5, is loaded at about 69% of its maximum MVA limit, while transformer T2, between buses 3 and 4, is loaded at about 53%.

Next, the bus 3 generation needs to be varied. This can be done a number of different ways in PowerWorld Simulator. The easiest (for this example) is to use the bus 3 generator MW oneline field to manually change the generation (see Figure 6.5). Right-click on the 520 MW field to the right of the bus 3 generator and select **Generator Field Information** dialog to view the **Generator Field Options** dialog. Set the Delta Per Mouse Click field to 10 and select OK. Small arrows are now visible next to this field on the oneline; clicking on the up arrow increases the generator's MW output by 10 MW, while clicking on the down arrow decreases the generation by 10 MW. Select **Tools, Play** to begin the simulation. Increase the generation until the pie chart for the transformer from bus 3 to 4 is loaded to 100%. This occurs at about 1000 MW. Notice that as the bus 3 generation is increased, the bus 1 slack generation decreases by a similar amount. Repeat the process, except now decreasing the generation. This unloads the transformer from bus 3 to 4, but increases the loading on the transformer from bus 1 to bus 5. The bus 1 to 5 transformer should reach 100% loading with the bus 3 generation equal to about 330 MW.

(*Continued*)

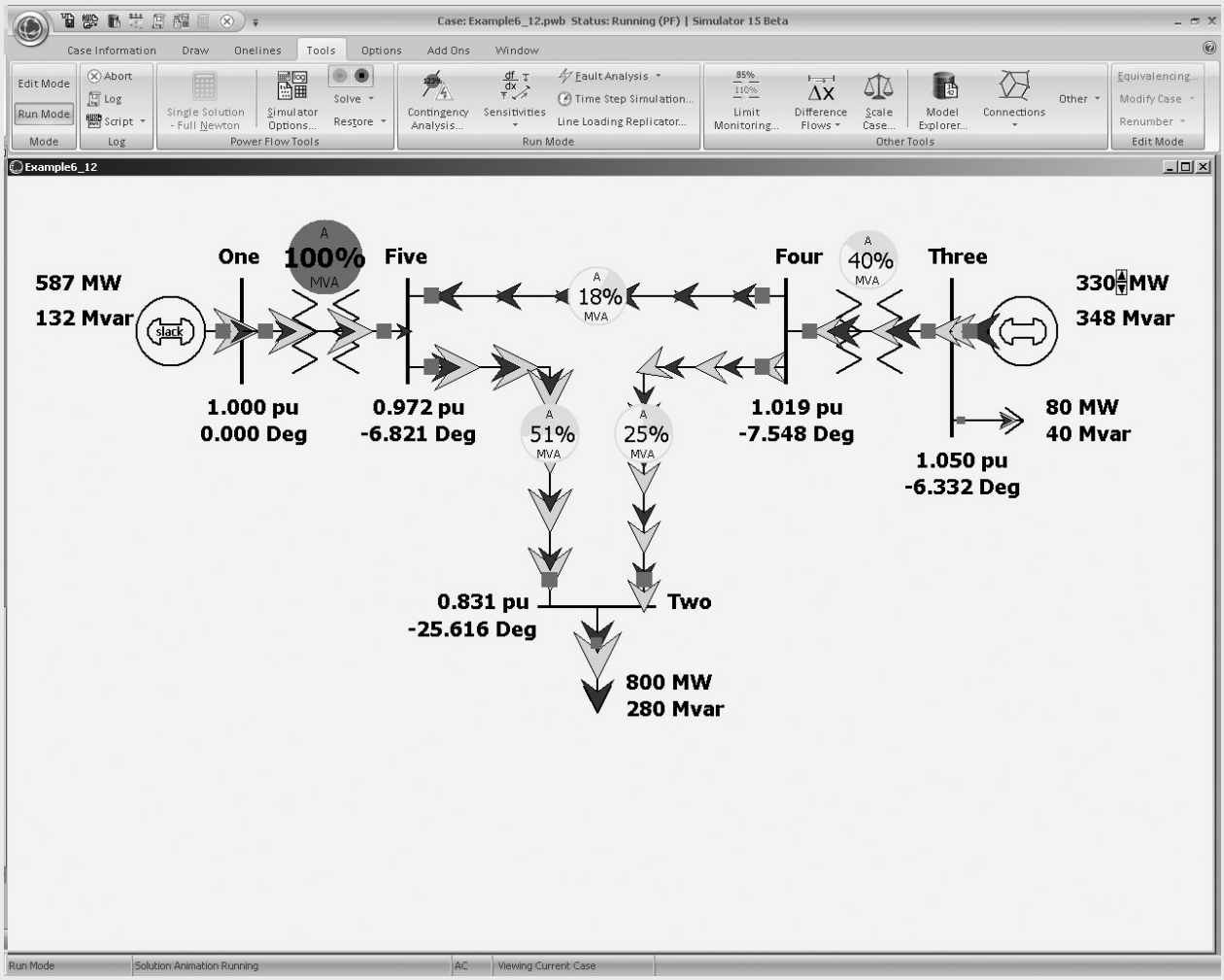

FIGURE 6.5

Screen for Example 6.12, Minimum Bus 3 Generator Loading

Voltage-controlled buses to which tap-changing or voltage-regulating transformers are connected can be handled by various methods. One method is to treat each of these buses as a load bus. The equivalent π circuit parameters (Figure 3.25) are first calculated with tap setting $c = 1.0$ for starting. During each iteration, the computed bus voltage magnitude is compared with the desired value specified by the input data. If the computed voltage is low (or high), c is increased (or decreased) to its next setting, and the parameters of the equivalent π circuit as well as $\boldsymbol{Y}_{\text{bus}}$ are recalculated. The procedure continues until the computed bus voltage magnitude equals the desired value within a specified tolerance or until the high

or low tap-setting limit is reached. Phase-shifting transformers can be handled in a similar way by using a complex turns ratio $c = 1.0\angle\alpha$ and by varying the phase-shift angle α.

A method with faster convergence makes c a variable and includes it in the **x** vector of (6.6.1). An equation is then derived to enter into the Jacobian matrix [4].

In comparing the Gauss-Seidel and Newton-Raphson algorithms, experience from power flow studies has shown that Newton-Raphson converges in many cases where Jacobi and Gauss-Seidel diverge. Furthermore, the number of iterations required for convergence is independent of the number of buses N for Newton-Raphson, but increases with N for Jacobi and Gauss-Seidel. The principal advantage of the Jacobi and Gauss-Seidel methods had been their more modest memory storage requirements and their lower computational requirements per iteration. However, with the vast increases in low-cost computer memory over the last several decades, coupled with the need to solve power flow problems with tens of thousands of buses, these advantages have been essentially eliminated. Therefore the Newton-Raphson, or one of the derivative methods discussed in Sections 6.9 and 6.10, are the preferred power flow solution approaches.

EXAMPLE 6.13

Power flow program: 37-bus system

To see a power flow example of a larger system, open PowerWorld Simulator case Example 6_13 (see Figure 6.6). This case models a 37-bus, 9-generator power system containing three different voltage levels (345 kV, 138 kV, and 69 kV) with 57 transmission lines or transformers. The oneline can be panned by pressing the arrow keys, and it can be zoomed by pressing the <ctrl> with the up arrow key to zoom in or with the down arrow key to zoom out. Use **Tools, Play** to animate the oneline and **Tools, Pause** to stop the animation.

Determine the lowest per-unit voltage and the maximum line/transformer loading both for the initial case and for the case with the line from bus OAK69 to WALNUT69 out of service.

SOLUTION

Use single solution to initially solve the power flow, and then **Case Information, Network, Buses…** to view a listing of all the buses in the case. To quickly determine the lowest per-unit voltage magnitude, left-click on the PU Volt column header to sort the column (clicking a second time reverses the sort). The lowest initial voltage magnitude is 0.990 at bus LOCUST69. Next, select **Case Information, Network, Lines and Transformers…** to view the Line and Transformer Records display. Left-click on % of Max Limit to sort the lines by percentage loading. Initially the highest percentage loading is 64.9% on the line between PEAR69 and PECAN69, circuit 1.

(*Continued*)

In the software, there are several ways to open the line between OAK69 and WALNUT69. One approach is to locate the line on the Line and Transformer Records display and then double-click on the Status field to change its value. An alternative approach is to find the line on the oneline (it is in the upper-lefthand portion) and then click on one of its circuit breakers. Once the line is removed, use single solution to resolve the power flow. The lowest per-unit voltage is now 0.911 at MAPLE69, and the highest percentage line loading is 135% on the line between PEACH69 to POPLAR69. Since there are now several bus and line violations, the power system is no longer at a reliable operating point. Control actions and/or design improvements are needed to correct these problems. The design projects at the end of the chapter discuss these options.

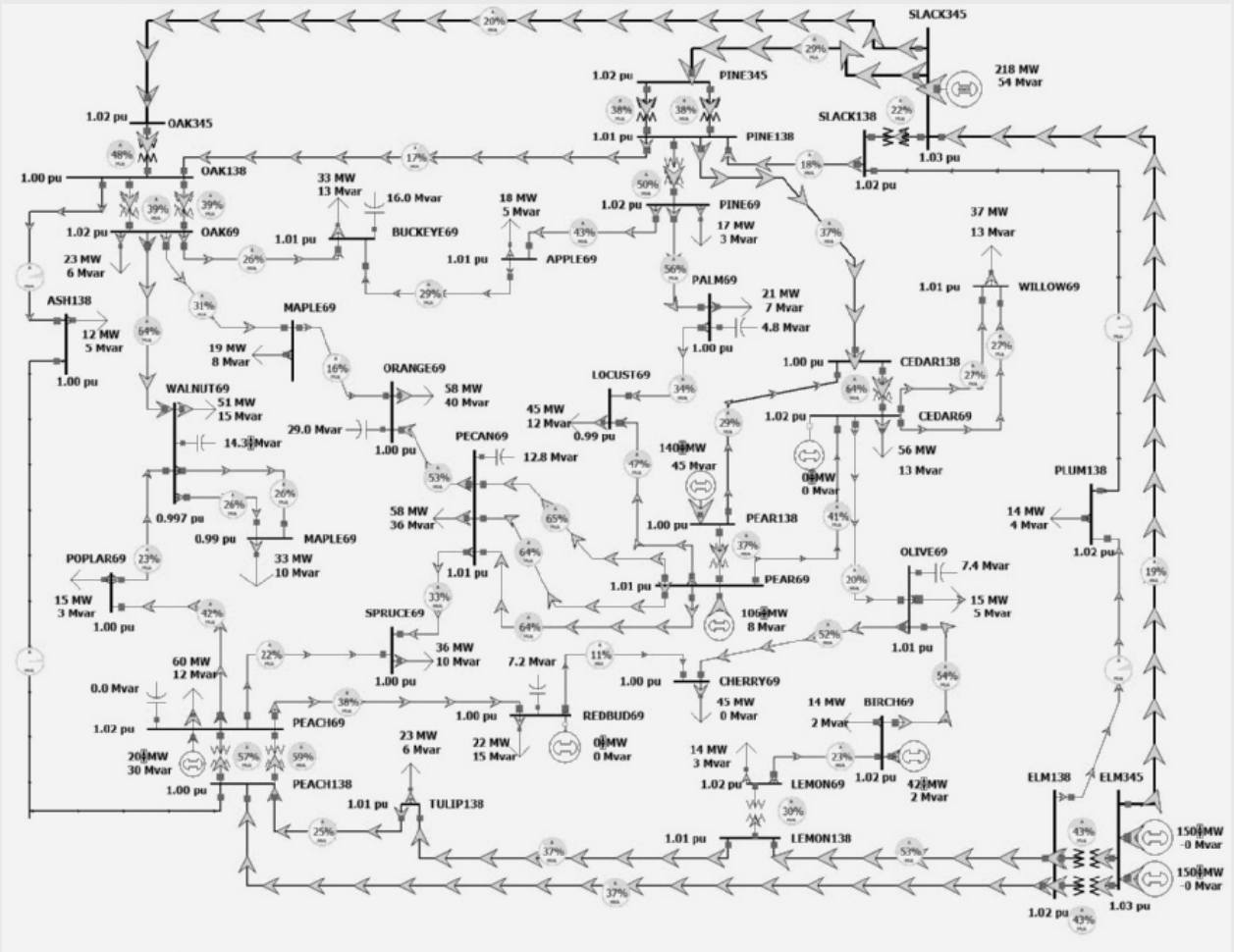

FIGURE 6.6

Screen for Example 6.13 showing the initial flows

6.7 CONTROL OF POWER FLOW

The following means are used to control system power flows:

1. Prime mover and excitation control of generators
2. Switching of shunt capacitor banks, shunt reactors, and static var systems
3. Control of tap-changing and regulating transformers

A simple model of a generator operating under balanced steady-state conditions is the Thévenin equivalent shown in Figure 6.7. V_t is the generator terminal voltage, E_g is the excitation voltage, δ is the power angle, and X_g is the positive-sequence synchronous reactance. From the figure, the generator current is

$$I = \frac{E_g e^{j\delta} - V_t}{jX_g} \tag{6.7.1}$$

and the complex power delivered by the generator is

$$\begin{aligned} S = P + jQ = V_t I^* &= V_t\left(\frac{E_g e^{-j\delta} - V_t}{-jX_g}\right) \\ &= \frac{V_t E_g(j\cos\delta + \sin\delta) - jV_t^2}{X_g} \end{aligned} \tag{6.7.2}$$

The real and reactive powers delivered are then

$$P = \text{Re}\, S = \frac{V_t E_g}{X_g}\sin\delta \tag{6.7.3}$$

$$Q = \text{Im}\, S = \frac{V_t}{X_g}(E_g\cos\delta - V_t) \tag{6.7.4}$$

Equation (6.7.3) shows that the real power P increases when the power angle δ increases. From an operational standpoint, when the prime mover increases the power input to the generator while the excitation voltage is held constant, the rotor speed increases. As the rotor speed increases, the power angle δ also increases, causing an increase in generator real power output P. There is also a decrease in reactive power output Q, given by (6.7.4). However, when δ is less than 15°, the increase in P is much larger than the decrease in Q. From the power flow standpoint, an increase in prime-move power corresponds to an increase in P at the constant-voltage bus to

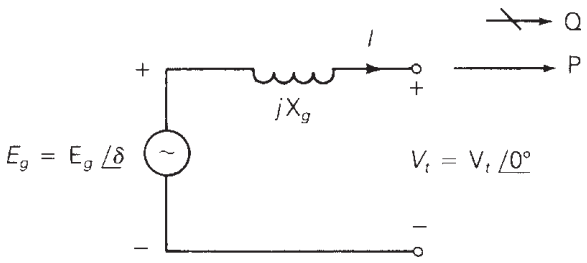

FIGURE 6.7
Generator Thévenin equivalent

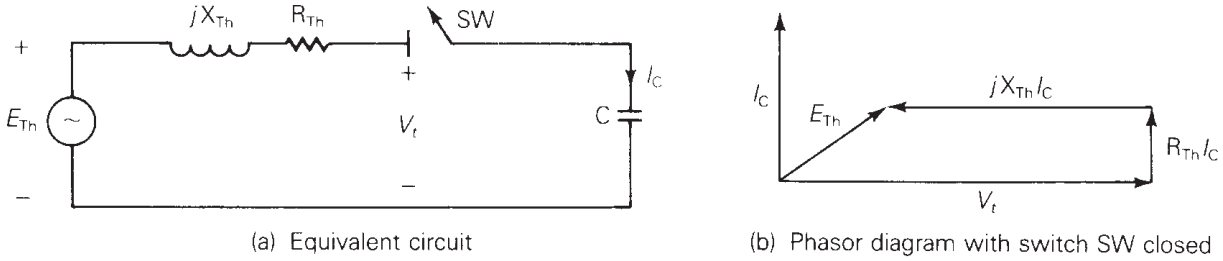

(a) Equivalent circuit (b) Phasor diagram with switch SW closed

FIGURE 6.8

Effect of adding a shunt capacitor bank to a power system bus

which the generator is connected. The power flow program computes the increase in δ along with the small change in Q.

Equation (6.7.4) shows that reactive power output Q increases when the excitation voltage E_g increases. From the operational standpoint, when the generator exciter output increases while holding the prime-mover power constant, the rotor current increases. As the rotor current increases, the excitation voltage E_g also increases, causing an increase in generator reactive power output Q. There is also a small decrease in δ required to hold P constant in (6.7.3). From the power flow standpoint, an increase in generator excitation corresponds to an increase in voltage magnitude at the constant-voltage bus to which the generator is connected. The power flow program computes the increase in reactive power Q supplied by the generator along with the small change in δ.

Figure 6.8 shows the effect of adding a shunt capacitor bank to a power system bus. The system is modeled by its Thévenin equivalent. Before the capacitor bank is connected, the switch SW is open and the bus voltage equals E_{Th}. After the bank is connected, SW is closed, and the capacitor current I_C leads the bus voltage V_t by 90°. The phasor diagram shows that V_t is larger than E_{Th} when SW is closed. From the power flow standpoint, the addition of a shunt capacitor bank to a load bus corresponds to the addition of a negative reactive load, since a capacitor absorbs negative reactive power. The power flow program computes the increase in bus voltage magnitude along with the small change in δ. Similarly, the addition of a shunt reactor corresponds to the addition of a positive reactive load, wherein the power flow program computes the decrease in voltage magnitude.

Tap-changing and voltage-magnitude-regulating transformers are used to control bus voltages as well as reactive power flows on lines to which they are connected. Similarly, phase-angle regulating transformers are used to control bus angles as well as real power flows on lines to which they are connected. Both tap-changing and regulating transformers are modeled by a transformer with an off-nominal turns ratio c (Figure 3.25). From the power flow standpoint, a change in tap setting or voltage regulation corresponds to a change in c. The power flow program computes the changes in $\boldsymbol{Y}_{\text{bus}}$, bus voltage magnitudes and angles, and branch flows.

Besides the above controls, the power flow program can be used to investigate the effect of switching in or out lines, transformers, loads, and generators. Proposed

system changes to meet future load growth, including new transmission, new transformers, and new generation can also be investigated. Power flow design studies are normally conducted by trial and error. Using engineering judgment, adjustments in generation levels and controls are made until the desired equipment loadings and voltage profile are obtained.

EXAMPLE 6.14

Power flow program: effect of shunt capacitor banks

Determine the effect of adding a 200-Mvar shunt capacitor bank at bus 2 on the power system in Example 6.9.

SOLUTION

Open PowerWorld Simulator case Example 6_14 (see Figure 6.9). This case is identical to Example 6.9 except that a 200-Mvar shunt capacitor bank has been added at bus 2. Initially this capacitor is open. Click on the capacitor's circuit to close the capacitor and then solve the case. The capacitor increases the bus 2 voltage from 0.834 per unit to a more acceptable 0.959 per unit. The insertion of the capacitor has also substantially decreased the losses, from 34.84 to 25.37 MW.

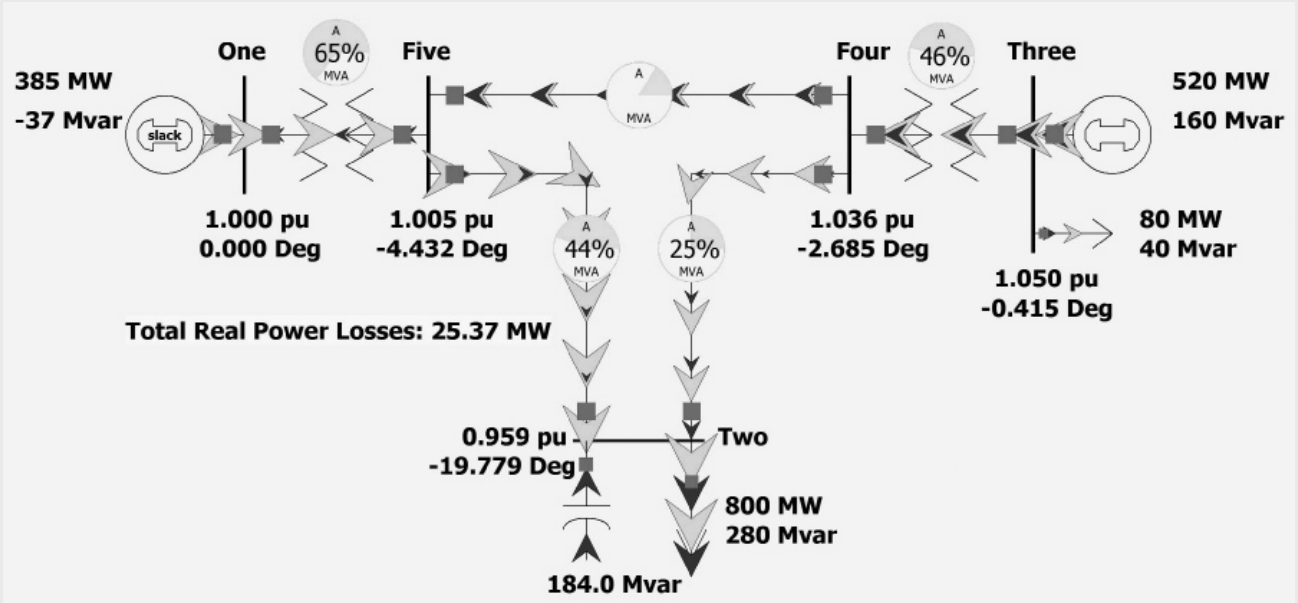

FIGURE 6.9

Screen for Example 6.14

(*Continued*)

Notice that the amount of reactive power actually supplied by the capacitor is only 184 Mvar. This discrepancy arises because a capacitor's reactive output varies with the square of the terminal voltage, $Q_{cap} = V_{cap}^2/X_c$ (see 2.3.5). A capacitor's Mvar rating is based on an assumed voltage of 1.0 per unit.

EXAMPLE 6.15

PowerWorld Simulator Case Example 6_15 (see Figure 6.10) modifies the Example 6.13 case by (1) opening one of the 138/69 kV transformers at the PEACH substation and (2) opening the 69-kV transmission line between CHERRY69 and OLIVE69. This causes a flow of 116 MVA on the remaining 138/69 kV

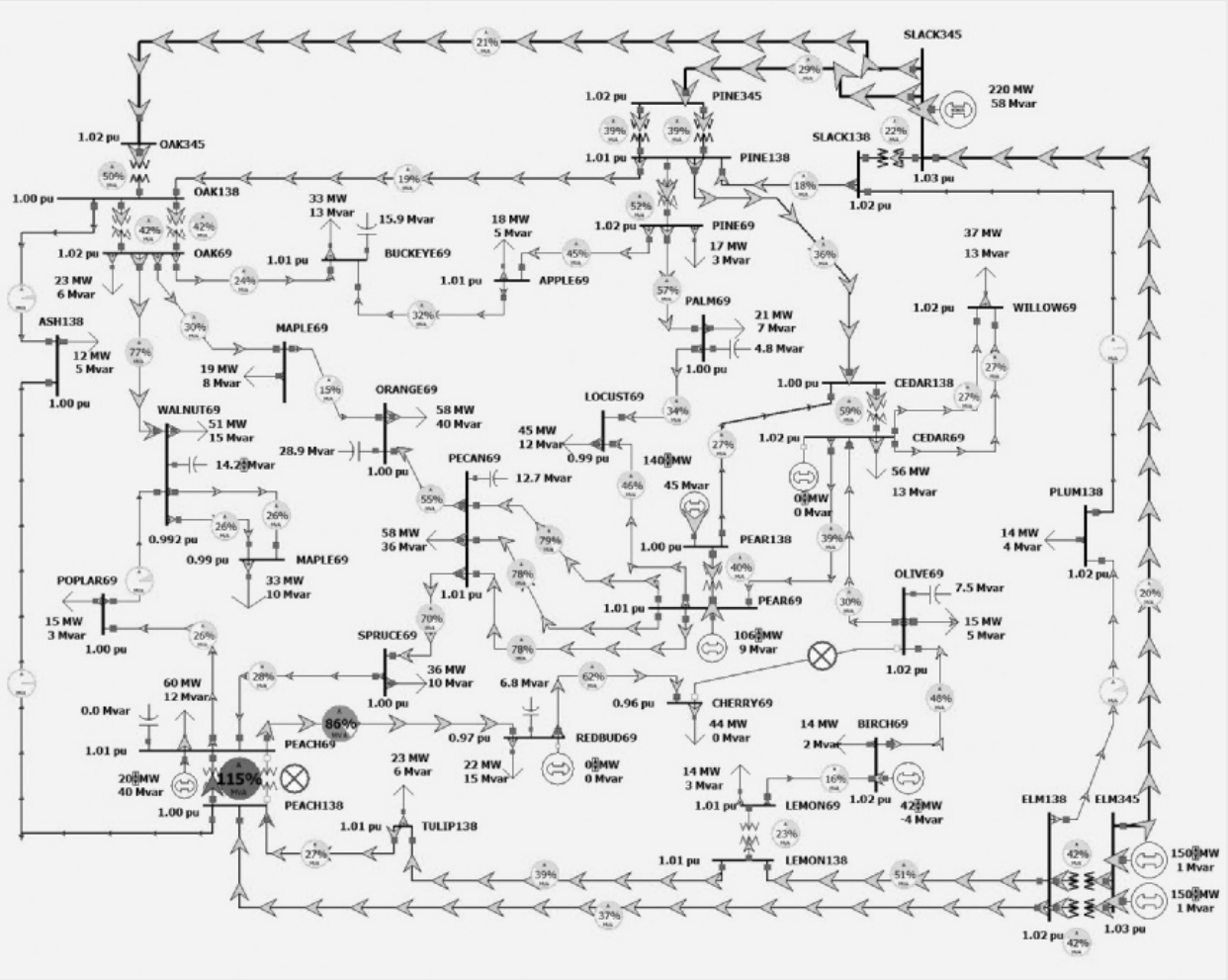

FIGURE 6.10

Screen for Example 6.15

transformer at PEACH. Since this transformer has a limit of 101 MVA, it results in an overload at 115%. Redispatch the generators in order to remove this overload.

SOLUTION

There are a number of solutions to this problem and several solution techniques. One solution technique would be to use engineering intuition, along with a trial-and-error approach (see Figure 6.11). Since the overload is from the 138 kV level to the 69 kV level and there is a generator directly connected to at the PEACH 69 kV bus, it stands to reason that increasing this generation would decrease the overload. Using this approach, the overload is removed by increasing the PEACH generation until the transformer flow is reduced to 100%. This occurs when the generation is increased from 20 MW to 51 MW. Notice that as the generation is

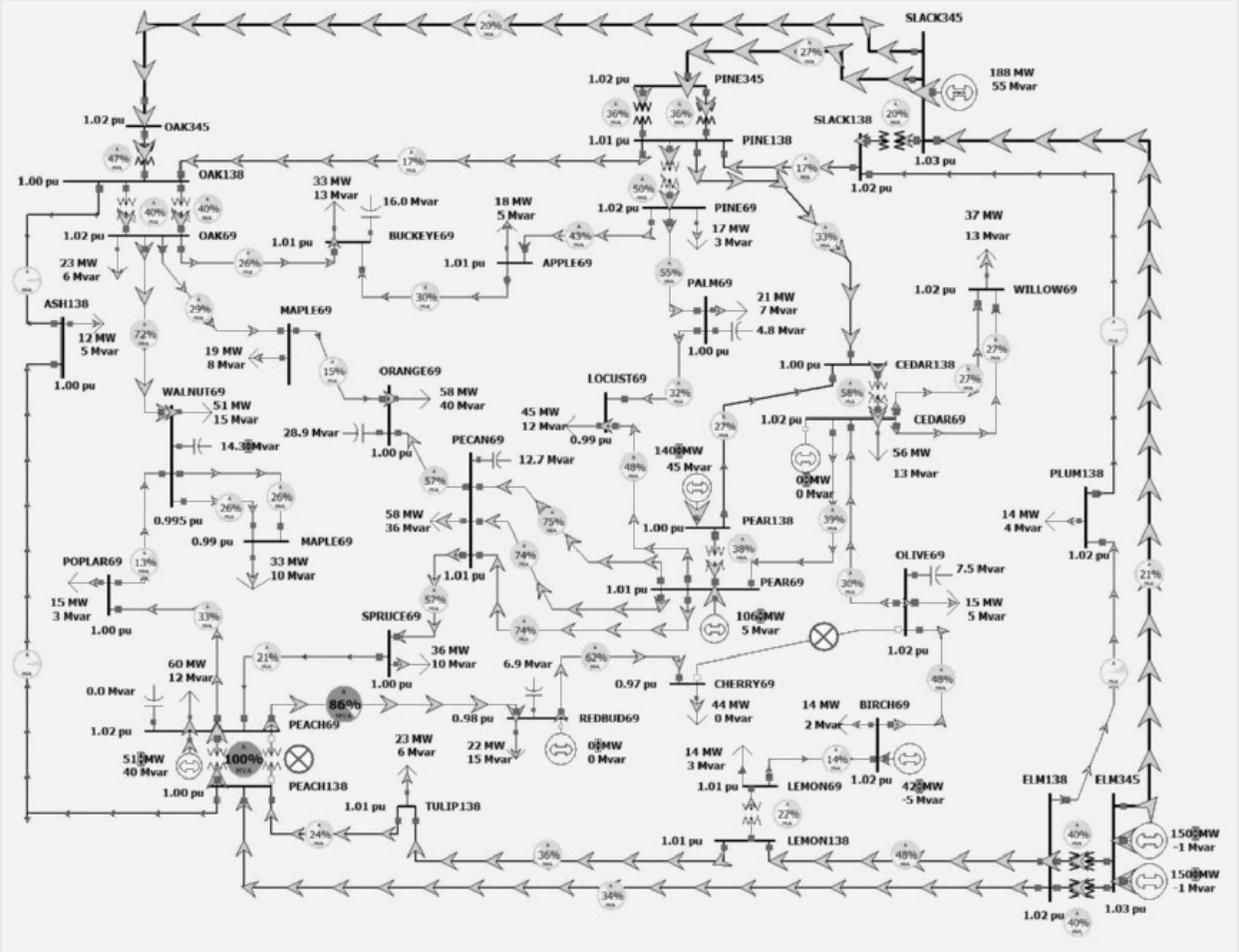

FIGURE 6.11

A solution to Example 6.15

(*Continued*)

increased, the slack bus (SLACK345) generation automatically decreases in order to satisfy the requirement that total system load plus losses must be equal to total generation.

An alternative possible solution is seen by noting that, since the overload is caused by power flowing from the 138 kV bus, decreasing the generation at ELM345 might also decrease this flow. This is indeed the case, but now the trial-and-error approach requires a substantial amount of work and ultimately doesn't solve the problem. Even when the total ELM345 generation is decreased from 300 MW to 0 MW, the overload is still present, albeit with its percentage decreased to 105%.

Another solution approach would be to first determine the generators with the most sensitivity to this violation and then adjust these (see Figure 6.12). This

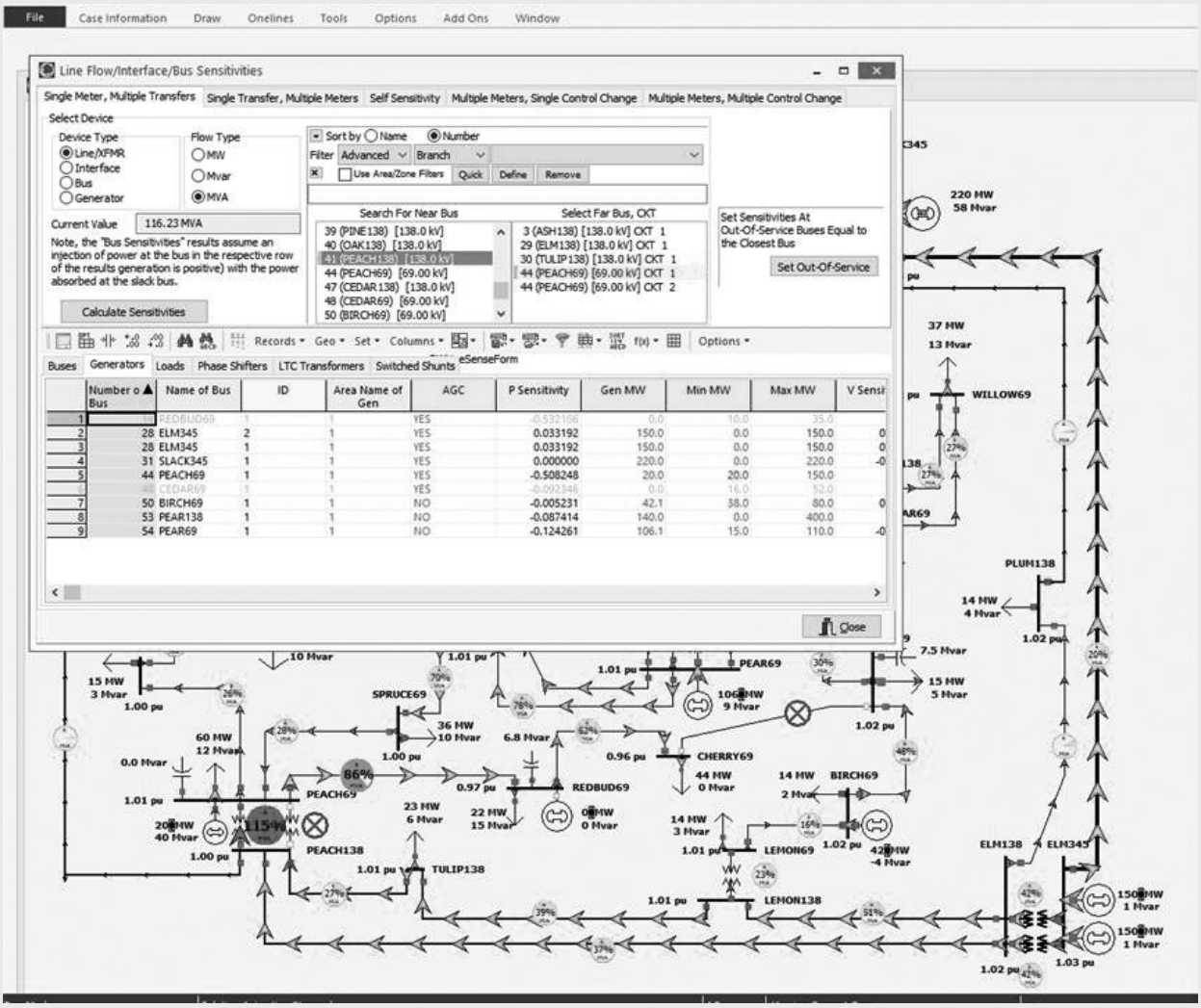

FIGURE 6.12

Example 6.15 Flow Sensitivities Dialog

can be done in PowerWorld Simulator by selecting **Tools, Sensitivities, Flows and Voltage Sensitivities** to calculate sensitivities. On the top of the page, select the PEACH138 to PEACH69 circuit 1 transformer; then click on the **Calculate Sensitivities** button, and select the Generator Sensitivities tab towards the bottom of the dialog. The "P Sensitivity" field tells how increasing the output of each generator by one MW would affect the MVA flow on this transformer. Note that the sensitivity for the PEACH69 generator is −0.508, indicating that if this generation is increased by 1 MW, the transformer MVA flow would decrease by 0.508 MVA. Hence, in order to decrease the flow by 15.2 MVA, increase the PEACH69 generator by 30 MW, which is exactly what was gotten by the trial-and-error approach. It is also clear that the ELM345 generators, with a sensitivity of just 0.033, would be relatively ineffective. In actual power system operation, these sensitivities, known as generator shift factors, are used extensively. These sensitivities are also used in the Optimal Power Flow (introduced in Section 6.13).

6.8 SPARSITY TECHNIQUES

A typical large power system has an average of fewer than three lines connected to each bus. As such, each row of $\boldsymbol{Y}_{\text{bus}}$ has an average of fewer than four nonzero elements: one off-diagonal for each line and the diagonal. Such a matrix, which has only a few nonzero elements, is said to be *sparse*.

Newton-Raphson power flow programs employ sparse matrix techniques to reduce computer storage and time requirements [2]. These techniques include compact storage of $\boldsymbol{Y}_{\text{bus}}$ and $\mathbf{J}(i)$ and reordering of buses to avoid fill-in of $\mathbf{J}(i)$ during Gauss elimination steps. Consider the following matrix:

$$\mathbf{S} = \begin{bmatrix} 1.0 & -1.1 & -2.1 & -3.1 \\ -4.1 & 2.0 & 0 & -5.1 \\ -6.1 & 0 & 3.0 & 0 \\ -7.1 & 0 & 0 & 4.0 \end{bmatrix} \tag{6.8.1}$$

One method for compact storage of S consists of the following four vectors:

$$\mathbf{DIAG} = [1.0\ 2.0\ 3.0\ 4.0] \tag{6.8.2}$$

$$\mathbf{OFFDIAG} = [1.1\ -2.1\ -3.1\ -4.1\ -5.1\ -6.1\ -7.1] \tag{6.8.3}$$

$$\mathbf{COL} = [2\ 3\ 4\ 1\ 4\ 1\ 1] \tag{6.8.4}$$

$$\mathbf{ROW} = [3\ 2\ 1\ 1] \tag{6.8.5}$$

DIAG contains the ordered diagonal elements and **OFFDIAG** contains the nonzero off-diagonal elements of **S**. **COL** contains the column number of each off-diagonal element. For example, the *fourth* element in **COL** is 1, indicating that the *fourth* element of **OFFDIAG**, −4.1, is located in column 1. **ROW** indicates the number of off-diagonal elements in each row of **S**. For example, the *first* element of **ROW** is 3, indicating the *first* three elements of **OFFDIAG**, −1.1, −2.1, and −3.1, are located in the *first* row. The *second* element of **ROW** is 2, indicating the next two elements of **OFFDIAG**, −4.1 and −5.1, are located in the *second* row. The **S** matrix can be completely reconstructed from these four vectors. Note that the dimension of **DIAG** and **ROW** equals the number of diagonal elements of **S**, whereas the dimension of **OFFDIAG** and **COL** equals the number of nonzero off-diagonals.

Now assume that computer storage requirements are 4 bytes to store each magnitude and 4 bytes to store each phase entry in $\boldsymbol{Y}_{\text{bus}}$ in an N-bus power system. Also assume $\boldsymbol{Y}_{\text{bus}}$ has an average of $3N$ nonzero off-diagonals (three lines per bus) along with its N diagonals. Using the preceding compact storage technique, $(4 + 4)$ $3N = 24N$ bytes are required for **OFFDIAG** and $(4 + 4)N = 8N$ bytes for **DIAG**. Also, assuming 2 bytes to store each integer, $6N$ bytes are required for **COL** and $2N$ bytes for **ROW**. Total computer memory required is then $(24 + 8 + 6 + 2)N = 40N$ bytes with compact storage of $\boldsymbol{Y}_{\text{bus}}$, compared to $8N^2$ bytes without compact storage. For a 1000-bus power system, this means 40 instead of 8000 kilobytes to store $\boldsymbol{Y}_{\text{bus}}$.

The Jacobian matrix is also sparse. From Table 6.5, whenever $Y_{kn} = 0$, $\text{J1}_{kn} = \text{J2}_{kn} = \text{J3}_{kn} = \text{J4}_{kn} = 0$. Compact storage of **J** for a 30,000-bus power system requires less than 10 megabytes with the above assumptions.

The other sparsity technique is to reorder buses. Suppose Gauss elimination is used to triangularize **S** in (6.8.1). After one Gauss elimination step, as described in Section 6.1, the result is

$$\mathbf{S}^{(1)} = \begin{bmatrix} 1.0 & -1.1 & -2.1 & -3.1 \\ 0 & -2.51 & -8.61 & -7.61 \\ 0 & -6.71 & -9.81 & -18.91 \\ 0 & -7.81 & -14.91 & -18.01 \end{bmatrix} \tag{6.8.6}$$

Note that the zeros in columns 2, 3, and 4 of **S** are filled in with nonzero elements in $\mathbf{S}^{(1)}$. The original degree of sparsity is lost.

One simple reordering method is to start with those buses having the fewest connected branches and to end with those having the most connected branches. For example, **S** in (6.8.1) has three branches connected to bus 1 (three off-diagonals in row 1), two branches connected to bus 2, and one branch connected to buses 3 and 4. Reordering the buses 4, 3, 2, 1 instead of 1, 2, 3, 4 results in

$$\mathbf{S}_{\text{recordered}} = \begin{bmatrix} 4.0 & 0 & 0 & -7.1 \\ 0 & 3.0 & 0 & -6.1 \\ -5.1 & 0 & 2.0 & -4.1 \\ -3.1 & -2.1 & -1.1 & 1.0 \end{bmatrix} \tag{6.8.7}$$

Now, after one Gauss elimination step,

$$\mathbf{S}^{(1)}_{\text{recorderd}} = \begin{bmatrix} 4.0 & 0 & 0 & -7.1 \\ 0 & 3.0 & 0 & -6.1 \\ 0 & 0 & 2.0 & -13.15 \\ 0 & -2.1 & -1.1 & -4.5025 \end{bmatrix} \tag{6.8.8}$$

Note that the original degree of sparsity is not lost in (6.8.8).

Reordering buses according to the fewest connected branches can be performed once, before the Gauss elimination process begins. Alternatively, buses can be renumbered during each Gauss elimination step in order to account for changes during the elimination process.

Sparsity techniques similar to those described in this section are a standard feature of today's Newton-Raphson power flow programs. As a result of these techniques, typical 30,000-bus power flow solutions require less than 10 megabytes of storage, less than one second per iteration of computer time, and less than 10 iterations to converge.

EXAMPLE 6.16

Sparsity in a 37-bus system

To see a visualization of the sparsity of the power flow $\boldsymbol{Y}_{\text{bus}}$ and Jacobian matrices in a *37*-bus system, open PowerWorld Simulator case Example 6_13.
Select **Case Information, Solution Details, Ybus** to view the bus admittance matrix. Then press <ctrl> Page Down to zoom the display out. Blank entries in the matrix correspond to zero entries. The 37 × 37 $\boldsymbol{Y}_{\text{bus}}$ has a total of 1369 entries, with only about 10% nonzero (see Figure 6.13). Select **Case Information, Solution Details, Power Flow Jacobian** to view the Jacobian matrix.

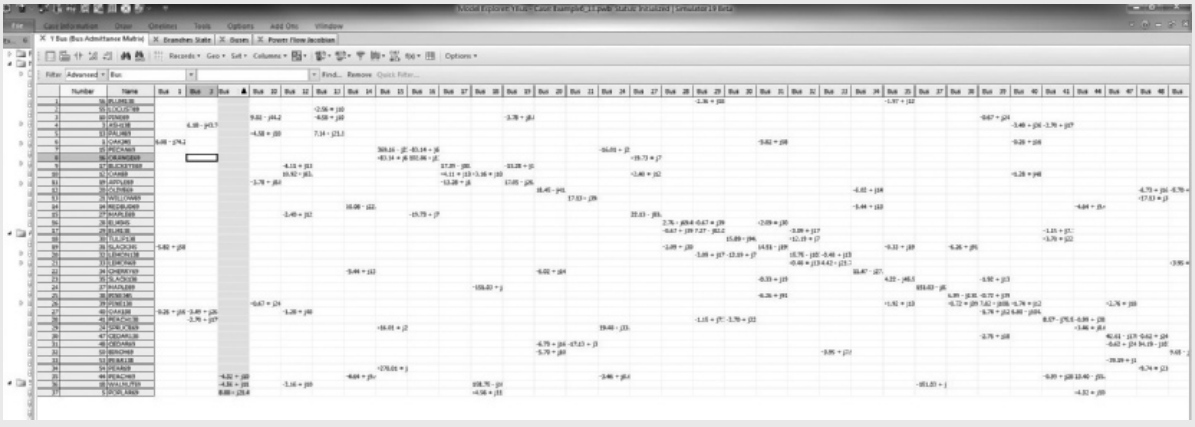

FIGURE 6.13

Screen for Example 6.16

6.9 FAST DECOUPLED POWER FLOW

Contingencies are a major concern in power system operations. For example, operating personnel need to know what power flow changes will occur due to a particular generator outage or transmission-line outage. Contingency information, when obtained in real time, can be used to anticipate problems caused by such outages and can be used to develop operating strategies to overcome the problems.

Fast power flow algorithms have been developed to give power flow solutions in seconds or less [8]. These algorithms are based on the following simplification of the Jacobian matrix. Neglecting $\mathbf{J}_2(i)$ and $\mathbf{J}_3(i)$, (6.6.6) reduces to two sets of decoupled equations:

$$\mathbf{J}_1(i)\,\boldsymbol{\Delta\delta}(i) = \Delta \mathrm{P}(i) \tag{6.9.1}$$

$$\mathbf{J}_4(i)\,\boldsymbol{\Delta V}(0) = \Delta \mathbf{Q}(i) \tag{6.9.2}$$

The computer time required to solve (6.9.1) and (6.9.2) is significantly less than that required to solve (6.6.6). Further reduction in computer time can be obtained from additional simplification of the Jacobian matrix. For example, assume $\mathrm{V}_k \approx \mathrm{V}_n \approx 1.0$ per unit and that the angle differences are small so the sin terms can be ignored. Then $\mathbf{J}_1$ and $\mathbf{J}_4$ are constant matrices whose elements in Table 6.5 are the negative of the imaginary components of $\boldsymbol{Y}_{\text{bus}}$. As such, $\mathbf{J}_1$ and $\mathbf{J}_4$ do not have to be recalculated during successive iterations.

The above simplifications can result in rapid power flow solutions for most systems. While the fast decoupled power flow usually takes more iterations to converge, it is usually significantly faster than the Newton-Raphson algorithm since the Jacobian does not need to be recomputed each iteration. And since the mismatch equations themselves have not been modified, the solution obtained by the fast decoupled algorithm is the same as that found with the Newton-Raphson algorithm. However, in some situations in which only an approximate power flow solution is needed, the fast decoupled approach can be used with a fixed number of iterations (typically one) to give an extremely fast, albeit approximate solution.

6.10 THE "DC" POWER FLOW

The power flow problem can be further simplified by extending the fast decoupled power flow to completely neglect the Q-V equations by assuming that the voltage magnitudes are constant at 1.0 per unit. With these simplifications, the power flow on the line from bus j to bus k with reactance X_{jk} becomes

$$P_{jk} = \frac{\delta_j - \delta_k}{X_{jk}} \tag{6.10.1}$$

and the real power balance equations reduce to a completely linear problem

$$-\mathbf{B}\boldsymbol{\delta} = \mathbf{P} \tag{6.10.2}$$

where **B** is the imaginary component of the of $\boldsymbol{Y}_{\text{bus}}$ calculated neglecting line resistance and excepting the slack bus row and column and **P** is the vector of real power injections (with generation assumed positive).

Because (6.10.2) is a linear equation with a form similar to that found in solving dc resistive circuits, this technique is referred to as the dc power flow. However, in contrast to the previous power flow algorithms, the dc power flow only gives an approximate solution with the degree of approximation system dependent. Nevertheless, with the advent of power system restructuring, the dc power flow has become a commonly used analysis technique.

EXAMPLE 6.17

Determine the dc power flow solution for the five bus system from Example 6.9.

SOLUTION

With bus 1 as the system slack, the **B** matrix and **P** vector for this system are

$$\mathbf{B} = \begin{bmatrix} -30 & 0 & 10 & 20 \\ 0 & -100 & 100 & 0 \\ 10 & 100 & -150 & 40 \\ 20 & 0 & 40 & -110 \end{bmatrix} \quad \mathbf{P} = \begin{bmatrix} -8.0 \\ 4.4 \\ 0 \\ 0 \end{bmatrix}$$

$$\boldsymbol{\delta} = -\mathbf{B}^{-1}\mathbf{P} = \begin{bmatrix} -0.3263 \\ 0.0091 \\ -0.0349 \\ -0.0720 \end{bmatrix} \text{ radians} = \begin{bmatrix} -18.70 \\ 0.5214 \\ -2.000 \\ -4.125 \end{bmatrix} \text{ degrees}$$

To view this example in PowerWorld Simulator, open case Example 6_17, which has this example solved using the dc power flow (see Figure 6.14). To view the dc power flow options, select **Options, Simulator Options** to show the PowerWorld Simulator Options dialog. Then select the Power Flow Solution category and the DC Options page.

(*Continued*)

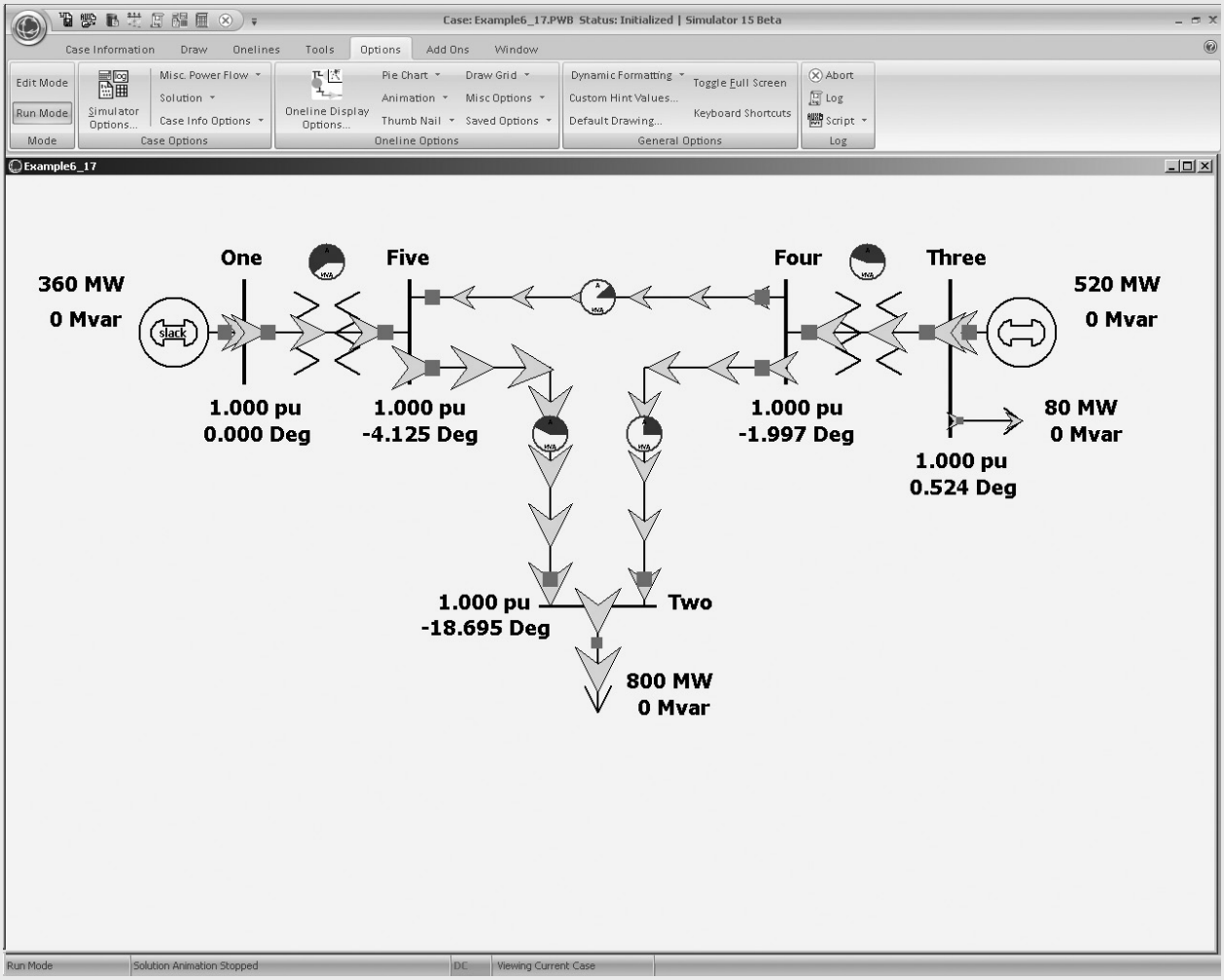

FIGURE 6.14

Screen for Example 6.17

6.11 POWER FLOW MODELING OF WIND GENERATION

As was mentioned in Chapter 1, the amount of renewable generation, particularly wind, being integrated into electric grids around the world is rapidly growing. For example, in 2013 Denmark obtained 33% of their total electric energy from wind while Spain got over 20%. In the United States the amount of wind capacity has been rapidly escalating from less than 2.5 GW in 2000 to more than 68 GW in 2015 (out of a total generation capacity of about 1065 GW), while worldwide, it was more than 360 GW in 2014.

Whereas most energy from traditional synchronous generators comes from large units with ratings of hundreds of MWs, comparatively speaking, individual wind turbine generator (WTG) power ratings are quite low, with common values for new land-based WTGs between one to three MWs, and offshore WTGs up to 6 MWs. This power is generated at low voltage (e.g., 600 V) and then usually stepped-up with a pad-mounted transformer at the base of the turbine to a distribution-level voltage (e.g., 34.5 kV). Usually dozens or even hundreds of individual WTGs are located in wind "farms" or "parks" that cover an area of many square miles, with most of the land still available for other uses such as farming. An underground and/or overhead collector system is used to transmit the power to a single interconnection point at which its voltage is stepped-up to a transmission level voltage (> 100 kV). The layout of such a system is shown in Figure 6.15.

From a power system analysis perspective for large-scale studies, the entire wind farm can usually be represented as a single equivalent generator that is either directly connected at the interconnection point transmission system bus or connected to this bus through an equivalent impedance that represents the impedance of the collector system and the step-up transformers. The parameters associated with the equivalent generator are usually just scaled values of the parameters for the individual WTGs.

There are four main types of WTGs [13,15] with more details on each type provided in Chapter 11. Here the focus is on their power flow characteristics. As is the case with traditional synchronous generators, the real power outputs for all the WTG types are considered to be a constant value in power flow studies. Of course how much real power a wind farm can actually produce at any moment depends upon the wind speed, with a typical wind speed versus power curve shown in Figure 6.16.

Type 1 WTGs are squirrel-cage induction machines. Since induction machines consume reactive power and their reactive power output cannot be independently

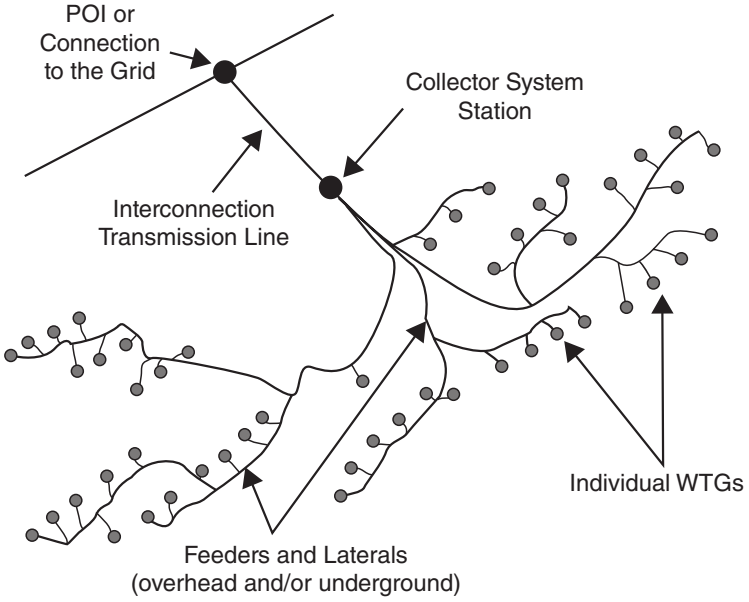

FIGURE 6.15

Wind power plant collector system topology [14] (Figure 1 from WECC Wind Generation Modeling Group, "WECC Wind Power Plant Power Flow Model Guide," WECC, May 2008, p. 2.)

FIGURE 6.16

Typical wind speed versus power curve

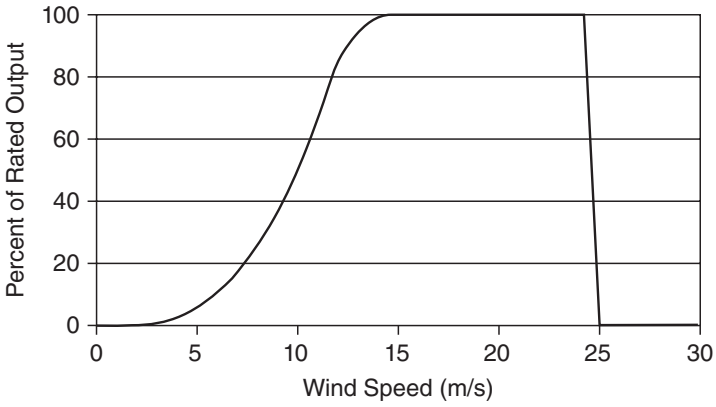

controlled, typically these machines are modeled as a constant power factor PQ bus. By themselves these machines have under-excited (consuming reactive power) power factors of between 0.85 and 0.9, but banks of switched capacitors are often used to correct the wind farm power factor. Type 2 WTGs are wound rotor induction machines in which the rotor resistance can be controlled. The advantages of this approach are discussed in Chapter 11; from a power flow perspective, they perform like Type 1 WTGs.

Most of the installed wind capacity and almost all new WTGs are either Type 3 or Type 4. Type 3 wind turbines are used to represent doubly-fed asynchronous generators (DFAGs), also sometimes referred to as doubly-fed induction generators (DFIGs). This type models induction machines in which the rotor circuit is also connected to the ac network through an ac-dc-ac converter, allowing for much greater control of the WTG. Type 4 wind turbines are fully asynchronous machines in which the full power output of the machine is coupled to the ac network through an ac-dc-ac converter. From a power flow perspective, both types are capable of full voltage control like a traditional bus generator with reactive power control between a power factor of up to ± 0.9. However, like traditional synchronous generators, how their reactive power is actually controlled depends on commercial considerations, with many generator owners desiring to operate at unity power factor to maximize their real power outputs.

6.12 ECONOMIC DISPATCH

This section describes how the real power output of a controlled generating unit is selected to meet a given load and to minimize the total operating costs. This is the *economic dispatch* problem [16]. In interconnected power systems, economic dispatch is often solved for smaller portions of the system, known as *areas*, in which the total generation in each area is controlled to match the total area load; further details are provided in Chapter 12.

This section begins by considering only fossil-fuel generating units, with no constraints on maximum and minimum generator outputs, and with no transmission losses. The economic dispatch problem is first solved for this idealized case. Then it is

expanded to include inequality constraints on generator outputs and to consider the impact of transmission losses. Finally, the dispatch of other types of units including solar and wind, nuclear, pumped-storage hydro, and hydro units is briefly discussed.

FOSSIL-FUEL UNITS, NO INEQUALITY CONSTRAINTS, NO TRANSMISSION LOSSES

Figure 6.17 shows the operating cost C_i, of a fossil-fuel generating unit versus its real power output P_i. Fuel cost is the major portion of the variable cost of operation, although other variable costs, such as maintenance, could have been included in the figure. Fixed costs, such as the capital cost of installing the unit, are not included. Only those costs that are a function of unit power output—that is, those costs that can be controlled by operating strategy—enter into the economic dispatch formulation.

In practice, C_i is constructed of piecewise continuous functions valid for ranges of output P_i based on empirical data. The discontinuities in Figure 6.17 may be due to the firing of equipment such as additional boilers or condensers as power output is increased. It is often convenient to express C_i in terms of BTU/hr, which is relatively constant over the lifetime of the unit, rather than \$/hr, which can change monthly or daily. C_i can be converted to \$/hr by multiplying the fuel input in BTU/hr by the cost of fuel in \$/BTU.

Figure 6.18 shows the unit incremental operating cost dC_i/dP_i versus unit output P_i, which is the slope or derivative of the C_i versus P_i curve in Figure 6.17. When C_i consists of only fuel costs, dC_i/dP_i is the ratio of the incremental fuel energy input in BTU to incremental energy output in kWh, which is called the incremental *heat rate.* Note that the reciprocal of the heat rate, which is the ratio of output energy to input energy, gives a measure of fuel efficiency for the unit. For the unit shown in Figure 6.17, maximum efficiency occurs at $P_i = 600$ MW, where the heat rate is $C_i/P_i = 5.4 \times 10^9/600 \times 10^3 = 9000$ BTU/kWh. The efficiency at this output is

$$\text{percentage efficency} = \left(\frac{1}{9000}\frac{\text{kWh}}{\text{BTU}}\right)\left(3413\,\frac{\text{BTU}}{\text{kWh}}\right) \times 100 = 37.92\%$$

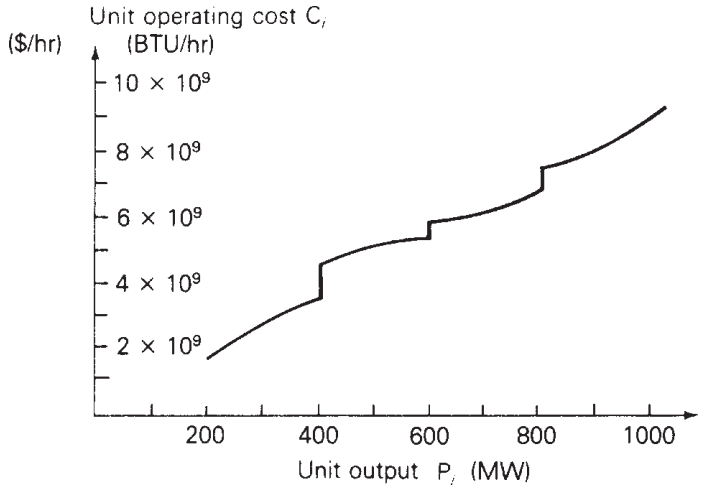

FIGURE 6.17
Unit operating cost versus real power output—fossil-fuel generating unit

FIGURE 6.18

Unit incremental operating cost versus real power output—fossil-fuel generating unit

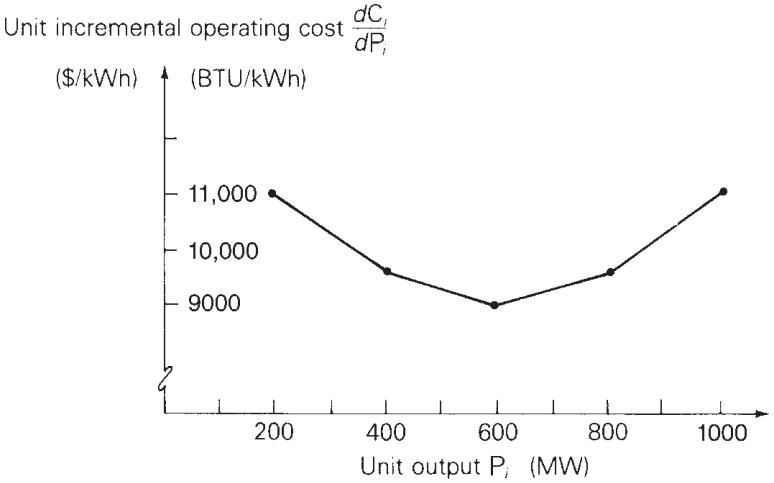

The dC_i/dP_i curve in Figure 6.18 is also represented by piecewise continuous functions valid for ranges of output P_i. For analytical work, the actual curves are often approximated by straight lines. The ratio dC_i/dP_i can also be converted to \$/kWh by multiplying the incremental heat rate in BTU/kWh by the cost of fuel in \$/BTU.

For the area of an interconnected power system consisting of N units operating on economic dispatch, the total variable cost C_T of operating these units is

$$C_T = \sum_{i=i}^{N} C_i$$

$$= C_1(P_1) + C_2(P_2) + \cdots + C_N(P_N) \quad \$/\text{hr} \tag{6.12.1}$$

where C_i, expressed in \$/hr, includes fuel cost as well as any other variable costs of unit i. Let P_T equal the total load demand in the area. Neglecting transmission losses.

$$P_1 + P_2 + \cdots + P_N = P_T \tag{6.12.2}$$

Due to relatively slow changes in load demand, P_T may be considered constant for periods of 2 to 10 minutes. The economic dispatch problem can be stated as follows:

> Find the values of unit outputs $P_1, P_2, \ldots, P_N$ that minimize C_T given by (6.12.1), subject to the equality constraint given by (6.12.2).

A criterion for the solution to this problem is: All units on economic dispatch should operate at equal incremental operating cost. That is,

$$\frac{dC_1}{dP_1} = \frac{dC_2}{dP_2} = \cdots = \frac{dC_N}{dP_N} \tag{6.12.3}$$

An intuitive explanation of this criterion is the following. Suppose one unit is operating at a higher incremental operating cost than the other units. If the output power of that unit is reduced and transferred to units with lower incremental operating costs, then the total operating cost C_T decreases. That is, reducing the output of the unit with the *higher* incremental cost results in a *greater cost decrease* than the

cost increase of adding that same output reduction to units with lower incremental costs. Therefore, all units must operate at the same incremental operating cost (the economic dispatch criterion).

A mathematical solution to the economic dispatch problem also can be given. The minimum value of C_T occurs when the total differential dC_T is zero. That is,

$$dC_T = \frac{\partial C_T}{\partial P_1} dP_1 + \frac{\partial C_T}{\partial P_2} dP_2 + \cdots + \frac{\partial C_T}{\partial P_N} dP_N = 0 \tag{6.12.4}$$

Using (6.12.1), (6.12.4) becomes

$$dC_T = \frac{dC_1}{dP_1} dP_1 + \frac{dC_2}{dP_2} dP_2 + \cdots + \frac{dC_N}{dP_N} dP_N = 0 \tag{6.12.5}$$

Also, assuming P_T is constant, the differential of (6.12.2) is

$$dP_1 + dP_2 + \cdots + dP_N = 0 \tag{6.12.6}$$

Multiplying (6.12.6) by λ and subtracting the resulting equation from (6.12.5),

$$\left(\frac{dC_1}{dP_1} - \lambda\right) dP_1 + \left(\frac{dC_2}{dP_2} - \lambda\right) dP_2 + \cdots + \left(\frac{dC_N}{dP_N} - \lambda\right) dP_N = 0 \tag{6.12.7}$$

Equation (6.12.7) is satisfied when each term in parentheses equals zero. That is,

$$\frac{dC_1}{dP_1} = \frac{dC_2}{dP_2} = \cdots = \frac{dC_N}{dP_N} = \lambda \tag{6.12.8}$$

Therefore, all units have the same incremental operating cost, denoted here by λ, in order to minimize the total operating cost C_T.

EXAMPLE 6.18

Economic dispatch solution neglecting generator limits and line losses

An area of an interconnected power system has two fossil-fuel units operating on economic dispatch. The variable operating costs of these units are given by

$$C_1 = 10P_1 + 8 \times 10^{-3}P_1^2 \quad \$/\text{hr}$$

$$C_2 = 8P_2 + 9 \times 10^{-3}P_2^2 \quad \$/\text{hr}$$

where P_1 and P_2 are in megawatts. Determine the power output of each unit, the incremental operating cost, and the total operating cost C_T that minimizes C_T as the total load demand P_T varies from 500 to 1500 MW. Generating unit inequality constraints and transmission losses are neglected.

(*Continued*)

SOLUTION

The incremental operating costs of the units are

$$\frac{dC_1}{dP_1} = 10 + 16 \times 10^{-3}P_1 \quad \$/\text{MWh}$$

$$\frac{dC_2}{dP_2} = 8 + 18 \times 10^{-3}P_2 \quad \$/\text{MWh}$$

Using (6.12.8), the minimum total operating cost occurs when

$$\frac{dC_1}{dP_1} = 10 + 16 \times 10^{-3}P_1 = \frac{dC_2}{dP_2} = 8 + 18 \times 10^{-3}P_2$$

Using $P_2 = P_T - P_1$, the preceding equation becomes

$$10 + 16 \times 10^{-3}P_1 = 8 + 18 \times 10^{-3}(P_T - P_1)$$

Solving for P_1,

$$P_1 = \frac{18 \times 10^{-3}P_T - 2}{34 \times 10^{-3}} = 0.5294P_T - 58.82 \quad \text{MW}$$

Also, the incremental operating cost when C_T is minimized is

$$\frac{dC_2}{dP_2} = \frac{dC_1}{dP_1} = 10 + 16 \times 10^{-3}P_1 = 10 + 16 \times 10^{-3}(0.5294P_T - 58.82)$$

$$= 9.0589 + 8.4704 \times 10^{-3}P_T \quad \$/\text{MWh}$$

P_T MW	P_1 MW	P_2 MW	dC_i/dP_1 \$/MWh	C_T \$/hr
500	206	294	13.29	5529
600	259	341	14.14	6901
700	312	388	14.99	8358
800	365	435	15.84	9899
900	418	482	16.68	11,525
1000	471	529	17.53	13,235
1100	524	576	18.38	15,030
1200	576	624	19.22	16,910
1300	629	671	20.07	18,875
1400	682	718	20.92	20,924
1500	735	765	21.76	23,058

TABLE 6.9

Economic dispatch solution for Example 6.18

and the minimum total operating cost is

$$C_T = C_1 + C_2 = (10P_1 + 8 \times 10^{-3}P_1^2) + (8P_2 + 9 \times 10^{-3}P_2^2) \quad \$/hr$$

The economic dispatch solution is shown in Table 6.9 for values of P_T from 500 to 1500 MW.

EFFECT OF INEQUALITY CONSTRAINTS

Each generating unit must not operate above its rating or below some minimum value. That is.

$$P_{i\min} < P_i < P_{i\max} \qquad i = 1, 2, \ldots, N \tag{6.12.9}$$

Other inequality constraints also may be included in the economic dispatch problem. For example, some unit outputs may be restricted so that certain transmission lines or other equipment are not overloaded. Also, under adverse weather conditions, generation at some units may be limited to reduce emissions.

When inequality constraints are included, modify the economic dispatch solution as follows. If one or more units reach their limit values, then these units are held at their limits, and the remaining units operate at equal incremental operating cost λ. The incremental operating cost of the area equals the common λ for the units that are not at their limits.

EXAMPLE 6.19

Economic dispatch solution including generator limits

Rework Example 6.18 if the units are subject to the following inequality constraints:

$$100 \leqq P_1 \leqq 600 \quad MW$$

$$400 \leqq P_2 \leqq 1000 \quad MW$$

SOLUTION

At light loads, unit 2 operates at its lower limit of 400 MW, where its incremental operating cost is $dC_2/dP_2 = 15.2$ \$/MWh. Additional load comes from unit 1 until $dC_1/dP_1 = 15.2$ \$/MWh, or

$$\frac{dC_1}{dP_1} = 10 + 16 \times 10^{-3}P_1 = 15.2$$

$$P_1 = 325 \quad MW$$

(*Continued*)

For P_T less than 725 MW, where P_1 is less than 325 MW, the incremental operating cost of the area is determined by unit 1 alone.

At heavy loads, unit 1 operates at its upper limit of 600 MW, where its incremental operating cost is $dC_1/dP_1 = 19.60$ \$/MWh. Additional load comes from unit 2 for all values of dC_2/dP_2 greater than 19.60 \$/MWh. At $dC_2/dP_2 =$ 19.60 \$/MWh,

$$\frac{dC_2}{dP_2} = 8 + 18 \times 10^{-3} P_2 = 19.60$$

$$P_2 = 644 \quad \text{MW}$$

For P_T greater than 1244 MW, where P_2 is greater than 644 MW, the incremental operating cost of the area is determined by unit 2 alone.

For $725 < P_T < 1244$ MW, neither unit has reached a limit value, and the economic dispatch solution is the same as that given in Table 6.9.

The solution to this example is summarized in Table 6.10 for values of P_T from 500 to 1500 MW.

P_T MW	P_1 MW	P_2 MW	dC/dP \$/MWh	C_T \$/hr
500	100	400	$\frac{dC_1}{dP_1}$ 11.60	5720
600	200	400	13.20	6960
700	300	400	14.80	8360
725	325	400	15.20	8735
800	365	435	15.84	9899
900	418	482	16.68	11,525
1000	471	529	17.53	13,235
1100	524	576	18.38	15,030
1200	576	624	19.22	16,910
1244	600	644	$\frac{dC_2}{dP_2}$ 19.60	17,765
1300	600	700	20.60	18,890
1400	600	800	22.40	21,040
1500	600	900	24.20	23,370

TABLE 6.10
Economic dispatch solution for Example 6.19

EXAMPLE 6.20

PowerWorld Simulator–economic dispatch, including generator limits

PowerWorld Simulator case Example 6_20 uses a five-bus, three-generator lossless case to show the interaction between economic dispatch and the transmission

system (see Figure 6.19). The variable operating costs for each of the units are given by

$C_1 = 10P_1 + 0.016P_1^2$ \$/hr

$C_2 = 8P_2 + 0.018P_2^2$ \$/hr

$C_4 = 12P_4 + 0.018P_4^2$ \$/hr

where P_1, P_2, and P_4 are the generator outputs in megawatts. Each generator has minimum/maximum limits of

$100 \leq P_1 \leq 400$ MW

$150 \leq P_2 \leq 500$ MW

$50 \leq P_4 \leq 300$ MW

In addition to solving the power flow equations, PowerWorld Simulator can simultaneously solve the economic dispatch problem to optimally allocate the generation in an area. To turn on this option, select **Case Information, Aggregation, Areas…** to view a list of each of the control areas in a case (just one in this example). Then toggle the AGC Status field to ED. Now anytime the power flow equations are solved, the generator outputs are also changed using the economic dispatch.

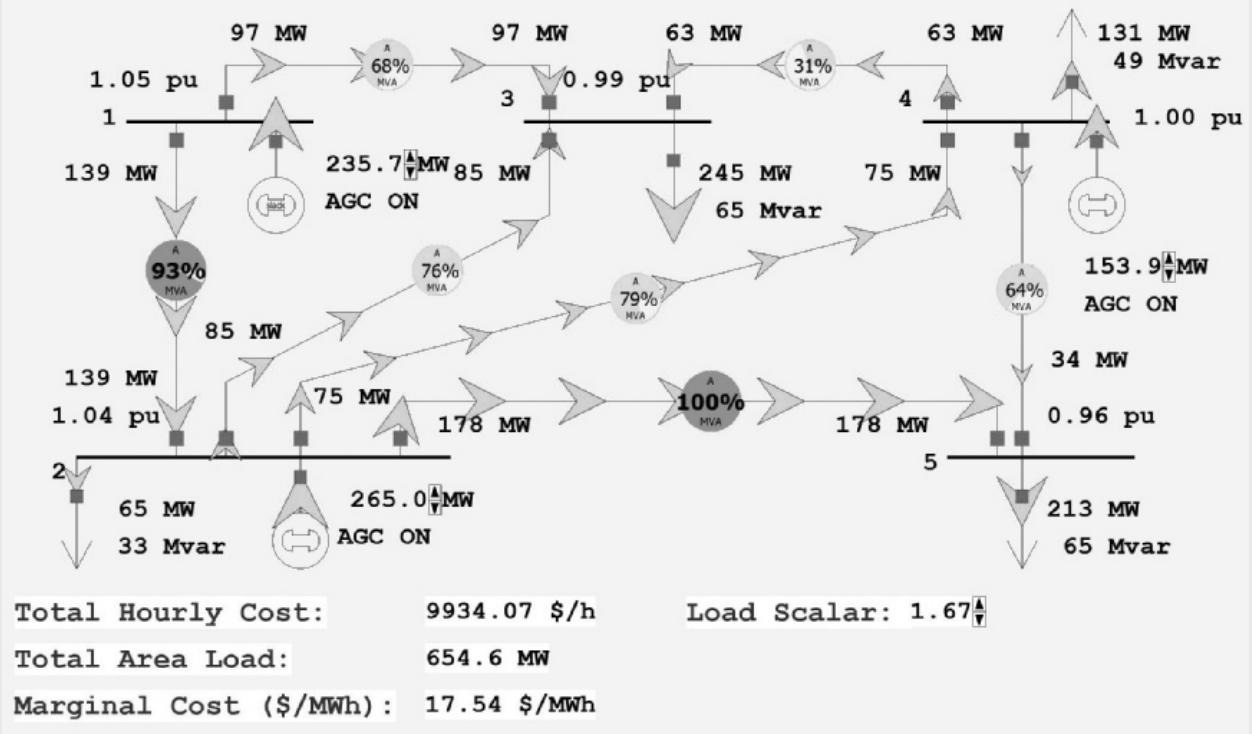

FIGURE 6.19

Example 6.20 with maximum economic loading

(*Continued*)

Initially, the case has a total load of 392 MW with an economic dispatch of $P_1 = 141$ MW, $P_2 = 181$, and $P_4 = 70$, and an incremental operating cost, λ, of 14.52 \$/MWh. To view a graph showing the incremental cost curves for all of the area generators, right-click on any generator to display the generator's local menu, and then select All Area Gen IC Curves (right-click on the graph's axes to change their scaling).

To see how changing the load impacts the economic dispatch and power flow solutions, first select **Tools, Play** to begin the simulation. Then, on the oneline, click on the up/down arrows next to the Load Scalar field. This field is used to scale the load at each bus in the system. Notice that the change in the Total Hourly Cost field is well approximated by the change in the load multiplied by the incremental operating cost.

Determine the maximum amount of load this system can supply without overloading any transmission line with the generators dispatched using economic dispatch.

SOLUTION

The maximum system economic loading is determined numerically to be 655 MW (which occurs with a Load Scalar of 1.67) with the line from bus 2 to bus 5 being the critical element.

EFFECT OF TRANSMISSION LOSSES

Although one unit may be very efficient with a low incremental operating cost, it also may be located far from the load center. The transmission losses associated with this unit may be so high that the economic dispatch solution requires the unit to decrease its output, while other units with higher incremental operating costs but lower transmission losses increase their outputs.

When transmission losses are included in the economic dispatch problem, (6.12.2) becomes

$$P_1 + P_2 + \cdots + P_N - P_L = P_T \tag{6.12.10}$$

where P_T is the total load demand and P_L is the total transmission loss in the area. In general, P_L is not constant but depends on the unit outputs P_1, P_2, …, P_N, The total differential of (6.12.10) is

$$(dP_1 + dP_2 + \cdots + dP_N) - \left(\frac{\partial P_L}{\partial P_1} dP_1 + \frac{\partial P_L}{\partial P_2} dP_2 + \cdots + \frac{\partial P_L}{\partial P_N} dP_N\right) = 0 \tag{6.12.11}$$

Multiplying (6.12.11) by λ and subtracting the resulting equation from (6.12.5),

$$\left(\frac{dC_1}{dP_1} + \lambda\frac{\partial P_L}{\partial P_1} - \lambda\right) dP_1 + \left(\frac{dC_2}{dP_2} + \lambda\frac{\partial P_L}{\partial P_2} - \lambda\right) dP_2$$

$$+ \cdots + \left(\frac{dC_N}{dP_N} + \lambda\frac{\partial P_L}{\partial P_N} - \lambda\right)dP_N = 0 \tag{6.12.12}$$

Equation (6.12.12) is satisfied when each term in parentheses equals zero. That is.

$$\frac{dC_i}{dP_i} + \lambda\frac{\partial P_L}{\partial P_i} - \lambda = 0$$

or

$$\lambda = \frac{dC_i}{dP_i}(L_i) = \frac{dC_i}{dP_i}\left(\frac{1}{1 - \dfrac{\partial P_L}{\partial P_i}}\right) \qquad i = 1, 2, \ldots, N \tag{6.12.13}$$

Equation (6.12.13) gives the economic dispatch criteria, including transmission losses. Each unit that is not at a limit value operates such that its incremental operating cost dC_i/dP_i multiplied by the *penalty factor* L_i is the same. Note that when transmission losses are negligible $\partial P_L/\partial P_i = 0$, $L_i = 1$, and (6.12.13) reduces to (6.12.8).

EXAMPLE 6.21

Economic dispatch solution including generator limits and line losses

Total transmission losses for the power system area given in Example 6.18 are given by

$$P_L = 1.5 \times 10^{-4}P_1^2 + 2 \times 10^{-5}P_1P_2 + 3 \times 10^{-5}P_2^2 \ \text{MW}$$

where P_1 and P_2 are given in megawatts. Determine the output of each unit, total transmission losses, total load demand, and total operating cost C_T when the area $\lambda = 16.00$ \$/MWh.

SOLUTION

Using the incremental operating costs from Example 6.18 in (6.12.13),

$$\frac{dC_1}{dP_1}\left(\frac{1}{1 - \dfrac{\partial P_L}{\partial P_1}}\right) = \frac{10 + 16 \times 10^{-3}P_1}{1 - (3 \times 10^{-4}P_1 + 2 \times 10^{-5}P_2)} = 16.00$$

$$\frac{dC_2}{dP_2}\left(\frac{1}{1 - \dfrac{\partial P_L}{\partial P_2}}\right) = \frac{8 + 18 \times 10^{-3}P_2}{1 - (6 \times 10^{-5}P_2 + 2 \times 10^{-5}P_1)} = 16.00$$

(*Continued*)

Rearranging the two equations,

$$20.8 \times 10^{-3}P_1 + 32 \times 10^{-5}P_2 = 6.00$$
$$32 \times 10^{-5}P_1 + 18.96 \times 10^{-3}P_2 = 8.00$$

Solving,

$$P_1 = 282 \quad \text{MW} \qquad P_2 = 417 \quad \text{MW}$$

Using the equation for total transmission losses,

$$P_L = 1.5 \times 10^{-4}(282)^2 + 2 \times 10^{-5}(282)(417) + 3 \times 10^{-5}(417)^2$$
$$= 19.5 \quad \text{MW}$$

From (6.12.10), the total load demand is

$$P_T = P_1 + P_2\, P_L = 282 + 417 - 19.5 = 679.5 \quad \text{MW}$$

Also, using the cost formulas given in Example 6.18, the total operating cost is

$$C_T = C_1 + C_2 = 10(282) + 8 \times 10^{-3}(282)^2 + 8(417) + 9 \times 10^{-3}(417)^2$$
$$= 8357 \quad \$/\text{h}$$

Note that when transmission losses are included, λ given by (6.12.13) is no longer the incremental operating cost of the area. Instead, λ is the unit incremental operating cost dC_i/dP_i multiplied by the unit penalty factor L_i.

EXAMPLE 6.22

PowerWorld Simulator—economic dispatch, including generator limits and line losses

This example repeats the Example 6.19 power system, except that now losses are included with each transmission line modeled with an R/X ratio of 1/3 (see Figure 6.20). The current value of each generator's loss sensitivity, $\partial P_L/\partial P_i$, is shown immediately below the generator's MW output field. Calculate the penalty factors L_i, and verify that the economic dispatch shown in the figure is optimal. Assume a Load Scalar of 1.0.

SOLUTION

From (6.12.13), the condition for optimal dispatch is

$$\lambda = dC_i/dP_i(1/(1 - \partial P_L/\partial P_i) = dC_i/dP_iL_i \qquad i = 1, 2, \ldots, N$$

with

$$L_i = 1/(1 - \partial P_L/\partial P_i)$$

Therefore, $L_1 = 1.0$, $L_2 = 0.9733$, and $L_4 = 0.9238$.

$$\text{with } P_1 = 130.1 \text{ MW}, \quad dC_1/dP_1 * L_1 = (10 + 0.032 * 130.1) * 1.0$$
$$= 14.16 \quad \$/\text{MWh}$$

$$\text{With } P_2 = 181.8 \text{ MW}, \quad dC_2/dP_2 * L_2 = (8 + 0.036 * 181.8) * 0.9733 = 14.16 \ \$/\text{MWh}$$

$$\text{With } P_4 = 92.4 \text{ MW}, \quad dC_4/dP_4 * L_4 = (12 + 0.036 * 92.4) * 0.9238 = 14.16 \ \$/\text{MWh}$$

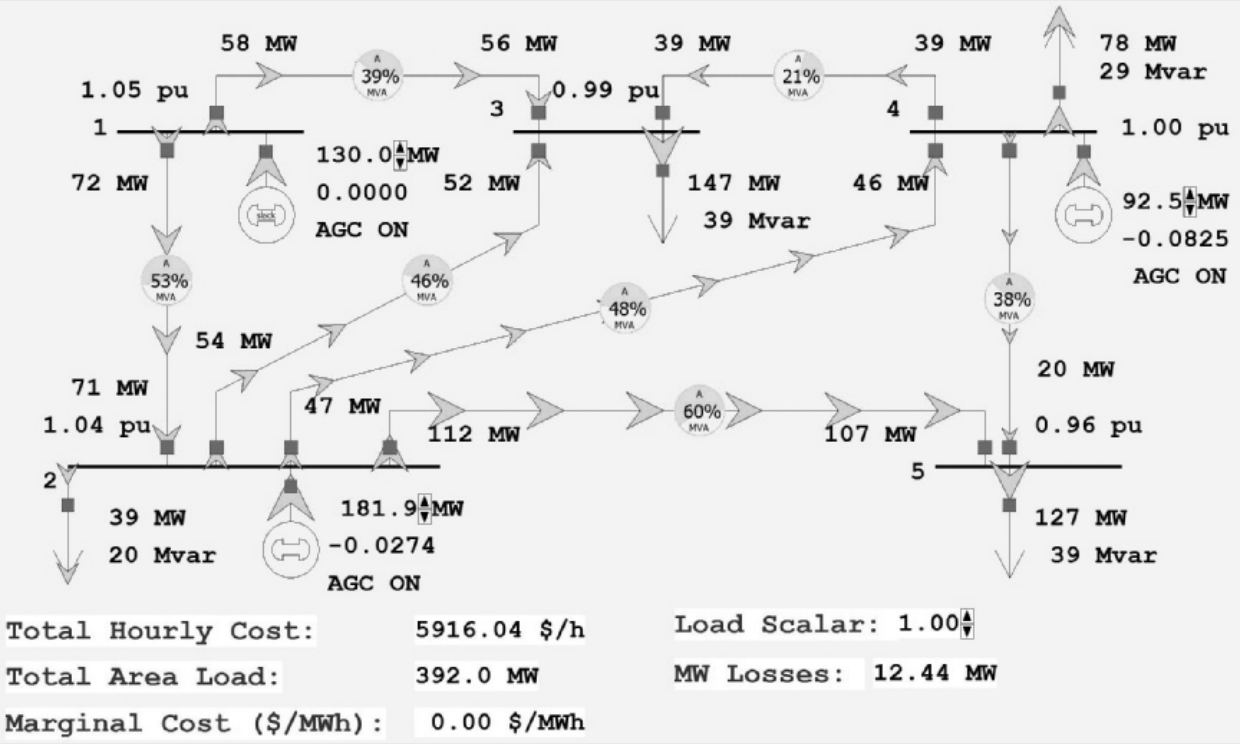

FIGURE 6.20

Example 6.22 five-bus case with transmission line losses

In Example 6.21, total transmission losses are expressed as a quadratic function of unit output powers. For an area with N units, this formula generalizes to

$$P_L = \sum_{i=1}^{N} \sum_{j=1}^{N} P_i B_{ij} P_j \tag{6.12.14}$$

where the B_{ij} terms are called *loss coefficients* or B *coefficients.* The B coefficients are not truly constant but vary with unit loadings. However, the B coefficients are often assumed constant in practice since the calculation of $\partial P_L/\partial P_i$ is thereby simplified. Using (6.12.14),

$$\frac{\partial P_L}{\partial P_i} = 2 \sum_{j=1}^{N} B_{ij} P_j \tag{6.12.15}$$

This equation can be used to compute the penalty factor L_i, in (6.12.13).

Various methods of evaluating B coefficients from power flow studies are available [17]. In practice, more than one set of B coefficients may be used during the daily load cycle.

When the unit incremental cost curves are linear, an analytic solution to the economic dispatch problem is possible, as illustrated by Examples 6.18 through 6.20. However, in practice, the incremental cost curves are nonlinear and contain discontinuities. In this case, an iterative solution can be obtained. Given the load demand P_T, the unit incremental cost curves, generator limits, and B coefficients, such an iterative solution can be obtained by the following nine steps. Assume that the incremental cost curves are stored in tabular form, such that a unique value of P_i can be read for each dC_i/dP_i.

STEP 1 Set iteration index $m = 1$.

STEP 2 Estimate mth value of λ.

STEP 3 Skip this step for all $m > 1$. Determine initial unit outputs P_i, ($i = 1, 2, \ldots, N$). Use $dC_i/dP_i = \lambda$ and read P_i from each incremental operating cost table. Transmission losses are neglected here.

STEP 4 Compute $\partial P_L/\partial P_i$ from (6.12.15) ($i = 1, 2, \ldots, N$).

STEP 5 Compute dC_i/dP_i from (6.12.13) ($i = 1, 2, \ldots, N$).

STEP 6 Determine updated values of unit output P_i ($i = 1, 2, \ldots, N$). Read P_i from each incremental operating cost table. If P_i exceeds a limit value, set P_i to the limit value.

STEP 7 Compare P_i determined in Step 6 with the previous value ($i = 1, 2, \ldots, N$). If the change in each unit output is less than a specified tolerance ε_1, go to Step 8. Otherwise, return to Step 4.

STEP 8 Compute P_L from (6.12.14).

STEP 9 If $\left|\left(\sum_{i=1}^{N} P_i\right) - P_L - P_T\right|$ is less than a specified tolerance ε_2, stop. Otherwise, set $m = m + 1$ and return to Step 2.

Instead of having their values stored in tabular form for this procedure, the incremental cost curves instead could be represented by nonlinear functions such as polynomials. Then, in Step 3 and Step 5, each unit output P_i would be computed from the nonlinear functions instead of being read from a table. Note that this procedure assumes that the total load demand P_T is constant. In practice, this economic dispatch program is executed every few minutes with updated values of P_T.

OTHER TYPES OF UNITS

The economic dispatch criterion has been derived for a power system area consisting of fossil-fuel generating units. In practice, however, an area has a mix of different types of units including fossil-fuel, nuclear, pumped-storage hydro, hydro, wind, and other types.

Wind and solar generation, which have no fuel costs, are represented with very low or negative cost. As such, they are preferred sources for economic dispatch and

are used by system operators whenever possible, unless there are generator operating limits or transmission constraints.

Although the fixed costs of a nuclear unit may be high, their operating costs are low due to inexpensive nuclear fuel. As such, nuclear units are normally base-loaded at their rated outputs. That is, the reference power settings of turbine-governors for nuclear units are held constant at rated output; therefore, these units do not participate in economic dispatch.

Pumped-storage hydro is a form of energy storage. During off-peak hours, these units are operated as synchronous motors to pump water to a higher elevation. Then during peak-load hours the water is released, and the units are operated as synchronous generators to supply power. As such, pumped-storage hydro units are used for light-load build-up and peak-load shaving. Economic operation of the area is improved by pumping during off-peak hours when the area λ is low, and by generating during peak-load hours when λ is high. Techniques are available for incorporating pumped-storage hydro units into economic dispatch of fossil-fuel units [18].

In an area consisting of hydro plants located along a river, the objective is to maximize the energy generated over the yearly water cycle rather than to minimize total operating costs. Reservoirs are used to store water during high-water or light-load periods, although some water may have to be released through spillways. Also, there are constraints on water levels due to river transportation, irrigation, or fishing requirements. Optimal strategies are available for coordinating outputs of plants along a river [19]. Economic dispatch strategies for mixed fossil-fuel/hydro systems are also available [20, 21, 22].

Techniques are also available for including reactive power flows in the economic dispatch formulation, whereby both active and reactive powers are selected to minimize total operating costs. In particular, reactive injections from generators, switched capacitor banks, and static var systems, along with transformer tap settings, can be selected to minimize transmission-line losses [22]. However, electric utility companies usually control reactive power locally. That is, the reactive power output of each generator is selected to control the generator terminal voltage, and the reactive power output of each capacitor bank or static var system located at a power system bus is selected to control the voltage magnitude at that bus. In this way, the reactive power flows on transmission lines are low, and the need for central dispatch of reactive power is eliminated.

6.13 OPTIMAL POWER FLOW

Economic dispatch has one significant shortcoming—it ignores the limits imposed by the devices in the transmission system. Each transmission line and transformer has a limit on the amount of power that can be transmitted through it, with the limits arising because of thermal, voltage, or stability considerations (Section 5.6). Traditionally, the transmission system was designed so that when the generation was dispatched economically there would be no limit violations. Hence, just solving economic dispatch was usually sufficient. However, with the worldwide trend toward deregulation of the electric utility industry, the transmission system is becoming

increasingly constrained (with these constraints sometimes called congestion). For example, in the PJM power market in the eastern United States, the costs associated with active transmission line and transformer limit violations (congestion) increased from $65 million in 1999 to almost $2.1 billion in 2005 and have averaged about $1 billion per year from 2008 to 2013 [23].

The solution to the problem of optimizing the generation while enforcing the transmission lines is to combine economic dispatch with either the full ac power flow, or a dc power flow. The result is known as the optimal power flow (OPF). There are several methods for solving the OPF with [24] providing a nice summary. One common approach is sequential linear programming (LP); this is the technique used with the PowerWorld Simulator. The LP OPF solution algorithm iterates between solving the power flow to determine the flow of power in the system devices and solving an LP to economically dispatch the generation (and possibility other controls) subject to the transmission system limits. In the absence of system elements loaded to their limits, the OPF generation dispatch is identical to the economic dispatch solution, and the marginal cost of energy at each bus is identical to the system λ. However, when one or more elements are loaded to their limits, the economic dispatch becomes constrained, and the bus marginal energy prices are no longer identical. In some electricity markets, these marginal prices are known as the Locational Marginal Prices (LMPs) and are used to determine the wholesale price of electricity at various locations in the system. For example, the real-time LMPs for the Midcontinent ISO (MISO) are available online at www.misoenergy.org/MarketsOperations.

EXAMPLE 6.23

PowerWorld Simulator—optimal power flow

PowerWorld Simulator case Example 6_23 duplicates the five-bus case from Example 6.20, except that the case is solved using PowerWorld Simulator's LP OPF algorithm (see Figure 6.21). To turn on the OPF option, first select **Case Information, Aggregation, Areas…,** and toggle the AGC Status field to OPF. Then, rather than solving the case with the "Single Solution" button, select **Add-ons, Primal LP** to solve using the LP OPF. Initially the OPF solution matches the ED solution from Example 6.20 since there are no overloaded lines. The green-colored fields on the screen immediately to the right of the buses show the marginal cost of supplying electricity to each bus in the system (i.e., the bus LMPs). With the system initially unconstrained, the bus marginal prices are all identical at $14.5/MWh, with a Load Scalar of 1.0.

Now increase the Load Scalar field from 1.00 to the maximum economic loading value, determined to be 1.67 in Example 6.20, and again select **Add-ons, Primal LP**. The bus marginal prices are still all identical, now at a value of $17.5/MWh, and with the line from bus 2 to 5 just reaching its maximum value. For load scalar values above 1.67, the line from bus 2 to bus 5 becomes constrained, with a result that the bus marginal prices on the constrained side of the line become higher than those on the unconstrained side.

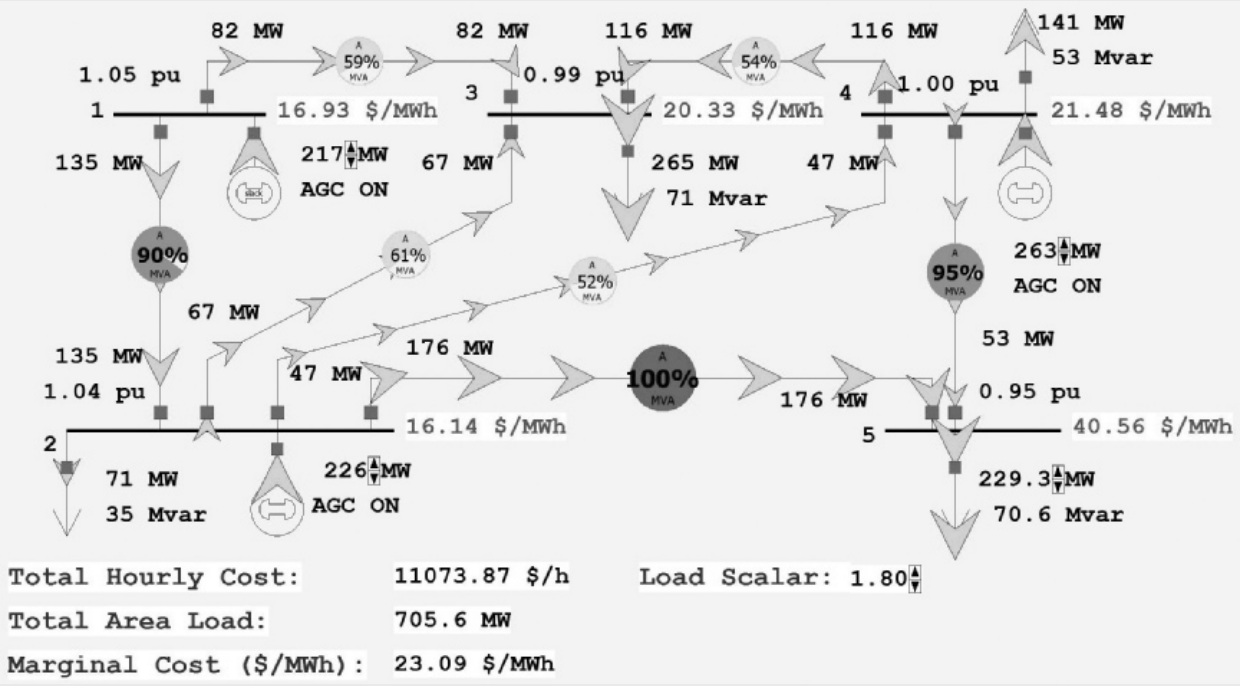

FIGURE 6.21

Example 6.23 optimal power flow solution with load multiplier = 1.80

With the load scalar equal to 1.80, numerically verify that the price of power at bus 5 is approximately \$40.60/MWh.

SOLUTION

The easiest way to numerically verify the bus 5 price is to increase the load at bus 5 by a small amount and compare the change in total system operating cost. With a load scalar of 1.80, the bus 5 MW load is 229.3 MW with a case hourly cost of \$11,073.90. Increasing the bus 5 load by 0.9 MW and resolving the LP OPF gives a new cost of \$11,110.40, which is a change of about \$40.60/MWh (note that this increase in load also increases the bus 5 price to over \$41/MWh). Because of the constraint, the price of power at bus 5 is actually more than double the incremental cost of the most expensive generator!

MULTIPLE CHOICE QUESTIONS

SECTION 6.1

6.1 For a set of linear algebraic equations in matrix format, $\mathbf{Ax} - \mathbf{y}$, for a unique solution to exist, det(**A**) should be _____.

6.2 For an $N \times N$ square matrix **A**, in $(N - 1)$ steps, the technique of Gauss elimination can transform into an _____ matrix.

SECTION 6.2

6.3 For the iterative solution to linear algebraic equations $\mathbf{Ax} - \mathbf{y}$, the **D** matrix in the Jacobi method is the _____ portion of **A**, whereas **D** for Gauss-Siedel is the _____ portion of **A**.

6.4 Is convergence guaranteed always with Jacobi and Gauss-Siedel methods, as applied to iterative solutions of linear algebraic equations?
(a) Yes (b) No

SECTION 6.3

6.5 For the iterative solutions to nonlinear algebraic equations with the Newton-Raphson method, the Jacobian matrix $\mathbf{J}(i)$ consists of the partial derivatives. Write down the elements of first row of $\mathbf{J}(i)$.

6.6 For the Newton-Raphson method to work, one should make sure that $\mathbf{J}^{-1}$ exists.
(a) True (b) False

6.7 The Newton-Raphson method in four steps makes use of Gauss elimination and back substitution.
(a) True (b) False

6.8 The number of iterations required for convergence is dependent/independent of the dimension N for Newton-Raphson method. Choose one.

SECTION 6.4

6.9 The swing bus or slack bus is a reference bus for which $V_1 \angle \delta_1$, typically $1.0 \angle 0°$ per unit, is input data. The power flow program computes _____. Fill in the blank.

6.10 Most buses in a typical power flow program are load buses, for which P_k and Q_k are input data. The power flow program computes _____.

6.11 For a voltage-controlled bus k, _____ are input data, while the power flow program computes _____.

6.12 When the bus k is a load bus with no generation and inductive load, in terms of generation and load, P_k = _____, and Q_k = _____.

6.13 Starting from a single-line diagram of a power system, the input data for a power flow problem consists of _____, _____, and _____.

SECTION 6.5

6.14 Nodal equations $\boldsymbol{I} = \boldsymbol{Y}_{\text{bus}}\, \boldsymbol{V}$ are a set of linear equations analogous to $\boldsymbol{y} = \boldsymbol{Ax}$.
(a) True (b) False

6.15 Because of the nature of the power flow bus data, nodal equations do not directly fit the linear-equation format, and power flow equations are

actually nonlinear. However, the Gauss-Siedel method can be used for the power flow solution.
(a) True (b) False

SECTION 6.6

6.16 The Newton-Raphson method is most well suited for solving the nonlinear power flow equations.
(a) True (b) False

6.17 By default, PowerWorld Simulator uses _____ method for the power flow solution.

SECTION 6.7

6.18 Prime-mover control of a generator is responsible for a significant change in _____, whereas excitation control significantly changes _____.

6.19 From the power flow standpoint, the addition of a shunt-capacitor bank to a load bus corresponds to the addition of a positive/negative reactive load. Choose the right word.

6.20 Tap-changing and voltage-magnitude-regulating transformers are used to control bus voltages and reactive power flows on lines to which they are connected.
(a) True (b) False

SECTION 6.8

6.21 A matrix, which has only a few nonzero elements, is said to be _____.

6.22 Sparse-matrix techniques are used in Newton-Raphson power flow programs in order to reduce computer _____ and _____ requirements.

6.23 Reordering buses can be an effective sparsity technique in power flow solutions.
(a) True (b) False

SECTION 6.9

6.24 While the fast decoupled power flow usually takes more iterations to converge, it is usually significantly faster than the Newton-Raphson method.
(a) True (b) False

SECTION 6.10

6.25 The "dc" power flow solution, giving approximate answers, is based on completely neglecting the Q-V equation and solving the linear real-power balance equations.
(a) True (b) False

PROBLEMS

SECTION 6.1

6.1 Using Gauss elimination, solve the following linear algebraic equations:

$$\begin{aligned} -25x_1 + 10x_2 + 10x_3 + 10x_4 &= 0 \\ 5x_1 - 10x_2 + 10x_3 &= 2 \\ 10x_1 + 5x_2 - 10x_3 + 10x_4 &= 1 \\ 10x_1 - 20x_4 &= -2 \end{aligned}$$

6.2 Using Gauss elimination and back substitution, solve

$$\begin{bmatrix} 8 & 2 & 1 \\ 4 & 6 & 2 \\ 3 & 4 & 14 \end{bmatrix} \begin{bmatrix} x_1 \\ x_2 \\ x_3 \end{bmatrix} = \begin{bmatrix} 3 \\ 4 \\ 2 \end{bmatrix}$$

6.3 Rework Problem 6.2 with the value of 8 changed to 4.

6.4 What is the difficulty in applying Gauss elimination to the following linear algebraic equations?

$$\begin{aligned} -5x_1 + 5x_2 &= 5 \\ 10x_1 - 10x_2 &= -5 \end{aligned}$$

6.5 Show that, after triangularizing $\mathbf{Ax} = \mathbf{y}$, the back substitution method of solving $\mathbf{A}^{(N-1)}\mathbf{x} = \mathbf{y}^{(N-1)}$ requires N divisions, $N(N-1)/2$ multiplications, and $N(N-1)/2$ subtractions. Assume that all the elements of $\mathbf{A}^{(N-1)}$ and $\mathbf{y}^{(N-1)}$are nonzero and real.

SECTION 6.2

6.6 Solve Problem 6.2 using the Jacobi iterative method. Start with $x_1(0) = x_2(0) = x_3(0) = 0$, and continue until (6.2.2) is satisfied with $\varepsilon = 0.01$.

6.7 Repeat Problem 6.6 using the Gauss-Seidel iterative method. Which method converges more rapidly?

6.8 Express the following set of equations in the form of (6.2.6), and then solve using the Jacobi iterative method with $\varepsilon = 0.05$ and with $x_1(0) = 1$, and $x_2(0) = 1$, $x_3(0) = 0$.

$$\begin{bmatrix} 10 & -2 & -4 \\ -2 & 6 & -2 \\ -4 & -2 & 10 \end{bmatrix} \begin{bmatrix} x_1 \\ x_2 \\ x_3 \end{bmatrix} = \begin{bmatrix} -2 \\ 3 \\ -1 \end{bmatrix}$$

6.9 Solve for x_1 and x_2 in the system of equations given by

$$x_2 - 3x_1 + 1.9 = 0$$
$$x_2 + x_1^2 - 3.0 = 0$$

using the Gauss method with an initial guess of $x_1 = 1$ and $x_2 = 1$.

6.10 Solve $x^2 - 4x + 1 = 0$ using the Jacobi iterative method with $x(0) = 1$. Continue until (6.2.2) is satisfied with $\varepsilon = 0.01$. Check using the quadratic formula.

6.11 Try to solve Problem 6.2 using the Jacobi and Gauss-Seidel iterative methods with the value of A_{33} changed from 14 to 0.14 and with $x_1(0) = x_2(0) = x_3(0) = 0$. Show that neither method converges to the unique solution.

6.12 Using the Jacobi method (also known as the Gauss method), solve for x_1 and x_2 in the following system of equations.

$$x_2 - 3x_1 + 1.9 = 0$$
$$x_2 + x_1^2 - 1.8 = 0$$

Use an initial guess of $x_1(0) = 1.0$ and $x_2 = (0) = 1.0$. Also, see what happens when you choose an uneducated initial guess of $x_1(0) = x_2(0) = 100$.

6.13 Use the Gauss-Seidel method to solve the following equations that contain terms that are often found in power flow equations.

$$x_1 = (1/(-20j)) * [(-1 + 0.5j)/(x_1)^* - (j10) * x_2 - (j10)]$$
$$x_2 = (1/(-20j)) * [(-3 + j)/(x_2)^* - (j10) * x_1 - (j10)]$$

Use an initial estimate of $x_1(0) = 1$ and $x_2(0) = 1$, and a stopping of $\varepsilon = 0.05$.

6.14 Find a root of the following equation by using the Gauss-Seidel method: (use an initial estimate of $x = 2$) $f(x) = x^3 - 6x^2 + 9x - 4 = 0$.

6.15 Use the Jacobi method to find a solution to $x^2 \cos x - x + 0.5 = 0$. Use $x(0) = 1$ and $\varepsilon = 0.01$. Experimentally determine the range of initial values that results in convergence.

6.16 Take the z-transform of (6.2.6) and show that $\mathbf{X}(z) = \mathbf{G}(z)\mathbf{Y}(z)$, where $\mathbf{G}(z) = (z\mathbf{U} - \mathbf{M})^{-1}\,\mathbf{D}^{-1}$ and $\mathbf{U}$ is the unit matrix.

Note: $\mathbf{G}(z)$ is the matrix transfer function of a digital filter that represents the Jacobi or Gauss-Seidel methods. The filter poles are obtained by solving $\det(z\mathbf{U} - \mathbf{M}) = 0$. The filter is stable if and only if all the poles have magnitudes less than 1.

6.17 Determine the poles of the Jacobi and Gauss-Seidel digital filters for the general two-dimensional problem ($N = 2$):

$$\left[\begin{array}{c|c} A_{11} & A_{12} \\ \hline A_{21} & A_{22} \end{array}\right] \begin{bmatrix} x_1 \\ x_2 \end{bmatrix} = \begin{bmatrix} y_1 \\ y_2 \end{bmatrix}$$

Then determine a necessary and sufficient condition for convergence of these filters when $N = 2$.

SECTION 6.3

6.18 Use Newton-Raphson to find a solution to the polynomial equation $f(x) = y$ where $y = 0$ and $f(x) = x^3 + 8x^2 + 2x - 40$. Start with $x(0) = 1$ and continue until (6.2.2) is satisfied with $\varepsilon = 0.001$.

6.19 Repeat 6.19 using $x(0) = -2$.

6.20 Use Newton-Raphson to find one solution to the polynomial equation $f(x) = y$, where $y = 7$ and $f(x) = x^4 + 3x^3 - 15x^2 - 19x + 30$. Start with $x(0) = 0$ and continue until (6.2.2) is satisfied with $\varepsilon = 0.001$.

6.21 Repeat Problem 6.20 with an initial guess of $x(0) = 4$.

6.22 For Problem 6.20, plot the function $f(x)$ between $x = 0$ and 4. Then provide a graphical interpretation why points close to $x = 2.2$ would be poorer initial guesses.

6.23 Use Newton-Raphson to find a solution to

$$\begin{bmatrix} e^{x_1 x_2} \\ \cos(x_1 + x_2) \end{bmatrix} = \begin{bmatrix} 1.2 \\ 0.5 \end{bmatrix}$$

where x_1 and x_2 are in radians. (a) Start with $x_1(0) = 1.0$ and $x_2(0) = 0.5$ and continue until (6.2.2) is satisfied with $\varepsilon = 0.005$. (b) Show that Newton-Raphson diverges for this example if $x_1(0) = 1.0$ and $x_2(0) = 2.0$.

6.24 Solve the following equations by the Newton-Raphson method:

$$2x_1 + x_2^2 - 8 = 0$$
$$x_1^2 - x_2^2 + x_1 x_2 - 3 = 0$$

Start with an initial guess of $x_1 = 1$ and $x_2 = 1$.

6.25 The following nonlinear equations contain terms that are often found in the power flow equations:

$$f_1(x) = 10x_1 \sin x_2 + 2 = 0$$
$$f_2(x) = 10\,(x_1)^2 - 10x_1 \cos x_2 + 1 = 0$$

Solve using the Newton-Raphson method starting with an initial guess of $x_1\,(0) = 1$ and $x_2(0) = 0$ radians and a stopping criteria of $\varepsilon = 10^{-4}$.

6.26 Repeat Problem 6.25 except using $x_1(0) = 0.25$ and $x_2(0) = 0$ radians as an initial guess.

6.27 For the Newton-Raphson method, the *region of attraction* (or *basin of attraction)* for a particular solution is the set of all initial guesses that converge to that solution. Usually initial guesses close to a particular solution will converge to that solution. However, for all but the simplest of multi-dimensional, nonlinear problems, the region of attraction boundary is often fractal. This makes it impossible to quantify the region of attraction and hence to guarantee convergence. Problem 6.25 has two

solutions when x_2 is restricted to being between $-\pi$ and π. With the x_2 initial guess fixed at 0 radians, numerically determine the values of the x_1 initial guesses that converge to the Problem 6.25 solution. Restrict your search to values of x_1 between 0 and 1.

SECTION 6.4

6.28 Consider the simplified electric power system shown in Figure 6.22 for which the power flow solution can be obtained without resorting to iterative techniques. (a) Compute the elements of the bus admittance matrix $\boldsymbol{Y}_{\text{bus}}$. (b) Calculate the phase angle δ_2 by using the real power equation at bus 2 (voltage-controlled bus). (c) Determine $|V_3|$ and δ_3 by using both the real and reactive power equations at bus 3 (load bus). (d) Find the real power generated at bus 1 (swing bus). (e) Evaluate the total real power losses in the system.

6.29 In Example 6.9, double the impedance on the line from bus 2 to bus 5. Determine the new values for the second row of $\boldsymbol{Y}_{\text{bus}}$. Verify your result using PowerWorld Simulator case Example 6_9.

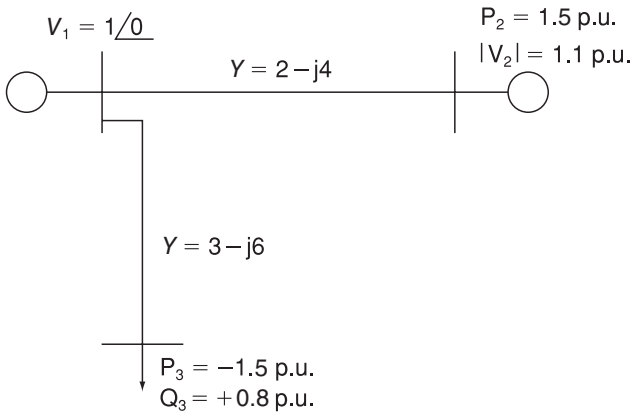

FIGURE 6.22
Problem 6.28

6.30 Determine the bus admittance matrix ($\boldsymbol{Y}_{\text{bus}}$) for the three-phase power system shown in Figure 6.23 with input data given in Table 6.11 and partial results in Table 6.12. Assume a three-phase 100 MVA per unit base.

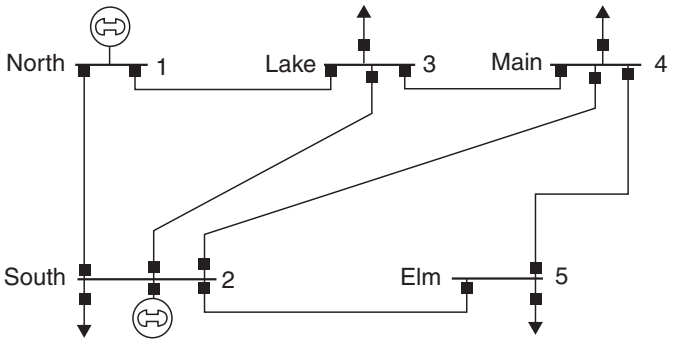

FIGURE 6.23
Sample System Diagram for Problem 6.30

Bus-to-Bus	R per unit	X per unit	B per unit
1-2	0.02	0.06	0.06
1-3	0.08	0.24	0.05
2-3	0.06	0.18	0.04
2-4	0.08	0.24	0.05
2-5	0.02	0.06	0.02
3-4	0.01	0.04	0.01
4-5	0.03	0.10	0.04

TABLE 6.11

Bus input data for Problem 6.30

$6.25 - j18.695$	$-5.00 + j15.00$	$-1.25 + j3.75$	0	0
$-5.00 + j15.00$				

TABLE 6.12

Partially Completed Bus Admittance Matrix ($\boldsymbol{Y}_{bus}$) for Problem 6.30

6.31 For the system from Problem 6.30, assume that a 75-Mvar shunt capacitance (three phase assuming one per unit bus voltage) is added at bus 4. Calculate the new value of Y_{44}.

SECTION 6.5

6.32 For a two-bus power system, a $0.7 + j0.4$ per unit load at bus 2 is supplied by a generator at bus 1 through a transmission line with series impedance of $0.05 + j0.1$ per unit. With bus 1 as the slack bus with a fixed per-unit voltage of $1.0\angle 0$, use the Gauss-Seidel method to calculate the voltage at bus 2 after three iterations.

6.33 Repeat Problem 6.32 with the slack bus voltage changed to $1.0\angle 30°$ per unit.

6.34 For the three-bus system whose $\boldsymbol{Y}_{bus}$ is given, calculate the second iteration value of V_3 using the Gauss-Seidel method. Assume bus 1 as the slack (with $V_1 = 1.0\angle 0°$), and buses 2 and 3 are load buses with a per-unit load of $S_2 = 1 + j0.5$ and $S_3 = 1.5 + j0.75$. Use voltage guesses of $1.0\angle 0°$ at both buses 2 and 3. The bus admittance matrix for a three-bus system is

$$\boldsymbol{Y}_{bus} = \begin{bmatrix} -j10 & j5 & j5 \\ j5 & -j10 & j5 \\ j5 & j5 & -j10 \end{bmatrix}$$

6.35 Repeat Problem 6.34 except assume the bus 1 (slack bus) voltage of $V_1 = 1.05\angle 0°$.

6.36 The bus admittance matrix for the power system shown in Figure 6.24 is given by

$$\boldsymbol{Y}_{\text{bus}} = \begin{bmatrix} 3 - j9 & -2 + j6 & -1 + j3 & 0 \\ -2 + j6 & 3.666 - j11 & -0.666 + j2 & -1 + j3 \\ -1 + j3 & -0.666 + j2 & 3.666 - j11 & -2 + j6 \\ 0 & -1 + j3 & -2 + j6 & 3 - j9 \end{bmatrix} \text{ per unit}$$

With the complex powers on load buses 2, 3, and 4 as shown in Figure 6.24, determine the value for V_2 that is produced by the first and second iterations of the Gauss-Seidel procedure. Choose the initial guess $V_2(0) = V_3(0) = V_4(0) = 1.0\angle 0°$ per unit.

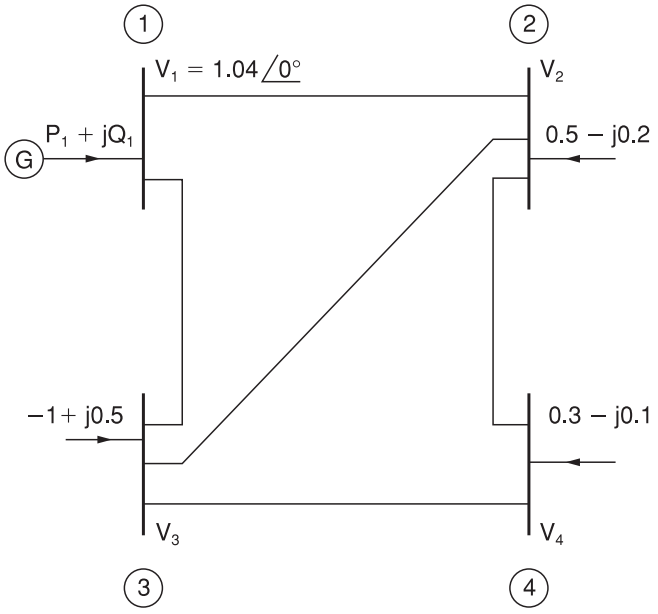

FIGURE 6.24
Problem 6.36

6.37 The bus admittance matrix of a three-bus power system is given by

$$\boldsymbol{Y}_{\text{bus}} = -j\begin{bmatrix} 7 & -2 & -5 \\ -2 & 6 & -4 \\ -5 & -4 & 9 \end{bmatrix} \text{ per unit}$$

with $V_1 = 1.0\angle 0°$ per unit; $V_2 = 1.0$ per unit; $P_2 = 60$ MW; $P_3 = -80$ MW; $Q_3 = -60$ Mvar (lagging) as a part of the power flow solution of the system. Find V_2 and V_3 within a tolerance of 0.01 per unit by using the Gauss-Seidel iteration method. Start with $\delta_2 = 0$, $V_3 = 1.0$ per unit, and $\delta_3 = 0$.

SECTION 6.6

6.38 A generator bus (with a 1.0 per unit voltage) supplies a 180 MW, 60 Mvar load through a lossless transmission line with per unit (100 MVA base) impedance of $j0.1$ and no line charging. Starting with an initial voltage guess of $1.0\angle 0°$, iterate until converged using the Newton-Raphson power flow method. For convergence criteria, use a maximum power flow mismatch of 0.1 MVA.

6.39 Repeat Problem 6.38 except use an initial voltage guess of $1.0\angle 30°$.

6.40 Repeat Problem 6.38 except use an initial voltage guess of $0.25\angle 0°$.

6.41 Determine the initial Jacobian matrix for the power system described in Problem 6.34.

6.42 Use the Newton-Raphson power flow to solve the power system described in Problem 6.34. For convergence criteria, use a maximum power flow mismatch of 0.1 MVA.

6.43 For a three-bus power system, assume bus 1 is the slack with a per unit voltage of $1.0\angle 0°$, bus 2 is a PQ bus with a per unit load of $2.0 + j0.5$, and bus 3 is a PV bus with 1.0 per unit generation and a 1.0 voltage setpoint. The per unit line impedances are $j0.1$ between buses 1 and 2, $j0.4$ between buses 1 and 3, and $j0.2$ between buses 2 and 3. Using a flat start, use the Newton-Raphson approach to determine the first iteration phasor voltages at buses 2 and 3.

6.44 Repeat Problem 6.43 except with the bus 2 real power load changed to 1.0 per unit.

PW **6.45** Load PowerWorld Simulator case Example 6_11; this case is set to perform a single iteration of the Newton-Raphson power flow each time **Single Solution** is selected. Verify that initially the Jacobian element J_{33} is 104.41. Then, give and verify the value of this element after each of the next three iterations (until the case converges).

PW **6.46** Load PowerWorld Simulator case Problem 6_46. Using a 100 MVA base, each of the three transmission lines have an impedance of $0.05 + j0.1$ p.u. There is a single 180 MW load at bus 3, while bus 2 is a PV bus with generation of 80 MW and a voltage setpoint of 1.0 p.u. Bus 1 is the system slack with a voltage setpoint of 1.0 p.u. Manually solve this case using the Newton-Raphson approach with a convergence criteria of 0.1 MVA. Show all your work. Then verify your solution by solving the case with PowerWorld Simulator.

PW **6.47** As was mentioned in Section 6.4, if a generator's reactive power output reaches its limit, then it is modeled as though it were a PQ bus. Repeat Problem 6.46, except assume the generator at bus 2 is operating with its reactive power limited to a maximum of 50 Mvar. Then verify your solution by solving the case with PowerWorld Simulator. To increase the reactive power output of the bus 2 generator, select **Tools, Play** to

begin the power flow simulation, then click on the up arrow on the bus 2 magenta voltage setpoint field until the reactive power output reaches its maximum.

PW **6.48** Load PowerWorld Simulator case Problem 6_46. Plot the reactive power output of the generator at bus 2 as a function of its voltage setpoint value in 0.005 p.u. voltage steps over the range between its lower limit of −50 Mvar and its upper limit of 50 Mvar. To change the generator 2 voltage set point first select **Tools, Play** to begin the power flow simulation, and then click on the up/down arrows on the bus 2 magenta voltage setpoint field.

SECTION 6.7

PW **6.49** Open PowerWorld Simulator case Problem 6_49. This case is identical to Example 6.9, except that the transformer between buses 1 and 5 is now a tap-changing transformer with a tap range between 0.9 and 1.1 and a tap step size of 0.00625. The tap is on the high side of the transformer. As the tap is varied between 0.975 and 1.1, show the variation in the reactive power output of generator 1, V_5, V_2, and the total real power losses.

PW **6.50** Use PowerWorld Simulator to determine the Mvar rating of the shunt capacitor bank in the Example 6_14 case that increases V_2 to 1.0 per unit. Also determine the effect of this capacitor bank on line loadings and the total real power losses (shown immediately below bus 2 on the oneline). To vary the capacitor's nominal Mvar rating, right-click on the capacitor symbol to view the Switched Shunt Dialog, and then change Nominal Mvar field.

PW **6.51** Use PowerWorld Simulator to modify the Example 6_9 case by inserting a second line between bus 2 and bus 5. Give the new line a circuit identifier of "2" to distinguish it from the existing line. The line parameters of the added line should be identical to those of the existing lines 2 to 5. Determine the new line's effect on V_2, the line loadings, and on the total real power losses.

PW **6.52** Open PowerWorld Simulator case Problem 6_52. Open the 69 kV line between buses REDBUD69 and PEACH69 (shown towards the bottom of the oneline). With the line open, determine the amount of Mvar (to the nearest 1 Mvar) needed from the REDBUD69 capacitor bank to correct the REDBUD69 voltage to at least 1.0 p.u.

PW **6.53** Open PowerWorld Simulator case Problem 6_53. Plot the variation in the total system real power losses as the generation at bus PEAR138 is varied in 20 MW blocks between 0 MW and 400 MW. What value of PEAR138 generation minimizes the total system losses?

PW **6.54** Repeat Problem 6.53, except first remove the 69 kV line between LOCUST69 and PEAR69.

SECTION 6.8

6.55 Using the compact storage technique described in Section 6.8, determine the vectors **DIAG**, **OFFDIAG**, **COL**, and **ROW** for the following matrix:

$$\mathbf{S} = \begin{bmatrix} 17 & -9.1 & 0 & 0 & -2.1 & -7.1 \\ -9.1 & 25 & -8.1 & -1.1 & -6.1 & 0 \\ 0 & -8.1 & 9 & 0 & 0 & 0 \\ 0 & -1.1 & 0 & 2 & 0 & 0 \\ -2.1 & -6.1 & 0 & 0 & 14 & -5.1 \\ -7.1 & 0 & 0 & 0 & -5.1 & 15 \end{bmatrix}$$

6.56 For the triangular factorization of the corresponding $\boldsymbol{Y}_{\text{bus}}$, number the nodes of the graph shown in Figure 6.9 in an optimal order.

SECTION 6.10

6.57 Compare the angles and line flows between the Example 6_17 case and results shown in Tables 6.6, 6.7, and 6.8.

6.58 Redo Example 6.17 with the assumption that the per-unit reactance on the line between buses 2 and 5 is changed from 0.05 to 0.03.

PW **6.59** Open PowerWorld Simulator case Problem 6_59, which models a seven-bus system using the dc power flow approximation. Bus 7 is the system slack. The real power generation/load at each bus is as shown, while the per-unit reactance of each of the lines (on a 100 MVA base) is as shown in yellow on the oneline. (a) Determine the six-by-six **B** matrix for this system and the **P** vector. (b) Use a matrix package such as Matlab to verify the angles as shown on the oneline.

PW **6.60** Using the PowerWorld Simulator case from Problem 6.59, if the rating on the line between buses 1 and 2 is 150 MW, the current flow is 101 MW (from bus 1 to bus 3), and the bus 1 generation is 160 MW, analytically determine the amount this generation can increase until this line reaches 100% flow. Assume any change in the bus 1 generation is absorbed at the system slack.

SECTION 6.11

PW **6.61** PowerWorld Simulator cases Problem 6_61_PQ and 6_61_PV model a seven-bus power system in which the generation at bus 4 is modeled as a Type 1 or 2 wind turbine in the first case and as a Type 3 or 4 wind turbine in the second. A shunt capacitor is used to make the net reactive power injection at the bus the same in both cases. Compare the bus 4 voltage between the two cases for a contingency in which the line between buses 2 and 4 is opened. What is an advantage of a Type 3 or 4 wind turbine with respect to voltage regulation following a contingency? What is the variation in the Mvar output of a shunt capacitor with respect to bus voltage magnitude?

SECTION 6.12

6.62 The fuel-cost curves for two generators are given as follows:

$$C_1(P_1) = 600 + 18 \cdot P_1 + 0.04 \cdot (P_1)^2$$

$$C_2(P_2) = 700 + 20 \cdot P_2 + 0.03 \cdot (P_2)^2$$

Assuming the system is lossless, calculate the optimal dispatch values of P_1 and P_2 for a total load of 1000 MW, the incremental operating cost, and the total operating cost.

6.63 Rework Problem 6.62, except assume that the limit outputs are subject to the following inequality constraints:

$$200 \leq P_1 \leq 800 \text{ MW}$$

$$100 \leq P_2 \leq 400 \text{ MW}$$

6.64 Rework Problem 6.62, except assume the 1000 MW value also includes losses, and the penalty factor for the first unit is 1.0 and for the second unit 0.95.

6.65 The fuel-cost curves for a two-generator power system are given as follows:

$$C_1(P_1) = 600 + 15 \cdot P_1 + 0.05 \cdot (P_1)^2$$

$$C_2(P_2) = 700 + 20 \cdot P_2 + 0.04 \cdot (P_2)^2$$

while the system losses can be approximated as

$$P_L = 2 \times 10^{-4}(P_1)^2 + 3 \times 10^{-4}(P_2)^2 - 4 \times 10^{-4}P_1P_2 \quad \text{MW}$$

If the system is operating with a marginal cost (λ) of \$60/hr, determine the output of each unit, the total transmission losses, the total load demand, and the total operating cost.

6.66 Expand the summations in (6.12.14) for $N = 2$, and verify the formula for $\partial P_L/\partial P_i$ given by (6.12.15). Assume $B_{ij} = B_{ji}$.

6.67 Given two generating units with their respective variable operating costs as

$$C_1 = 0.01P_{G1}^2 + 2P_{G1} + 100 \quad \$/\text{hr} \qquad \text{for } 25 \leq P_{G1} \leq 150 \quad \text{MW}$$

$$C_2 = 0.004P_{G2}^2 + 2.6P_{G2} + 80 \quad \$/\text{hr} \qquad \text{for } 30 \leq P_{G2} \leq 200 \quad \text{MW}$$

determine the economically optimum division of generation for $55 \leq P_L \leq 350$ MW. In particular, for $P_L = 282$ MW, compute P_{G1} and P_{G2}. Neglect transmission losses.

PW **6.68** Resolve Example 6.20, except with the generation at bus 2 set to a fixed value (i.e., modeled as off of Automatic Generation Control). Plot the variation in the total hourly cost as the generation at bus 2 is varied between 1000 and 200 MW in 5 MW steps, resolving the economic dispatch at each step. What is the relationship between bus 2 generation at the minimum point on this plot and the value from economic dispatch in Example 6.20? Assume a Load Scalar of 1.0.

PW **6.69** Using PowerWorld case Example 6_22 with the Load Scalar equal to 1.0, determine the generation dispatch that minimizes system losses *(Hint:* Manually vary the generation at buses 2 and 4 until their loss sensitivity values are zero). Compare the operating cost between this solution and the Example 6_22 economic dispatch result. Which is better?

PW **6.70** Repeat Problem 6.69, except with the Load Scalar equal to 1.4.

SECTION 6.13

PW **6.71** Using LP OPF with PowerWorld Simulator case Example 6_23, plot the variation in the bus 5 marginal price as the Load Scalar is increased from 1.0 in steps of 0.02. What is the maximum possible load scalar without overloading any transmission line? Why is it impossible to operate without violations above this value?

PW **6.72** Load PowerWorld Simulator case Problem 6_72. This case models a slightly modified, lossless version of the 37-bus case from Example 6.13 with generator cost information, but also with the transformer between buses PEAR138 and PEAR69 open. When the case is loaded, the "Total Cost" field shows the economic dispatch solution, which results in an overload on several lines. Before solving the case, select **Add-Ons, OPF Case Info, OPF Buses** to view the bus LMPs, noting that they are all identical. Then Select **Add-Ons, Primal LP** to solve the case using the OPF, and again view the bus LMPs. Verify the LMP at the PECAN69 bus by manually changing the load at the bus by one MW, and then noting the change in the Total Cost field. Repeat for the LOCUST69 bus. *Note*: Because of solution convergence tolerances, the manually calculated results may not exactly match the OFP calculated bus LMPs.

CASE STUDY QUESTIONS

a. What are the operational impacts on fossil-fueled power plants due to high penetrations of wind and solar generation into a power grid?

b. Do high penetrations of wind and solar generation increase the wear and tear costs of fossil-fueled generation? Why?

c. Which has more forecast uncertainty, wind generation or solar generation? Why?

DESIGN PROJECT I: NEW LOAD

As a result of the low electric rates from the local utility, Metropolis Light and Power (MLP), several large server farms and a new factory are going to be built in the eastern portion of the MLP service territory (see Figure 6.25). With an anticipated peak load of about 75 MW and 20 Mvar, this new load also brings additional revenue to MLP. However, in order to supply this additional load, the new TULIP substation will need to be constructed. While they would like to receive electricity at the

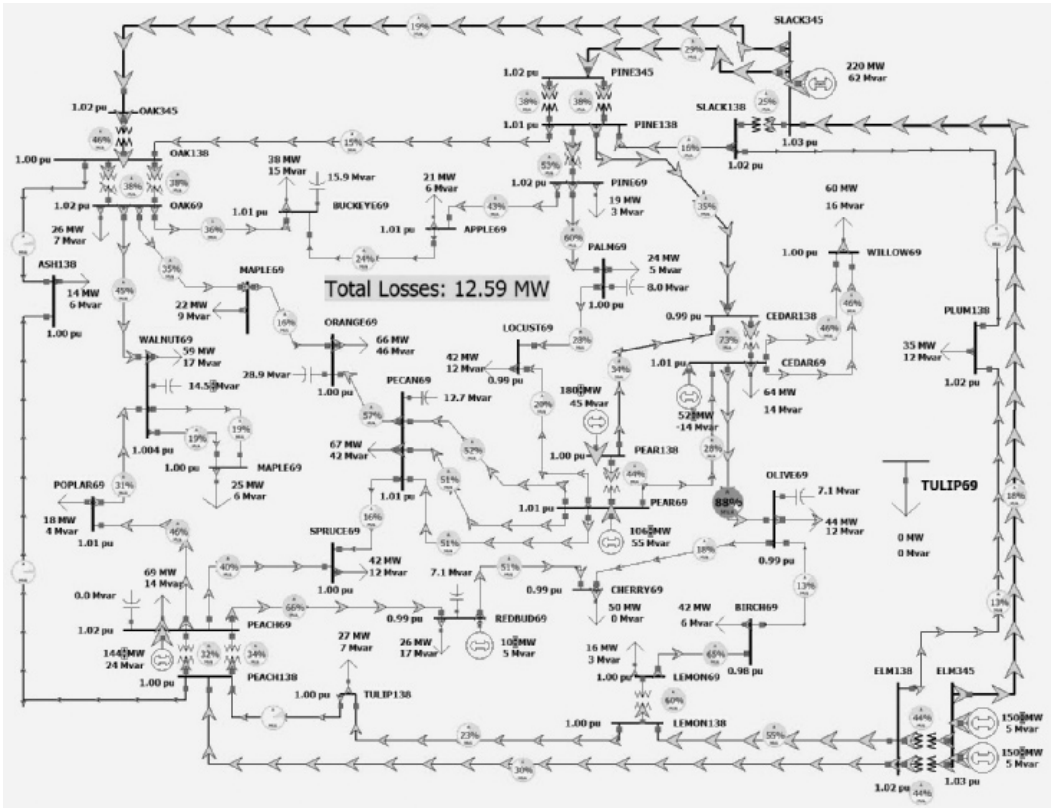

FIGURE 6.25

Design Case 1 System Oneline Diagram

69 kV level, the new substation location is large enough to accommodate a 138/69 kV transformer if needed. Additionally, for reliability purposes, the TULIP substation needs to have at least two separate lines into their substation.

As a planning engineer for MLP, your job is to make recommendations to ensure that, with new TULIP loads under peak loading conditions, the transmission system in the eastern region is adequate for any base case or first contingency loading situation. This is also a good opportunity not only to meet the new load, but also to fix some existing first contingency violations in the eastern portion of the MLP service territory. Table 6.13 shows the available right-of-way distances that

Right-of-Way/Substation	Right-of-Way Distance (km)
TULIP to ELM	15
TULIP to PLUM	12
TULIP to OLIVE	8
TULIP to CEDAR	10
TULIP to BIRCH	14
CEDAR to PLUM	13
WILLOW to PLUM	8
OLIVE TO CEDAR	10

TABLE 6.13

Available New Rights-of-Way

can be used for the construction of new 69 kV and/or new 138 kV lines. All existing 69 kV-only substations are large enough to accommodate 138 kV as well. The DesignCase1_2015 provides a power flow model of the initial conditions.

Design Procedure

1. Load DesignCase1_2015 into PowerWorld Simulator. Perform an initial power-flow solution to verify the base case system operation without the TULIP load. Note that the entire line flows and bus voltage magnitudes are within their limits. Assume all line MVA flows must be at or below 100% of the limit A values, and all voltages must be between 0.95 and 1.10 per unit.
2. Repeat the above analysis considering the impact of any single transmission line or transformer outage. This is known as contingency analysis. To simplify this analysis, PowerWorld Simulator has the ability to automatically perform a contingency analysis study. Select **Tools, Contingency Analysis** to show the Contingency Analysis display. Note that the 57 single line/transformer contingencies are already defined. Select **Start Run** to automatically see the impact of removing any single element. This system has line violations for several different contingencies.
3. Using the rights-of-way and the transmission line parameters/costs given in the cost section (see page 409), iteratively determine the least expensive system additions so that the base case and all the contingences result in reliable operation points (i.e., one with no violations) with the new TULIP load. The parameters of the new transmission lines(s) need to be derived using the tower configurations and conductor types. Tower configurations are provided by the instructor with default values given with the cost data. Several different conductor types are available in the cost section. The total cost of an addition is defined as the construction costs minus the savings associated with any decrease in system losses over the next 5 years.
4. Write a detailed report discussing the initial system problems, your approach to optimally solving the system problems, and the justification for your final recommendation.

Simplifying Assumptions

To simplify the analysis, several assumptions are made:

1. You need only consider the base case loading level given in DesignCase1_2015. In a real design, typically a number of different operating points/loading levels must be considered.
2. You should consider the generator outputs as fixed values; any changes in the losses and the new TULIP load are always picked up by the system slack generator.
3. You should not modify the status of the capacitors or the transformer taps.
4. You should assume that the system losses remain constant over the 5-year period and need only consider the impact the new design has on the base case losses. Electricity is priced at \$60/MWh.

DESIGN PROJECT 2: NEW WIND GENERATION AND GENERATION RETIREMENT

As a planning engineer for Island Electric Company (IEC), you have been tasked with determining the transmission system changes required to locate a new 600 MW wind farm in the western portion of your service territory (see Figure 6.26). IEC uses 345 and 161 kV transmission grids, so your changes are restricted to these existing voltages. The wind farm would like to connect at the 161 kV level and requires at least two transmission lines into the NewWind substation (which can be at either 161 and/or 345 kV). Since the location is usually quite windy, it is expected to have a capacity factor of at least 40%. However, the wind also can be quite variable, including during times of maximum system loading, so this generation cannot be counted on for firm capacity. Simultaneous with the addition of the new wind farm, IEC would like to retire the existing 300 MW generator at the Pheasant substation.

Hence, your job is to make recommendations on the least-cost design for the construction of new lines and transformers to ensure that the transmission system in the IEC system is adequate for any base case or first-contingency loading situation when then wind farm is installed and operating at either its maximum output of 600 or 0 MW and with the Pheasant generator removed from service. Note, this will also involve fixing some existing first-contingency violations. Since the wind farm will be built with Type 3 DFAG wind turbines, you can model the wind farm in the power flow as a single equivalent, traditional PV bus generator with a fixed output of either 0 or 600 MW, a voltage setpoint of 1.03 per unit, and with reactive power limits of ±250 Mvar.

Table 6.14 shows the right-of-way distances that are available for the construction of new 161 kV and/or new 345 kV lines. All existing 161-kV only substations are large enough to accommodate 345 kV as well, as is the NewWind substation.

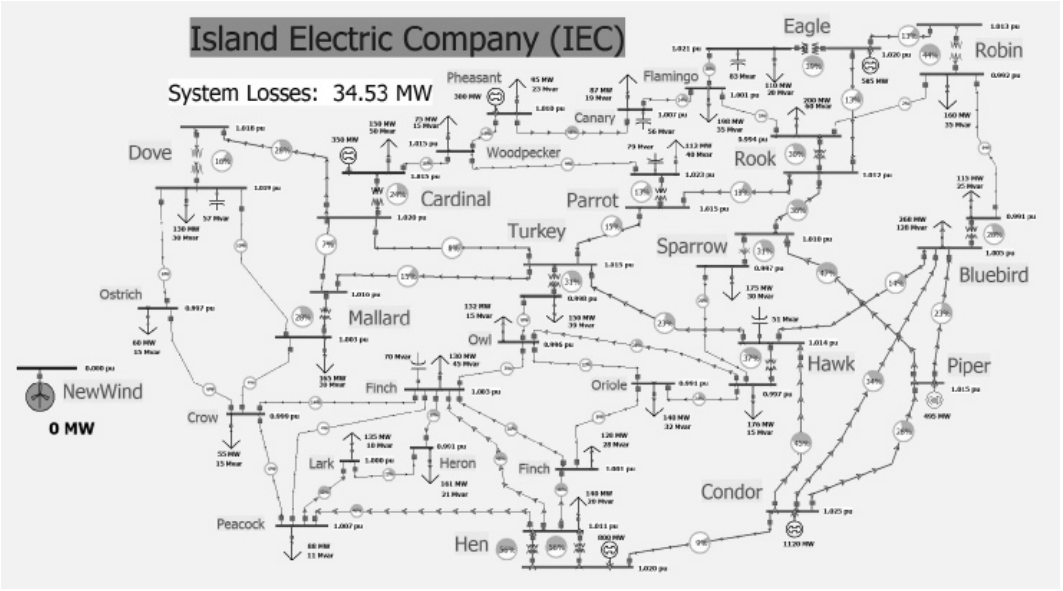

FIGURE 6.26

Design Case 2 System Oneline Diagram

Right-of-Way/Substation	Right-of-Way Distance (km)
NewWind to Ostrich	15
NewWind to Dove	55
NewWind to Crow	30
NewWind to Peacock	53
NewWind to Hen	70
Ostrich to Mallard	45
Peakcock to Hen	20
Dove to Cardinal	40

TABLE 6.14
Available New Rights-of-Way

Design Procedure

1. Load DesignCase2_2015 into PowerWorld Simulator, which contains the system power flow case and the disconnected NewWind generator and bus. Perform an initial power flow solution to verify the base case system operation. Note that all of the line flows and bus voltage magnitudes are within their limits. Assume all line MVA flows must be at or below 100% of their limit values, and all voltages must be between 0.92 and 1.10 per unit.
2. Repeat the above analysis, considering the impact of any single transmission line or transformer outage. This is known as contingency analysis. To simplify this analysis, PowerWorld Simulator has the ability to automatically perform a contingency analysis study. Select **Tools, Contingency Analysis** to show the Contingency Analysis display. Note that the 60 single line/transformer contingencies are already defined. Select **Start Run** (towards the bottom right corner of the display) to automatically see the impact of removing any single element. Note that there are several existing violations.
3. Open the existing 300 MW generator at the Pheasant substation, and repeat parts 1 and 2.
4. Using the rights-of-way given in Table 6.14 and the transmission line parameters/costs, iteratively determine the least-expensive system additions so that the base case and all the contingences result in reliable operation points with the NewWind generation connected with an output of either 0 or 600 MW. When the output is at 0 MW, the wind farm is still considered on-line and hence should be modeled as a PV bus regulating its voltage to 1.03 p.u. The parameters of the new transmission lines(s) need to be derived using the tower configurations and conductor types provided by the instructor. In addition, the transmission changes you propose will modify the total system losses, indicated by the large field

on the oneline diagram. In your design, you should consider the impact on total system losses in the studied condition for the next 5 years. Hence, you should minimize the total construction costs minus the savings associated with any decrease in system losses over the next 5 years.

5. Write a detailed report discussing the initial system problems, your approach to optimally solving the system problems, and the justification for your final recommendation.

Simplifying Assumptions

To simplify the analysis, several assumptions are made:

1. You need only consider the base case loading level given with the modification of opening the Pheasant generation. In a real design, typically a number of different operating points/loading levels must be considered.
2. You should consider all the generator real power outputs as fixed values with the exception that the NewWind generator should be studied at both 0 and 600 MW. The change in the total system generation and any changes in the system losses are always picked up by the system slack.
3. You should not modify the status of the capacitors or the transformer taps.
4. You should assume that the system losses remain constant over the 5-year period and need only consider the impact the new design has on the base case losses, assuming the NewWind generation is at 600 MW. The price for losses can be assumed to be \$50/MWh.
5. You do not need to consider contingencies involving the new transmission lines and possibly any transformers you may be adding.
6. While an appropriate control response to a contingency might be to decrease the wind farm output (by changing the pitch on the wind turbine blades), your supervisor has specifically asked you not to consider this possibility. Therefore the NewWind generator should always have either a 0 or 600 MW output.

DESIGN PROJECTS 1 AND 2: SAMPLE TRANSMISSION SYSTEM DESIGN COSTS

Transmission Lines (69 kV, 138 kV, 161 kV, 345 kV)

New transmission lines include a fixed cost and a variable cost. The fixed cost is for the design work, the purchase/installation of the three-phase circuit breakers, associated relays, and changes to the substation bus structure. The fixed costs are \$2,400,000 for a 345 kV line, \$1,100,000 for at 161 kV line, \$850,000 for a 138 kV line, and \$500,000 for a 69 kV line. The variable costs depend on the type of conductor and the length of the line. The assumed cost in \$/km are given in Table 6.15.

Conductor Type	Current Rating (Amps)	345-kV Lines	161-kV Lines	138-kV Lines	69-kV Lines
Rook	770				$200,000/km
Crow	830		$390,000/km	$330,000/km	$220,000/km
Condor	900		$410,000/km	$350,000/km	$240,000/km
Cardinal	1110	$600,000/km	$430,000/km	$370,000/km	
Pheasant	1200	$650,000/km	$450,000/km		
Falcon	1380	$700,000/km			

TABLE 6.15
Assumed costs

Lined impedance data and MVA ratings are determined based on the conductor type and tower configuration. The conductor characteristics are given in Table A.4 of the book. For these design problems, assume a symmetric tower configurations. Often the spacings between conductors are provided by the instructor and may be student specific. If no values are given, assume a GMD of 2 m for 69 kV, 4 m for 138 kV, 5 m for 161 kV, and 8 m for 345 kV.

Transformers

Transformer costs include associated circuit breakers, relaying, and installation.

138/69 kV, 101 MVA	$1,500,000
138/69 kV, 168 MVA	$1,800,000
345/161 kV, 560 MVA	$7,500,000

Assume any new 138/69 kV transformer has 0.0025 per unit resistance and 0.07 per unit reactance, and any new 345/161 kV transformer has 0.0004 per unit resistance and 0.025 per unit reactance (all on a 100 MVA base).

Bus Work

Upgrade 69-kV substation to also include 138 kV	$900,000
Upgrade 161-kV substation to also include 345 kV	$3,500,000

DESIGN PROJECT 3: POWER FLOW/SHORT CIRCUITS

Time given: 3 weeks
Approximate time required: 15 hours
Each student is assigned one of the single-line diagrams shown in Figures 6.27 and 6.28. Also, the length of line 2 in these figures is varied for each student.

Assignment I: Power Flow Preparation

For the single-line diagram that you have been assigned (Figure 6.27 or 6.28), convert all positive-sequence impedance, load, and voltage data to per unit using the given

system base quantities. Then using the PowerWorld Simulator, create three input data files: bus input data, line input data, and transformer input data. Note that bus 1 is the swing bus. Your output for this assignment consists of three power-flow input data files.

The purpose of this assignment is to get started and to correct errors before going to the next assignment. It requires a knowledge of the per-unit system, which was covered in Chapter 3, but may need review.

Assignment 2: Power Flow

Case 1. Run the power flow program and obtain the bus, line, and transformer input/output data files that you prepared in Assignment 1.

Case 2. Suggest one method of increasing the voltage magnitude at bus 4 by 5%. Demonstrate the effectiveness of your method by making appropriate changes to the input data of case 1 and by running the power flow program.

Your output for this assignment consists of 12 data files, 3 input, and 3 output data files for each case, along with a one-paragraph explanation of your method for increasing the voltage at bus 4 by 5%.

During this assignment, course material contains voltage control methods, including use of generator excitation control, tap changing and regulating transformers, static capacitors, static var systems, and parallel transmission lines.

This project continues in Chapters 7 and 9.

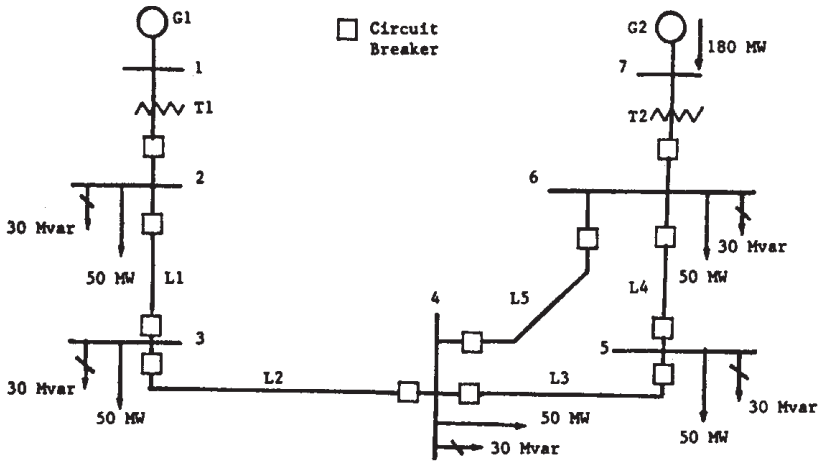

FIGURE 6.27
Single-line diagram for Design Project 3—transmission loop

Generator Ratings
G1: 100 MVA,13.8 kV, $x'' = 0.12, x_2 = 0.14, x_0 = 0.05$ per unit
G2: 200 MVA,15.0 kV, $x'' = 0.12, x_2 = 0.14, x_0 = 0.05$ per unit
The generator neutrals are solidly grounded
Transformer Ratings
T1: 100 MVA,13.8 kVΔ/230 kVY, x=0.1 per unit
T2: 200 MVA, 15 kVΔ/230 kVY, x=0.1 per unit
The transformer neutrals are solidly grounded
Transmission Line Ratings
All Lines: 230 kV, $z_1 = 0.08 + j0.5\ \Omega/km$,
$z_0 = 0.2 + j1.5\ \Omega/km$, $y_1 = j3.3$ E-6 S/km,
Maximum MVA = 400
Line Lengths: $L_1 = 15$ km, L_2 assigned by the instructor (20 to 50 km), $L_3 = 40$ km, $L_4 = 15$ km, $L_5 = 50$ km.

Power Flow Data
Bus 1 : Swing bus, $V_1 = 13.8$ kV, $\partial_1 = 0^o$
Bus 2,3,4,5,6 : Load buses
Bus 7 : Constant voltage magnitude bus, $V_7 = 15$ kV,
$P_{G7} = 180$ MW, -87 Mvar $< Q_{G7} < +87$ Mvar
System Base Quantities
$S_{base} = 100$ MVA (three-phase)
$V_{base} = 13.8$ kV (line-to-line) in the zone of G1

FIGURE 6.28

Single-line diagram for Design Project 3—radial distribution feeder

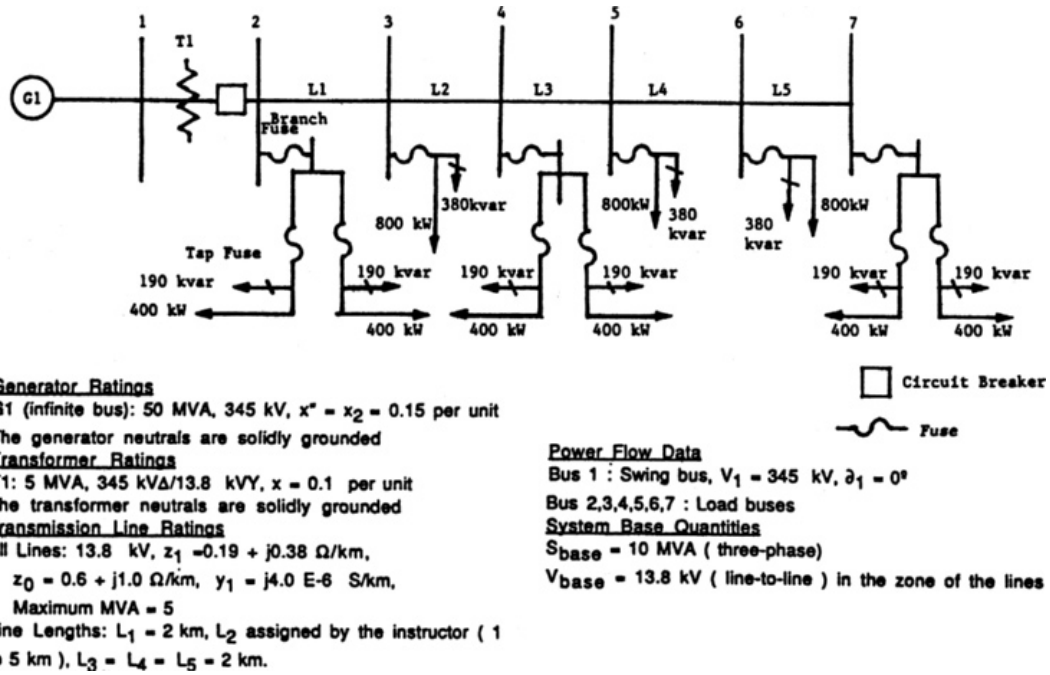

REFERENCES

1. W. F. Tinney and C. E. Hart, "Power Flow Solutions by Newton's Method," *IEEE Trans. PAS*, *86* (November 1967), p. 1449.
2. W. F. Tinney and J. W. Walker, "Direct Solution of Sparse Network Equations by Optimally Ordered Triangular Factorization," *Proc. IEEE*, *55* (November 1967), pp. 1801–1809.
3. Glenn W. Stagg and Ahmed H. El-Abiad, *Computer Methods in Power System Analysis* (New York: McGraw-Hill, 1968).
4. N. M. Peterson and W. S. Meyer, "Automatic Adjustment of Transformer and Phase Shifter Taps in Newton Power Flow," *IEEE Trans. PAS*, *90* (January-February 1971), pp. 103–108.
5. W. D. Stevenson, Jr., *Elements of Power Systems Analysis*, 4th ed. (New York: McGraw-Hill, 1982).
6. A. Bramellar and R. N. Allan, *Sparsity* (London: Pitman, 1976).
7. C. A. Gross, *Power Systems Analysis* (New York: Wiley, 1979).
8. B. Stott, "Fast Decoupled Load Flow," *IEEE Trans. PAS*, Vol. PAS 91 (September–October 1972), pp. 1955–1959.
9. T. Overbye and J. Weber, "Visualizing the Electric Grid," *IEEE Spectrum*, 38, 2 (February 2001), pp. 52–58.
10. Westinghouse Electric Corporation, *Transmission and Distribution Reference Book*, 4th ed. (Pittsburgh: Westinghouse, 1964).

11. Aluminum Association, *The Aluminum Electrical Conductor Handbook* (Washington, D.C.: Aluminum Association).

12. A. J. Wood and B. F. Wollenberg, *Power Generation*, *Operation and Control*, 2nd ed. (New York: John Wiley & Sons, 1996).

13. A. Ellis, "Wind Power Plant Models for System Studies," Tutorial on Fundamentals of Wind Energy, Section V, *IEEE PES GM* (Calgary, AB: July 2009).

14. WECC Wind Generator Modeling Group, "WECC Wind Power Plant Power Flow Modeling Guide," *WECC*, May 2008.

15. E.H. Camm et al., "Characteristics of Wind Turbine Generators for Wind Power Plants," *Proc. IEEE* 2009 General Meeting (Calgary, AB: July 2009).

16. L. K. Kirchmayer, *Economic Operation of Power Systems* (New York: Wiley, 1958).

17. L. K. Kirchmayer and G. W. Stagg, "Evaluation of Methods of Coordinating Incremental Fuel Costs and Incremental Transmission Losses," *Transactions AIEE*, vol. 71, part III (1952), pp. 513–520.

18. G. H. McDaniel and A. F. Gabrielle, "Dispatching Pumped Storage Hydro," *IEEE Transmission PAS*, vol. PAS-85 (May 1966), pp. 465–471.

19. E. B. Dahlin and E. Kindingstad, "Adaptive Digital River Flow Predictor for Power Dispatch," *IEEE Transactions PAS*, vol. PAS-83 (April 1964), pp. 320–327.

20. L. K. Kirchmayer, *Economic Control of Interconnected Systems* (New York: Wiley, 1959).

21. J. H. Drake et al., "Optimum Operation of a Hydrothermal System," *Transactions AIEE* (*Power Apparatus and Systems)*, vol. 62 (August 1962), pp. 242–250.

22. A. J. Wood and B. F. Wollenberg, *Power Generation*, *Operation*, *and Control* (New York: Wiley, 1989).

23. 2005 and 2014 PJM State of the Market Report, available online at http://www.monitoringanalytics.com/reports/PJM_State_of_the_Market/2014.shtml.

24. A. Castillo and R. P. O'Neill, "Survey of Approaches to Solving the ACOPF," *U.S. FERC* (March 2013).